

Foam properties of proteins, low molecular weight surfactants and their complexes

Frederik J. Lech

Thesis committee

Promotor

Prof. Dr H. Gruppen
Professor of Food Chemistry
Wageningen University

Co-promotors

Dr P.A. Wierenga
Assistant Professor, Laboratory of Food Chemistry
Wageningen University

Dr M.B.J. Meinders
Senior Scientist, Food and Biobased Research
Wageningen UR

Other members

Prof. Dr S.D. Stoyanov, Wageningen University
Prof. Dr R. Tuinier, Delft University of Technology, The Netherlands
Dr R. Miller, Max Planck-Institute Colloids and Interfaces, Golm/Potsdam, Germany
Dr L.M.C. Sagis, Wageningen University

This research was conducted under the auspices of the Graduate School VLAG (Advanced studies in Food Technology, Agrobiotechnology, Nutrition and Health Sciences).

Foam properties of proteins, low molecular weight surfactants and their complexes

Frederik J. Lech

Thesis

submitted in fulfilment of the requirements for the degree of doctor
at Wageningen University
by the authority of the Rector Magnificus
Prof. Dr A.P.J. Mol
in the presence of the
Thesis committee appointed by the Academic Board
to be defended in public
on Friday 22 January 2016
at 11 a.m. in the Aula.

Frederik J. Lech

Foam properties of proteins, low molecular weight surfactants and their complexes

128 pages.

PhD thesis, Wageningen University, Wageningen, NL (2015)

With references, with summary in English

ISBN: 978-94-6257-624-7

Abstract

This thesis shows the effects that the addition of low molecular weight surfactants (LMWS) to proteins has on the foam stability of the mixture. For this, the bulk, interfacial, thin liquid films and foam properties are determined for different protein-LMWS mixtures at different molar ratios (MR). It was shown that the MR as well as the charge of the protein and LMWS determine the foam stability of the mixtures. For all mixtures it was found that the proteins have a select number of high affinity binding sites. So, the concentration of free LMWS in the solution is 0 until a critical MR (MR_{cr}), at which all high affinity binding sites are saturated. Above this MR_{cr} , part of the LMWS binds to low affinity binding sites of the proteins. The low affinity binding sites have a binding ratio < 1 , which determines the concentration of bound and free LMWS. For similarly charged protein-LMWS mixtures (i.e. β -lactoglobulin (BLG) and sodium dodecyl sulphate (SDS) and bovine serum albumin (BSA) and SDS at pH 7) the foam stability typically decreases from the foam stability of the pure protein solution (MR 0) until MR_{cr} is reached. At $MR > MR_{cr}$ the foam stability is dominated by the amount of free LMWS. For oppositely charged protein-LMWS mixtures, the binding of the LMWS to the proteins can be described in a similar way, although the number of high affinity sites and low affinity binding ratio are different. There is also a regime of MRs in which the protein-LMWS complexes form large aggregates. These aggregates were in some cases found to increase foam stability (lysozyme (LYS) and SDS and BLG-SDS at pH 3), while in another case (BLG and cetyltrimethylammonium bromide (CTAB)) they lead to decreased foam stability. Still, in all cases it was found that above MR_D the aggregates dissociate and the foam stability becomes dominated by free surfactants, equivalent to what was observed for similarly charged protein-LMWS mixtures.

A multi-scale model was developed to describe the stability of thin liquid films in terms of rupture time and thickness. Initially, the model was used to predict the stability of surfactant free films of water and electrolyte solutions. Later, it was used to predict the foam stability in LYS-SDS mixtures. For that purpose, the model was combined with a foam drainage model to provide theoretical estimations of foam stability. This model is the basis to understand coalescence of bubbles in foam. Finally, the concept of the critical MRs and the free LMWS was introduced. Using this, the foam properties of protein-LMWS mixtures can partly be predicted by relative charge of the components and the binding to both high and low affinity binding sites.

Table of contents

Chapter 1	<i>General Introduction</i>	1
Chapter 2	<i>Stability properties of surfactant free thin films at different ionic strengths: Measurements and modelling</i>	21
Chapter 3	<i>Identification of critical concentrations determining foam ability and stability of β-lactoglobulin</i>	31
Chapter 4	<i>Identifying changes in chemical, interfacial and foam properties of β-lactoglobulin-sodium dodecyl sulphate mixtures</i>	47
Chapter 5	<i>Comparing foam and interfacial properties of similarly charged mixtures of protein and low molecular weight surfactants</i>	69
Chapter 6	<i>Aggregation in mixtures of lysozyme and sodium dodecyl sulphate determines foam stability by stabilization of thin films</i>	81
Chapter 7	<i>General Discussion</i>	97
Summary		113
Acknowledgements		117
About the author		119

1. General Introduction

Proteins and low molecular weight surfactants (LMWS) are commonly used as foaming agents in foods. Each type of molecule has a specific role in the formation and stabilization of foam. To be able to control the foam stability of complex systems, e.g. food products, the individual contributions of proteins, LMWS and that of their mixtures to the foam stability need to be sufficiently understood. Although foam properties of individual protein and LMWS have been known for a long time, the foam properties of mixed protein LMWS systems are not understood yet. The aim of this thesis is to understand the foam properties of protein-LMWS mixtures. For this, coherent data on several aspects of mixed protein-LMWS systems, i.e. the interaction of proteins and LMWS in bulk, at the interface of the mixtures and in the foam are needed.

A short introduction into the principles of foam

Foam is a dispersion of gas bubbles in a continuous liquid or (semi)solid phase. Two important characteristics can be used to describe foam properties of solutions: Foam ability and foam stability. Processes acting at different time scales are important for the foam formation and stabilization. The short time scales are in the range of milliseconds to seconds and related to the creation of bubbles and the adsorption rate of interfacial-active components. Adsorption of interfacial-active components leads to a decrease of the interfacial tension, which is commonly expressed as the interfacial pressure (Π) (equation 1).

$$(1) \quad \Pi = \gamma_0 - \gamma$$

Where Π is the interfacial pressure (N m^{-1}), γ_0 is the interfacial tension of the solvent (N m^{-1}) and γ is the interfacial tension of the solution containing the interfacial-active component (N m^{-1}). The interfacial pressure describes the energy that is needed to create new interfacial area between two immiscible phases. The foam ability of a solution is related to the equilibrium between bubble creation and bubble disappearance, the latter through coalescence with the environment. The foam ability is a characteristic that describes how much foam can be produced in a certain time, i.e. how much gas is incorporated in a fixed volume of solution. Bubbles can be created in different ways, using mechanical, chemical and biological methods, e.g. by whipping, supersaturation of a liquid with gas (e.g. champagne) or by yeast fermentation, respectively. These different methods have recently been reviewed and put in a historical perspective¹. The sparging of gas through porous plates or disks has been proven to be one of the most robust ways to create foam in a reproducible way¹. Therefore, this method was chosen for foam formation in this thesis. In order to obtain a predominantly monodisperse foam, the gas flow rate has to be adjusted to such a rate that the bubbles are created by a 'bubbling' mechanism and not by jetting the gas into the liquid¹. The transition between bubbling

Chapter 1

and jetting is characterized by a critical capillary number (ratio of the Weber and the Reynolds number), which depends mainly on the flow rate of gas and on the viscosity and density of the solution in which the air is injected¹. Two cases can be distinguished in the bubbling regime. In the case of constant gas flow rate, the viscosity and the flow rate mainly determine the bubble volume. In the case of constant pressure, the bubble volume is determined by the pressure, the viscosity, the interfacial tension and by the size and shape of the holes².

After their formation, bubbles cream due to density differences and gravity. In this process, the bubbles come close together and liquid drains through the channels between the bubbles. When the liquid volume fraction (ϵ_l) of the bubble dispersion is about that of a random closed packed system of spheres ($\epsilon_{lc} \sim 0.36$) one speaks about a wet foam while at smaller liquid volume fraction it is called a dry foam. When two bubbles come into close contact, their interfaces confine a thin layer of liquid. When the distance between the layers reaches about 100 nm, a thin liquid film is formed where the surfaces are plane parallel. A schematic depiction of a single (deformed) bubble in foam is shown in figure 1.1, showing the thin liquid films, which are the liquid layers separating the bubbles, the Plateau borders, which are the place where 3 or more thin films join and nodes of the Plateau borders. The properties of the thin films to withstand rupture determine the foam stability against coalescence of two bubbles. The stability of the thin films originates in the balance between opposing forces (i.e. repulsive electrostatic forces and attractive van der Waals forces). The coalescence of two bubbles can be caused by the growth of thickness fluctuations in the thin film or by thermal capillary waves in the film^{3, 4}. The coalescence of bubbles can be affected by electrostatic as well as by steric repulsion between the adsorbed interfacial layers.

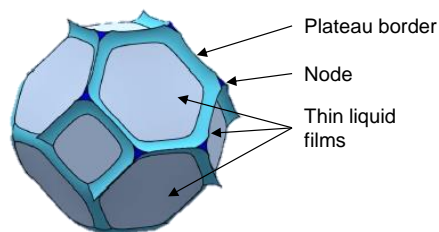


Figure 1.1: Schematic depiction of a dodecahedral shaped bubble in foam.

Another important mechanism of foam deterioration is disproportionation. The disproportionation or coarsening of foam is the shrinking of smaller bubbles and growth of larger bubbles due to differences of the Laplace pressure between the bubbles. The difference in Laplace pressure causes a difference in the amount of dissolved gas around the bubbles and thus a concentration gradient. Due to this gradient, dissolved gas will diffuse from the smaller to the larger bubbles. In addition, the atmosphere, which is contact with the foam and which can be considered as an infinitely large bubble, will take up gas. Disproportionation can be slowed down when the interface is visco-elastic like for protein stabilized foams⁵. It might even be stopped when the interface is purely elastic or

contains molecules or particles that do not desorb, as has been shown for LMWS with a condensed layer of aliphatic molecules⁶ and inorganic particles⁷.

A way to compare the foam stability is to compare the half-life time ($t_{1/2}$). $t_{1/2}$ is the time at which half of the initial foam volume has disappeared (equation 2)

$$(2) \quad t_{1/2} \rightarrow V_m/V_0=0.5$$

where $t_{1/2}$ is the half-life time (min), V_0 and V_m are the volume (cm^3) of foam at $t = 0$ and $t = m$ minutes, respectively.

Besides different time scales also different length scales have to be taken into account to understand foam formation and stabilization. The underlying physical rules describing the formation and stabilization of foam have been developed for each class of surfactants e.g. LMWS, proteins and particles. There are different sets of baseline assumptions for the different classes of surfactants. For example, the Marangoni mechanism is important in LMWS stabilized foam while the formation of an interfacial network is assumed to be an important mechanism for protein stabilized foams. The length scales, at which the mechanisms work in foam range from the molecular level of surfactant molecules in solution to the macroscopic level of the foam itself (figure 1.2). The molecular properties of the interfacial-active material (e.g. charge) depend on the conditions of the solution (e.g. pH, ionic strength). Interfacial-active molecules can adsorb to the gas-liquid interface if there is a gain of free energy. These adsorbed molecules form the adsorbed layer. The properties of the thin films between bubbles in close contact depend on the concentration and the conditions (e.g. pH) in solution and on the properties of the adsorbed layer. However, how these relate to foam is not yet clear.

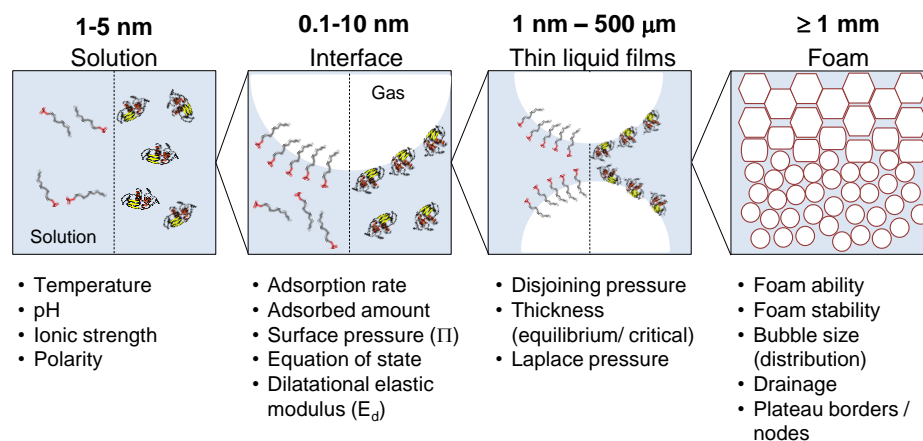


Figure 1.2: Schematic overview of different length scales of foam and accompanying parameters. The dotted lines separate LMWS and protein systems.

LMWS

For an elaborated overview of the influence of the type of LMWS on foam and interfacial properties, we refer to a review by Denkov *et al.*⁸. In short, LMWS are small molecules (hydrodynamic radius ~ 0.5-2 nm) containing a hydrophilic part and a hydrophobic part. Typically, LMWS are differentiated based by the polar group of the hydrophilic part. This

Chapter 1

part can be anionic, cationic, uncharged or zwitterionic. The LMWS used in this thesis and their properties, such as their critical micelle concentration (CMC) or equilibrium interfacial pressure (Π_{eq} , at concentrations above the CMC), are listed in table 1.1.

Table 1.1: Properties of LMWS used in this thesis.

Name	Molecular mass	Length C-chain	CMC _{H2O}	CMC _{bf*}	$\Pi_{eq, bf*}$	Polar group
Unit	[Da]	[-]	[mM]	[mM]	[mN m ⁻¹]	[-]
Sodium dodecyl sulphate (SDS)	289.0	12	8.0 ⁹	2.0 ⁹	38 ⁹	anionic
Cetyltrimethyl ammonium bromide (CTAB)	364.5	16	0.6 ⁹	0.2 ⁹	32 ¹⁰	cationic
Tween 20	1227.5	12	0.05 ¹¹	nd	40 ¹²	non-ionic

*Sodium phosphate buffer, 5 mM, pH 7.0

Adsorption of LMWS to the interface reduces the contact between the solvent molecules and the hydrophobic parts of the surfactant molecule. Because of the small size of the LMWS molecules and thus high diffusion coefficient, the equilibrium adsorbed amount is reached within milliseconds¹³. In dynamic systems, such as draining foam, the liquid flow can induce a concentration gradient of LMWS at the interface. This causes a gradient in interfacial tension. LMWS will move along the gradient of the interfacial tension (Marangoni flow) thereby moving bulk liquid against the direction of the drainage¹⁴. The resulting flow patterns can be observed as density fluctuations in thin films of LMWS (figure 1.3¹⁵).

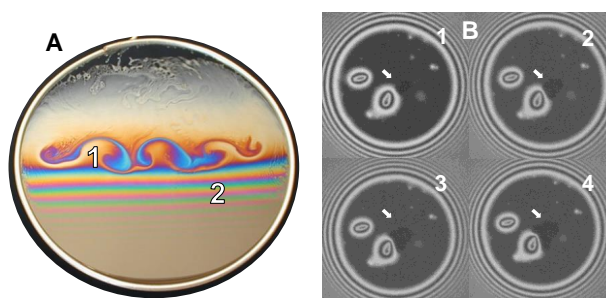


Figure 1.3: A) Flow patterns (1) and interference fringes (2) in a vertical soap film. Image taken from¹⁵. B) Black spot formation and growth, indicated by the white arrow in a thin film of lysozyme (10 mg mL⁻¹, pH 7). at 53, 54, 55 and 56 s after formation of the film. Panel 4 is captures just before rupture of the thin film.

Due to the Marangoni flow and the fast adsorption and desorption of LMWS, interfacial tension gradients are reduced thereby stabilizing the thin film.

In addition, the fast adsorption and desorption lead to low values of the dilatational interfacial elasticity (E_d , typical values for SDS $< 10 \text{ mN m}^{-1}$, this thesis), which is defined (equation 3)³.

$$(3) \quad E_d = \frac{d\gamma}{d\ln A}$$

Where E_d is the dilatational elastic modulus (N m^{-1}), γ is the interfacial tension (N m^{-1}) and $d\ln A$ is the change in interfacial area.

Drainage of the liquid in thin films results in thinning films. The thinning can be quantified by studying the interference fringes and colour/intensity if reflected by microinterferometry¹⁶. Under certain conditions (i.e. concentration, pH, I), the drainage in thin liquid films leads to the formation of so-called black spots, which can merge to form so called Newton black film⁶ (figure 1.3¹⁷). In those Newton black films almost all liquid is expelled and the ionic groups of the two opposing LMWS layers are in close vicinity, only separated by the repulsive electrostatic contribution of the disjoining pressure¹⁸. Although the black films are very thin, e.g. 3 nm in the case of 1 mM SDS in 0.2 M NaCl solution¹⁹, which is a little more than two times the size of the SDS molecule (1.4 nm), they can be very stable^{17, 18}.

Proteins

The literature on protein-stabilized foams has been extensively reviewed. For a detailed description we refer to the following reviews²⁰⁻²⁵. In general, proteins (hydrodynamic radius of 2.1 nm for β -lactoglobulin (18.4 kDa)²⁶ and BSA 3.4 nm (66.4 kDa)²⁷ are larger than LMWS. They consist of a chain of amino acids (AA), linked by peptide bonds. Usually, the protein chain is built up by 20 different AAs. The order of AA in the chain is called the primary structure. The AAs are distinguished by their side groups, which can be e.g. ionic, non-ionic or hydrophobic. The AA chain is folded into secondary structural elements, called e.g. α -helix, β -sheet or random coil. These structural elements are further ordered into a tertiary structure, which is stabilized by covalent (e.g. S-S bridges) and/or non-covalent bonds. A distinction can be made between globular, random coil and fibrillar proteins. Globular proteins have defined structural elements in a 'fixed' arrangement, e.g. β -lactoglobulin and bovine serum albumin, while flexible 'random coil' proteins consist predominantly of random coil elements without a fixed structure, e.g. β -casein. Fibrillar proteins are typically insoluble in water in their 'native' state, e.g. collagen or myosin. In this thesis, we focus on globular proteins. The uneven distribution of polar (charged and uncharged) and hydrophobic AAs, makes a protein amphiphilic. The adsorption rate constant of proteins depends on their diffusion rate, exposed hydrophobicity²⁸ and charge²⁹. The adsorption rate increases with increased hydrophobicity with decreased charge. longer adsorption time, the adsorbed amount increases. This reduces the chance to adsorb and slows down the effective adsorption rate of the protein. Once a globular protein is adsorbed to the interface, it only desorbs under extensive compression of the interface³⁰. This can be enhanced by increasing the temperature³¹. The desorption barrier is related to the size and exposed hydrophobicity of the protein. Once adsorbed to the interface, proteins form an adsorbed layer, which is typically described as a viscoelastic network^{22, 32}. The nature of this network is subject of

Chapter 1

debate. Some scientists speculate about a gelled network of denatured proteins³³, while others describe it as a jammed system of colloidal particles^{34, 35}. The interactions between the adsorbed proteins result in a cohesive interfacial layer with a relatively large dilatational modulus (E_d). This causes strong changes of the interfacial tension as a response to a change of the area of the interface. Due to this, protein foams are more stable against disproportionation than LMWS foams, yet they cannot fully stop the disproportionation. However, the role of proteins in coalescence of the thin films is far from understood.

The bubble size distribution in foam can vary over the length of the foam column. Typically, when the bulk concentration of protein (or any surfactant in this case) is high enough to cover the interface, the bubbles at the top of the foam are larger because of disproportionation and coalescence. When the bulk concentration is too low to fully cover the interfaces, the opposite can occur (i.e. small bubbles at the top equalling higher liquid volume fraction, larger bubbles at the bottom equalling lower liquid volume fraction)³⁶. This is mainly due to coalescence of bubbles and disproportionation, which leads to the coarsening of foam. It was reported that LMWS foams the coarsening of a protein foam is slower than the coarsening of LMWS foam³⁷. This was attributed to the visco-elasticity of the adsorbed protein layer³⁷.

Aggregates and particles

Under certain conditions (e.g. ionic strength, pH and temperature) monomeric proteins can cluster and form aggregates. These can vary in size from several nm to several 100 nm³⁸. These aggregates are visible in the thin liquid films as bright spots where they can form a so called 'pizza film'³⁹ (figure 1.4).

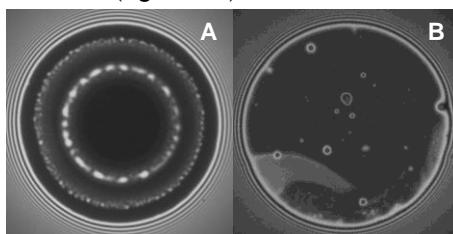


Figure 1.4: Micrographs of thin liquid films containing aggregated BLG at pH 7 10 mg mL⁻¹ (A) and 2 mg mL⁻¹ (B), obtained during this research.

The size and with it the diffusion rate of protein aggregates can be similar to inorganic particles³⁸. Foam properties of foams made from solutions containing inorganic particles are comprehensively described in several reviews^{25, 40-42}. The adsorption (and desorption) of particles is mainly determined by their size, charge and wetting angle (a measure of hydrophobicity). Loosely packed interfaces of particles can enhance the foam stability by preventing coalescence⁴³. Once adsorbed, particles can form a jammed interface, which can stop disproportionation⁷. This stabilization mechanism is called Pickering stabilization. Also, non-adsorbed particles can influence the foam properties by hindering the drainage from Plateau borders and thin films^{44, 45}. It was shown that the drainage of films of latex particles lead to stratification, a situation in which the particles are expelled layer by

layer from the film⁴⁶. Similar phenomena are observed for LMWS systems with concentrations beyond the CMC⁴⁷.

Summary of single surfactant systems

In the current understanding, LMWS, proteins, and particles stabilize foams in different ways. While the protein foam is stabilized by the viscoelastic network, LMWS stabilize the foam by fast adsorption and desorption and the Marangoni mechanism. It was suggested that in protein foams high values of E_d are needed to stabilize foams⁴⁸, while in the case of LMWS foam, Π should increase rapidly to stabilize foam⁴⁹. These opposing concepts of foam stabilization raises the question how to predict the foam stability of a mixture in which both substances are present? In other words, when do the rules for protein-stabilized foams apply and above which LMWS concentration do the rules for LMWS take over?

Interactions between proteins and LMWS

The interactions between proteins and LMWS usually lead to the formation of complexes by non-covalent bonds, e.g. hydrophobic interactions. Hydrophobic interactions occur between the aliphatic chain of the LMWS molecules and hydrophobic amino acid residues of the proteins. For a detailed description of the interactions between proteins and LMWS, we refer to a recent review⁵⁰.

Binding of LMWS

The binding of LMWS to proteins is typically described by binding isotherms in which the concentration of free LMWS molecules over the total amount of LMWS is plotted⁵¹. Typically, at low LMWS concentrations, binding occurs at specific high affinity binding sites of the proteins (region I, figure 1.5). Because of the high affinity for the LMWS molecules, there will be no free LMWS in the solution, only the protein-LMWS complexes. The existence of these high affinity binding sites has been shown for BLG⁵² and BSA^{53, 54}. Next to the high affinity binding, LMWS bind to non-specific low affinity binding sites of proteins (figure 1.5, region II). Above a certain concentration at the end of the non-cooperative binding region, the protein can unfold, which exposes additional low affinity binding sites. This leads to so-called co-operative binding⁵⁵. At the end of the co-operative binding region (region III, figure 1.5.), the protein becomes saturated with LMWS, which results in a steep increase of free surfactant molecules with further addition of LMWS,

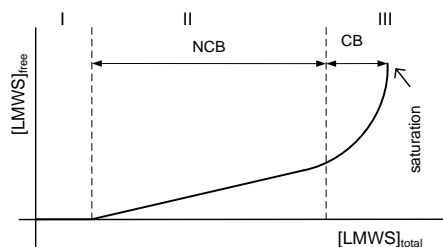


Figure 1.5: Schematic drawing of the concentration of free LMWS as a function of total LMWS concentration. Region (I) specific binding to high affinity binding sites, region (II) non-cooperative binding (NCB) and region (III) co-operative binding (CB) to low affinity binding sites. Saturation of the protein with LMWS is indicated by an arrow. Adapted from Jones (1975)⁵¹.

Several models of interaction between LMWS and unfolded protein have been proposed⁵⁶. Those models include the ‘rod-like’ model in which the LMWS forms a shell around the protein, the ‘pearl necklace’ model, where submicelles of LMWS are formed at different points of the primary protein structure and the ‘protein decorated micelle’ model, where the protein chain ‘ties up’ the micelle⁵⁶. As can be seen from the schematic drawing of the isotherm (figure 1.5), from the moment where the high affinity binding sites are fully saturated, the mixtures comprise complexes of protein and LMWS as well free LMWS monomers. To compare different protein-LMWS mixtures as presented in different studies, the concentration of LMWS can be expressed in multiples of the protein concentration. This is known as the molar ratio (MR) LMWS/protein. However, it must be noted that for foam and interfacial properties, the absolute concentrations of protein and LMWS are important as well.

Current state of knowledge on protein-LMWS interaction in literature

The interfacial properties as well as the bulk interaction in protein-LMWS mixtures have been thoroughly investigated and a part of those studies is compiled in table 1.2, which is summarized schematically in figure 1.6. The table is based on a literature search using the following keywords: Proteins, LMWS interaction and specified for the proteins and LMWS used in this thesis (i.e. BLG, BSA and LYS and of SDS, CTAB and Tween and their mixtures). It was expanded to include information on foam and interfacial properties by using the following keywords: Foam stability, foam ability, ‘interfacial properties’, interfacial pressure and interfacial dilatational elasticity, surface properties, thin liquid films and foam films in combination with the other keywords that were mentioned earlier. The resulting list of 74 articles is summarized in table 1.2. In general, the literature on the interfacial properties focuses mainly on the interfacial properties (i.e. Π and E_a) of the mixtures. Although the concept of protein-LMWS interaction is mentioned in most of those papers (40/47) only a limited number (8/47) provide actual data. Similarly, a high number (38/57) of the studies stress the importance of interfacial measurements to understand foam properties but only 10 from 74 provide actual foam data. A combination of measurements on the binding of LMWS, interfacial properties and foam was only provided by 2 of the 74 studies.

Table 1.2: Literature overview of studies on protein-LMWS interaction.

Ref.	Main LMWS	Main protein	Min MR	Max MR	B*	PS**	IP***	TLF*	Foam	(B+PS) + IP	Complexes mentioned	Importance for foam mentioned
57	SDS	BLG	130	23000	✓							
58	SDS	BLG	6	71	✓							
59	SDS	BLG	9.0	2200	✓	✓						✓
60	SDS	BLG	4	35	✓							✓
61	SDS	BLG	0.7	670	✓							✓
62	SDS	BLG	0.3	30	✓							✓
63	FA	BLG	0.8	200	✓							✓
64	SURV	BSA	1.0	1000	✓							✓
65	FA	BSA	1.0	1000	✓							✓
66	SDS	BSA	1.0	1000	✓							✓
67	CTAB	BSA	1.0	1000	✓							✓
68	SDS	Casein	1.0	500000	✓							✓
69	PFO	Casein	1.0	500000	✓							✓
70	SDS	Casein	1.0	500000	✓							✓
71	CTAB	BLG	1.0	100	✓	✓						✓
72	SDS	BLG	1.0	100	✓							✓
73	SDS	BSA	0.8	1000	✓							✓
74	SDS	BSA	0.8	1000	✓							✓
75	SDS	BSA	26	740	✓							✓
76	SDS	BSA	8.0	530	✓							✓
77	SDS	BSA	1.0	14000	✓							✓
78	SDS	BSA	1.0	20	✓							✓
79	SDS	BSA	0.02	0.7	✓							✓
80	SDS	BSA	200	4000	✓							✓
81	SDS	BSA	0.0	1300	✓							✓
82	SDS	BSA	0.3	400	✓							✓
83	SDS	Casein	1.0	11	✓							✓
84	SDS	Casein	1.0	11	✓							✓
85	SDS	Casein	1.0	11	✓							✓
86	SDS	Casein	1.0	11	✓							✓
87	SDS	Casein	1.0	11	✓							✓
88	SDS	Casein	1.0	11	✓							✓
89	SDS	Casein	1.0	11	✓							✓
90	SDS	Casein	1.0	11	✓							✓
91	SDS	Casein	1.0	11	✓							✓
92	SDS	Casein	1.0	11	✓							✓
93	SDS	Casein	1.0	11	✓							✓
94	SDS	Casein	1.0	11	✓							✓
95	SDS	Casein	1.0	11	✓							✓
96	SDS	Casein	1.0	11	✓							✓
97	SDS	Casein	1.0	11	✓							✓
98	SDS	Casein	1.0	11	✓							✓
99	SDS	Casein	1.0	11	✓							✓
100	SDS	Casein	1.0	11	✓							✓
101	SDS	Casein	1.0	11	✓							✓
102	SDS	Casein	1.0	11	✓							✓
103	SDS	Casein	1.0	11	✓							✓
104	SDS	Casein	1.0	11	✓							✓
105	SDS	Casein	1.0	11	✓							✓
106	SDS	Casein	1.0	11	✓							✓
107	SDS	Casein	1.0	11	✓							✓
108	SDS	Casein	1.0	11	✓							✓
109	SDS	Casein	1.0	11	✓							✓
110	SDS	Casein	1.0	11	✓							✓
111	SDS	Casein	1.0	11	✓							✓
112	SDS	Casein	1.0	11	✓							✓
113	SDS	Casein	1.0	11	✓							✓
114	SDS	Casein	1.0	11	✓							✓
115	SDS	Casein	1.0	11	✓							✓
116	SDS	Casein	1.0	11	✓							✓
117	SDS	Casein	1.0	11	✓							✓
118	SDS	Casein	1.0	11	✓							✓
119	SDS	Casein	1.0	11	✓							✓
120	SDS	Casein	1.0	11	✓							✓
121	SDS	Casein	1.0	11	✓							✓
122	SDS	Casein	1.0	11	✓							✓
123	SDS	Casein	1.0	11	✓							✓
124	SDS	Casein	1.0	11	✓							✓
125	SDS	Casein	1.0	11	✓							✓
126	SDS	Casein	1.0	11	✓							✓

*Binding studies: ITC and equilibrium dialysis

**Protein structure: CD, Fluorescence, SAXS, SANS and NMR

***Interfacial properties: P and E_d

xTLF: Thin liquid films

Chapter 1

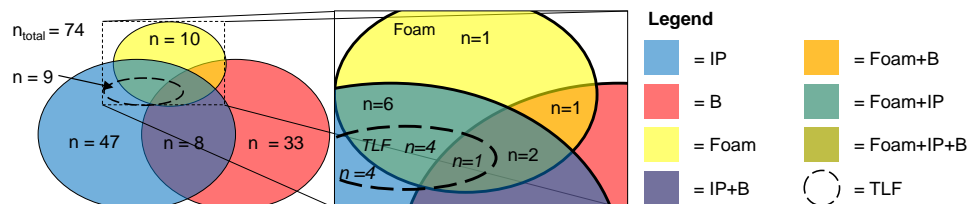


Figure 1.6: Overview of the distribution of literature on protein-LMWS mixtures. Total number of references was 74. The zoom shows the number of references related to foam and thin film (TLF) studies in relation to studies on bulk interaction (B) and interfacial properties (IP).

Effect and quantification of binding between proteins and LMWS

Several methods are used to determine the interactions between proteins and LMWS; they are summarized under binding and protein structure (B and PS) in table 1.2. These methods can further be classified in three subclasses. The first class of methods determine the crystal structure of the complex using, e.g. crystallography^{65, 127} or nuclear magnetic resonance (NMR)^{57, 128}. Amongst others, it was identified by crystallography that BLG can bind aliphatic substances in a hydrophobic pocket, called the calyx^{65, 127}. The second class of methods determine the affinity between substances by isothermal titration calorimetry (ITC) or equilibrium dialysis⁸⁹. Using ITC, the binding affinity (i.e. interactions with high enthalpy) between a protein and binding substances can be determined^{54, 60, 129}. The third class contains methods that can quantify the changes of the secondary and tertiary structure of the protein, including circular dichroism (CD)^{71, 130} or fluorescence techniques e.g. intrinsic fluorescence^{104, 131}. These techniques can only be used when the complexes do not aggregate and become insoluble and sediment. For these samples, the binding interaction can be visualized by measuring the turbidity in the solution^{129, 132}.

Interfacial properties of protein-LMWS mixtures

A large body of literature on the interfacial properties (Π and E_d) exists for protein-LMWS mixtures. Studies that determine these properties are summarized under interfacial properties (IP) in table 1.2. The effect of adding LMWS to proteins on interfacial properties strongly depends on the MR as well as the total concentration of the protein and LMWS. Increasing the MR leads to a faster increase of the interfacial pressure, compared to the protein alone. This was shown, for instance, for mixtures of the random coil protein β -casein and SDS⁶⁸ and the globular BSA and SDS¹¹³. In a recent review, this increase of the interfacial pressure, compared to the protein alone, was claimed to be related to the foam ability of the mixtures¹³³. Analogous to this, the final interfacial pressure values (or values obtained in the plateau region of the Π /time curve) increase with increasing MR until the value of the mixtures is similar to the values of the pure LMWS. This was shown for BLG-SDS¹²³, LYS-SDS⁸⁴ and Tween80-BSA¹⁰⁴ mixtures. In addition to Π , the E_d of the interfacial layer depends on the MR at a fixed protein concentration. This was recently demonstrated BSA-SDS and BLG-SDS mixtures^{119, 121}. They found that the E_d of the interfacial layer at low MR is similar to that of pure protein and with increasing MR it decreases to become similar to the response of SDS¹¹⁹. It can be assumed that this is a generic observation, since it was also found in oppositely charged mixtures (LYS-SDS)⁸².

as well as non-ionic LMWS-protein mixtures (Tween20-BSA)⁸⁶. A generic conclusion of the aforementioned studies is that the LMWS molecules displace the adsorbed proteins from the interface. However, this statement was based on sequential adsorption studies, in which first a layer of protein is adsorbed and subsequently LMWS was added to the solution. In competitive adsorption experiments, where proteins (in that case β -casein) and LMWS are mixed in bulk, a displacement of protein was not observed, since the interface was covered with complexes and free LMWS⁶⁸. Currently, there are two main conceptual models of the composition of mixed protein-LMWS interfaces (figure 1.7). The separate adsorption model (S-A model, figure 1.7 A), claims a mixture of non-interacting species. At a given concentration, the LMWS cover the interface while the proteins are in solution. Beyond the CMC, LMWS micelles are formed, in which proteins are incorporated^{102, 122}. The complex-adsorption model (C-A model, figure 1.7 B), assumes that LMWS bind to proteins. Initially, all LMWS bind to the protein and the complexes adsorb to the interface. At higher concentration, more LMWS binds to the protein, but free LMWS are able to adsorb to the interface as well. At very high LMWS concentrations, the interface is covered with LMWS and the complexes are dissolved in the bulk. Beyond the CMC, the protein-LMWS complexes are part of the LMWS micelles. The S-A model originates from the orogenic displacement theories from sequential adsorption studies^{110, 115, 117, 134, 135}. The C-A model originates from competitive adsorption studies^{82, 136, 137}. In most cases, Π and E_d , follow monotonous curves as a function of the LMWS concentration from values close to that of pure protein at low MR (0.01-1) towards values typically found for pure LMWS systems (MR >100). One exception being the mixture of LYS-SDS (at pH 7), which shows a non-monotonous change of E_d ⁷⁴.

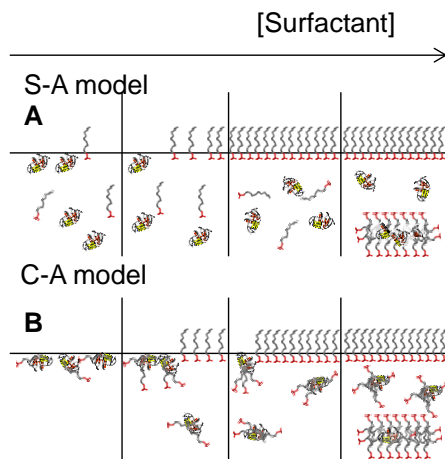


Figure 1.7: Schematic depiction of interfaces of protein-LMWS mixtures as a function of the concentration of LMWS. A) Separate adsorption (S-A) model. B) Complex adsorption (C-A) model.

Properties of thin liquid films of protein-LMWS mixtures

Mixing proteins and LMWS influences the properties of thin films. However, little quantitative data is available for thin films. Most of the studies focus on non-ionic LMWS

Chapter 1

mixtures, such as the mixing of BSA with n-dodecyl- β -D-maltoside¹⁸. The interaction leads to thicker thin liquid films than pure for BSA, since the protein-LMWS complexes are bigger than a BSA monomer¹⁸. However, the presence of the complexes and aggregates in the thin films can lead to irregular drainage patterns, which both impede the thickness measurements¹³⁸. Another study on non-ionic mixtures using LYS and decyl-dimethyl phosphine oxide showed common black films with black spots at MR 1 and Newton black films at MR 500. This indicates that at low MR the interfacial is covered by complexes, while at high MR mainly LMWS are at the interface¹²⁰. Also in other mixtures of BSA with non-ionic LMWS (Tween80), the protein-LMWS complexes stabilize regions of black foam films (MR 50-230)¹³⁹. Similar to the non-ionic mixtures, in the case of LYS-SDS mixtures, at low MR (MR < 20) the thin films entrapped protein-LMWS complexes, while at high MR (MR > 200), the interface of film is dominated by SDS and no complexes were observed¹²⁰. These findings indicate the importance of the MR to predict the behaviour of the mixed system.

Foam properties of protein-LMWS mixtures

It is generally assumed that the addition of LMWS to proteins decreases the foam stability of mixtures^{112, 140, 141}. However, this assumption is underpinned by very little quantitative data on foam properties of protein-LMWS mixtures as can be seen from table 1.2 and figure 1.6. A study on BSA-SDS mixtures showed a decrease of the foam ability (foam made by shaking in glass tubes of 30 mL) between MR 0 and 50, while from MR 50 onwards, the foam ability increases and becomes similar to the LMWS alone¹¹⁸. Not only the foam ability is affected by the addition of LMWS to protein but also the foam stability of the mixtures. It was shown that MR 1.7 mixtures of whey protein isolate and oligofructose palmitic acid had a foam stability (determined by image analysis) similar to WPI, while at MR 3.7, the foam stability was similar to that of the pure LMWS¹²⁶. In mixtures of BLG-Tween20, the foam stability (determined by conductimetry) decreased from MR 1 to 5 compared to the foam stability of pure BLG, while from MR 5 onwards, the foam stability increased with increasing MR to become similar to Tween20¹¹². The decrease in foam stability as a function of MR at low MR is not observed in all cases of mixed protein-LMWS solutions. A study on LPC-BLG mixture showed a 22 % increase in the foam stability (determined by conductimetry) with increasing MR until a MR 5. Between MR 5 and 10 a minimum in foam stability was observed, while >MR 10, the foam stability is similar to the foam stability of the pure LMWS¹¹⁶. As discussed above it can be seen that the multitude of techniques to determine the foam properties, the range of MR and the choice of proteins and LMWS are diverse. This diversity impedes the comparison of foam properties from different studies, which complicates the identification and understanding of the important underlying principles.

Aim, hypothesis and approach of the thesis

The aim of this thesis is to understand the mechanisms that control foam stability and ability of different protein-LMWS mixtures as model systems for complex foods.

From previous sections, it is clear that the interaction between the LMWS and the proteins influences the foam properties. As there are different interactions between the components, properties of the complexes as well as the overall composition of the liquid solution will depend on MR. Size and hydrophobicity of the protein-LMWS complex will change upon binding of the LMWS. Therefore, it is hypothesized that the formation of the complexes as well as the composition of the mixtures i.e. the presence of protein-LMWS complexes and free LMWS determine the foam properties of the mixtures. Both proteins and LMWS can be similarly or oppositely charged to each other. Hence, the addition of LMWS to protein will lead to different protein-LMWS complexes depending on the relative charge of components. It is, therefore, hypothesized that the foam properties of the mixtures / complexes depend on the relative charge both substances possess in solution and on the effect this has on interfacial and thin film properties.

To what extent these various mechanisms control foam ability and stability is far from clear and is subject of the research in presented thesis. To increase quantitative understanding of protein-LMWS mixtures, systematic studies on molecular, interfacial, thin film, and foam properties are performed.

In the first experimental chapter (**chapter 2**), quantitative understanding of the role of disjoining pressure on the stability of thin liquid films in a surfactant free model system is generated. In **chapter 3**, the influence of the bulk properties on the foam ability and stability of a pure protein system is investigated. Further, the foam properties of mixtures of proteins with a LMWS as a function of the MR are investigated. Next, the extent of the effect of the bulk interaction of a protein mixed with a similarly charged LMWS is characterized (**chapter 4**). Subsequently, the effects of high and low affinity binding sites on the composition of a protein-LMWS mixture is determined (**chapter 5**). The importance of the charge of the individual protein and surfactant on the bulk interaction as well as the foam properties is shown in **chapter 6**. In the last chapter (**chapter 7**), the main results obtained in the previous chapters are discussed.

References

1. Drenckhan, W.; Saint-Jalmes, A., The science of foaming. *Advances in Colloid and Interface Science* **2015**, *222*, 228-259.
2. Davidson, J. F.; Schüler, B. O. G., Bubble formation at an orifice in a viscous liquid. *Chemical Engineering Research and Design* **1997**, *75*, Supplement, S105-S115.
3. Lucassen-Reynders, E. H.; Lucassen, J., Properties of capillary waves. *Advances in Colloid and Interface Science* **1970**, *2*, 347-395.
4. Vrij, A.; Overbeek, J. T. G., Rupture of thin liquid films due to spontaneous fluctuations in thickness. *Journal of the American Chemical Society* **1968**, *90*, 3074-3078.
5. Kloek, W.; van Vliet, T.; Meinders, M., Effect of bulk and interfacial rheological properties on bubble dissolution. *Journal of Colloid and Interface Science* **2001**, *237*, 158-166.
6. Tcholakova, S.; Mitinova, Z.; Golemanov, K.; Denkov, N. D.; Vethamuthu, M.; Ananthapadmanabhan, K. P., Control of Ostwald ripening by using surfactants with high surface modulus. *Langmuir* **2011**, *27*, 14807-14819.
7. Maestro, A.; Rio, E.; Drenckhan, W.; Langevin, D.; Salonen, A., Foams stabilised by mixtures of nanoparticles and oppositely charged surfactants: relationship between bubble shrinkage and foam coarsening. *Soft Matter* **2014**, *10*, 6975-6983.
8. Denkov, N. D.; Tcholakova, S.; Golemanov, K.; Ananthapadmanabhan, K. P.; Lips, A., The role of surfactant type and bubble surface mobility in foam rheology. *Soft Matter* **2009**, *5*, 3389-3408.

Chapter 1

9. Bahri, M. A.; Hoebeke, M.; Grammenos, A.; Delanaye, L.; Vandewalle, N.; Seret, A., Investigation of SDS, DTAB and CTAB micelle microviscosities by electron spin resonance. *Colloids and Surfaces A: Physicochemical and Engineering Aspects* **2006**, 290, 206-212.
10. Taylor, D. J. F.; Thomas, R. K.; Penfold, J., The adsorption of oppositely charged polyelectrolyte/surfactant mixtures: Neutron reflection from dodecyl trimethylammonium bromide and sodium poly(styrene sulfonate) at the air/water interface. *Langmuir* **2002**, 18, 4748-4757.
11. Mittal, K. L., Determination of CMC of polysorbate 20 in aqueous solution by surface tension method. *Journal of Pharmaceutical Sciences* **1972**, 61, 1334-1335.
12. Clark, D. C.; Wilde, P. J.; Wilson, D. R., Destabilization of α -lactalbumin foams by competitive adsorption of the surfactant Tween20. *Colloids and surfaces* **1991**, 59, 209-223.
13. Walstra, P., Surface Phenomena. In *Physical Chemistry of Foods*, Marcel Dekker, Inc.: New York, NY, USA, **2003**; pp 316-396.
14. Scriven, L. E.; Sternling, C. V., The Marangoni effects. *Nature* **1960**, 187, 186-188.
15. Carboni, G. Surface phenomena and colloids. http://www.funsci.com/fun3_en/exper2/exper2.htm (9.9.2015),
16. Scheludko, A., Thin liquid films. *Advances in Colloid and Interface Science* **1967**, 1, 391-464.
17. Exerowa, D.; Nikolov, A.; Zacharieva, M., Common black and Newton film formation. *Journal of Colloid and Interface Science* **1981**, 81, 419-429.
18. Angarska, Z. K.; Elenskyi, A. A.; Yampolskaya, G. P.; Tachev, K. D., Foam films from mixed solutions of bovine serum albumin and n-dodecyl- β -D-maltoside. *Colloids and Surfaces A: Physicochemical and Engineering Aspects* **2011**, 382, 102-112.
19. Yaros, H. D.; Newman, J.; Radke, C. J., Evaluation of DLVO theory with disjoining-pressure and film-conductance measurements of common-black films stabilized with sodium dodecyl sulfate. *Journal of Colloid and Interface Science* **2003**, 262, 442-455.
20. Damodaran, S., Protein stabilization of emulsions and foams. *Journal of Food Science* **2005**, 70, R54-R66.
21. Dickinson, E., Proteins at interfaces and in emulsions stability, rheology and interactions. *Journal of the Chemical Society, Faraday Transactions* **1998**, 94, 1657-1669.
22. Dickinson, E., Adsorbed protein layers at fluid interfaces: interactions, structure and surface rheology. *Colloids and Surfaces B: Biointerfaces* **1999**, 15, 161-176.
23. Murray, B. S., Stabilization of bubbles and foams. *Current Opinion in Colloid and Interface Science* **2007**, 12, 232-241.
24. Murray, B. S., Rheological properties of protein films. *Current Opinion in Colloid and Interface Science* **2011**, 16, 27-35.
25. Murray, B. S.; Ettelaie, R., Foam stability: proteins and nanoparticles. *Current Opinion in Colloid and Interface Science* **2004**, 9, 314-320.
26. Aymard, P.; Durand, D.; Nicolai, T., The effect of temperature and ionic strength on the dimerisation of β -lactoglobulin. *International Journal of Biological Macromolecules* **1996**, 19, 213-221.
27. Valstar, A.; Almgren, M.; Brown, W.; Vasilescu, M., The interaction of bovine serum albumin with surfactants studied by light scattering. *Langmuir* **2000**, 16, 922-927.
28. Wierenga, P. A.; Meinders, M. B. J.; Egmond, M. R.; Voragen, A. G. J.; de Jongh, H. H. J., Protein exposed hydrophobicity reduces the kinetic barrier for adsorption of ovalbumin to the air-water interface. *Langmuir* **2003**, 19, 8964-8970.
29. Wierenga, P. A.; Meinders, M. B. J.; Egmond, M. R.; Voragen, A. G. J.; de Jongh, H. H. J., Quantitative description of the relation between protein net charge and protein adsorption to air-water interfaces. *The Journal of Physical Chemistry B* **2005**, 109, 16946-16952.
30. MacRitchie, F., Desorption of proteins from the air/water interface. *Journal of Colloid and Interface Science* **1985**, 105, 119-123.
31. Fainerman, V. B.; Leser, M. E.; Michel, M.; Lucassen-Reynders, E. H.; Miller, R., Kinetics of the desorption of surfactants and proteins from adsorption layers at the solution/air interface. *The Journal of Physical Chemistry B* **2005**, 109, 9672-9677.
32. Kinsella, J. E., Functional properties of proteins: possible relationships between structure and function in foams. *Food Chemistry* **1981**, 7, 273-288.
33. Kudryashova, E. V.; Visser, A. J. W. G.; De Jongh, H. H. J., Reversible self-association of ovalbumin at air-water interfaces and the consequences for the exerted surface pressure. *Protein Science* **2005**, 14, 483-493.

34. Wierenga, P. A.; Gruppen, H., New views on foams from protein solutions. *Current Opinion in Colloid and Interface Science* **2010**, *15*, 365-373.
35. Wijmans, C. M.; Dickinson, E., Simulation of interfacial shear and dilatational rheology of an adsorbed protein monolayer modeled as a network of spherical particles. *Langmuir* **1998**, *14*, 7278-7286.
36. Buckingham, J. H., Effect of pH, concentration, and temperature on the strength of cytoplasmic protein foams. *Journal of the Science of Food and Agriculture* **1970**, *21*, 441-445.
37. Saint-Jalmes, A.; Peugeot, M. L.; Ferraz, H.; Langevin, D., Differences between protein and surfactant foams: Microscopic properties, stability and coarsening. *Colloids and Surfaces A: Physicochemical and Engineering Aspects* **2005**, *263*, 219-225.
38. Dhayal, S. K.; *Mesoscale structure and techno-functional properties of enzymatically cross-linked α -lactalbumin nanoparticles*, PhD thesis, Wageningen University: Wageningen, The Netherlands, **2015**.
39. Rullier, B.; Axelos, M. A. V.; Langevin, D.; Novales, B., β -Lactoglobulin aggregates in foam films: Effect of the concentration and size of the protein aggregates. *Journal of Colloid and Interface Science* **2010**, *343*, 330-337.
40. Binks, B. P., Particles as surfactants—similarities and differences. *Current Opinion in Colloid and Interface Science* **2002**, *7*, 21-41.
41. Gonzenbach, U. T.; Studart, A. R.; Tervoort, E.; Gauckler, L. J., Stabilization of foams with inorganic colloidal particles. *Langmuir* **2006**, *22*, 10983-10988.
42. Horozov, T. S., Foams and foam films stabilised by solid particles. *Current Opinion in Colloid and Interface Science* **2008**, *13*, 134-140.
43. Lai, K.; Dixit, N., Additives for foams. In *Foams*, Prud'homme, R.; Khan, S., Eds. Marcel Dekker, Inc.: New York, NY, USA, **1995**; pp 315-338.
44. Carn, F.; Colin, A.; Pitois, O.; Backov, R., Foam drainage study during plateau border mineralisation. *Soft Matter* **2012**, *8*, 61-65.
45. Carn, F.; Colin, A.; Pitois, O.; Vignes-Adler, M.; Backov, R., Foam drainage in the presence of nanoparticle-surfactant mixtures. *Langmuir* **2009**, *25*, 7847-7856.
46. Basheva, E. S.; Danov, K. D.; Kralchevsky, P. A., Experimental study of particle structuring in vertical stratifying films from latex suspensions. *Langmuir* **1997**, *13*, 4342-4348.
47. Langevin, D.; Marquez-Beltran, C.; Delacotte, J., Surface force measurements on freely suspended liquid films. *Advances in Colloid and Interface Science* **2011**, *168*, 124-134.
48. Walstra, P., Formation of emulsions and foams. In *Physical Chemistry of Foods*, 1 ed.; Marcel Dekker: New York, NY, USA, **2003**; p 807.
49. Acharya, D. P.; Gutiérrez, J. M.; Aramaki, K.; Aratani, K.-i.; Kunieda, H., Interfacial properties and foam stability effect of novel gemini-type surfactants in aqueous solutions. *Journal of Colloid and Interface Science* **2005**, *291*, 236-243.
50. Otzen, D., Protein-surfactant interactions: A tale of many states. *Biochimica et Biophysica Acta (BBA) - Proteins and Proteomics* **2011**, *1814*, 562-591.
51. Jones, M. N., A theoretical approach to the binding of amphipathic molecules to globular proteins. *Biochemical Journal* **1975**, *151*, 109.
52. Gutiérrez-Magdaleno, G.; Bello, M.; Portillo-Téllez, M. C.; Rodríguez-Romero, A.; García-Hernández, E., Ligand binding and self-association cooperativity of β -lactoglobulin. *Journal of Molecular Recognition* **2012**, *26*, 67-75.
53. Kelley, D.; McClements, D. J., Interactions of bovine serum albumin with ionic surfactants in aqueous solutions. *Food Hydrocolloids* **2003**, *17*, 73-85.
54. Nielsen, A. D.; Borch, K.; Westh, P., Thermochemistry of the specific binding of C12 surfactants to bovine serum albumin. *Biochimica et Biophysica Acta (BBA) - Protein Structure and Molecular Enzymology* **2000**, *1479*, 321-331.
55. Turro, N. J.; Lei, X.-G.; Ananthapadmanabhan, K. P.; Aronson, M., Spectroscopic probe analysis of protein-surfactant interactions: The BSA/SDS system. *Langmuir* **1995**, *11*, 2525-2533.
56. Gudiksen, K. L.; Gitlin, I.; Moustakas, D. T.; Whitesides, G. M., Increasing the net charge and decreasing the hydrophobicity of bovine carbonic anhydrase decreases the rate of denaturation with sodium dodecyl sulfate. *Biophysical Journal* **2006**, *91*, 298-310.
57. Chen, A.; Wu, D.; Johnson, C. S. J., Determination of the binding isotherm and size of the bovine serum albumin-sodium dodecyl sulfate complex by diffusion-ordered 2D NMR. *The Journal of Physical Chemistry* **1995**, *99*, 828-834.

Chapter 1

58. Roth, S.; Murray, B. S.; Dickinson, E., Interfacial sheer rheology of aged and heat-treated β -lactoglobulin films: Displacement by nonionic surfactant. *Journal of Agricultural and Food Chemistry* **2000**, *48*, 1491-1497.
59. Ulaganathan, V.; Bergenstahl, B.; Krägel, J.; Miller, R., Adsorption and shear rheology of β -lactoglobulin/SDS mixtures at water/hexane and water/MCT interfaces. *Colloids and Surfaces A: Physicochemical and Engineering Aspects* **2012**, *413*, 136-141.
60. Hansted, J. G.; Wejse, P. L.; Bertelsen, H.; Otzen, D. E., Effect of protein-surfactant interactions on aggregation of β -lactoglobulin. *Biochimica et Biophysica Acta (BBA) - Proteins and Proteomics* **2011**, *1814*, 713-723.
61. Wüstneck, R.; Krägel, J.; Miller, R.; Wilde, P. J.; Clark, D. C., The adsorption of surface-active complexes between β -casein, β -lactoglobulin and ionic surfactants and their shear rheological behaviour. *Colloids and Surfaces A: Physicochemical and Engineering Aspects* **1996**, *114*, 255-265.
62. Jones, M. N.; Wilkinson, A., The interaction between β -lactoglobulin and sodium n-dodecyl sulphate. *Biochemistry Journal* **1976**, *153*, 713-718.
63. Jung, J.-M.; Savin, G.; Pouzot, M.; Schmitt, C.; Mezzenga, R., Structure of heat-induced β -lactoglobulin aggregates and their complexes with sodium-dodecyl sulfate. *Biomacromolecules* **2008**, *9*, 2477-2486.
64. Georgiev, G. A.; Vassileff, C.; Jordanova, A.; Tsanova, A.; Lalchev, Z., Foam film study of albumin inhibited lung surfactant preparations: effect of added hydrophilic polymers. *Soft Matter* **2012**, *8*, 12072-12079.
65. Loch, J. I.; Polit, A.; Bonarek, P.; Olszewska, D.; Kurpiewska, K.; Dziedzicka-Wasylewska, M.; Lewiński, K., Structural and thermodynamic studies of binding saturated fatty acids to bovine β -lactoglobulin. *International Journal of Biological Macromolecules* **2012**, *50*, 1095-1102.
66. Noskov, B.; Mikhailovskaya, A., Adsorption kinetics of globular proteins and protein/surfactant complexes at the liquid-gas interface. *Soft Matter* **2013**, *9*, 9392-9402.
67. Maulik, S.; Dutta, P.; Chatteraj, D. K.; Moulik, S. P., Biopolymer-surfactant interactions: 5 Equilibrium studies on the binding of cetyltrimethyl ammonium bromide and sodium dodecyl sulfate with bovine serum albumin, beta-lactoglobulin, hemoglobin, gelatin, lysozyme and deoxyribonucleic. *Colloids and Surfaces B: Biointerfaces* **1998**, *11*, 1-8.
68. Dan, A.; Kotsmar, C.; Ferri, J. K.; Javadi, A.; Karbaschi, M.; Kragel, J.; Wustneck, R.; Miller, R., Mixed protein-surfactant adsorption layers formed in a sequential and simultaneous way at water-air and water-oil interfaces. *Soft Matter* **2012**, *8*, 6057-6065.
69. Schwieger, C.; Ropers, M.-H., Binding of a perfluorinated surfactant to β -lactoglobulin in aqueous solutions. *Food Hydrocolloids* **2013**, *30*, 241-248.
70. Kotsmar, C.; Aksenenko, E. V.; Fainerman, V. B.; Pradines, V.; Krägel, J.; Miller, R., Equilibrium and dynamics of adsorption of mixed β -casein/surfactant solutions at the water/hexane interface. *Colloids and Surfaces A: Physicochemical and Engineering Aspects* **2010**, *354*, 210-217.
71. Taheri-Kafrani, A.; Asgari-Mobarakeh, E.; Bordbar, A.-K.; Haertlé, T., Structure-function relationship of β -lactoglobulin in the presence of dodecyltrimethyl ammonium bromide. *Colloids and Surfaces B: Biointerfaces* **2010**, *75*, 268-274.
72. Alahverdijeva, V.; Fainerman, V.; Aksenenko, E.; Leser, M.; Miller, R., Adsorption of hen egg-white lysozyme at the air-water interface in presence of sodium dodecyl sulphate. *Colloids and Surfaces A: Physicochemical and Engineering Aspects* **2008**, *317*, 610-617.
73. Ding, Y.; Shu, Y.; Ge, L.; Guo, R., The effect of sodium dodecyl sulfate on the conformation of bovine serum albumin. *Colloids and Surfaces A: Physicochemical and Engineering Aspects* **2007**, *298*, 163-169.
74. Alahverdijeva, V. S.; Grigoriev, D. O.; Fainerman, V. B.; Aksenenko, E. V.; Miller, R.; Möhwald, H., Competitive adsorption from mixed hen egg-white lysozyme/surfactant solutions at the air-water interface studied by tensiometry, ellipsometry, and surface dilational rheology. *The Journal of Physical Chemistry B* **2008**, *112*, 2136-2143.
75. Chernysheva, M. G.; Ivanov, R. A.; Soboleva, O. A.; Badun, G. A., Do low surfactants concentrations change lysozyme colloid properties? *Colloids and Surfaces A: Physicochemical and Engineering Aspects* **2013**, *436*, 1121-1129.
76. Lund, H.; Christensen, B. P.; Nielsen, A. D.; Westh, P., Proton exchange coupled to the specific binding of alkylsulfonates to serum albumins. *Biochimica et Biophysica Acta (BBA) - Proteins and Proteomics* **2006**, *1764*, 1243-1251.
77. Gimel, J. C.; Brown, W., A light scattering investigation of the sodium dodecyl sulfate-lysozyme system. *The Journal of Chemical Physics* **1996**, *104*, 8112-8117.

78. Green, R. J.; Su, T. J.; Joy, H.; Lu, J. R., Interaction of lysozyme and sodium dodecyl sulfate at the air-liquid interface. *Langmuir* **2000**, 16, 5797-5805.
79. Reynolds, J. A.; Gallagher, J. P.; Steinhardt, J., Effect of pH on the binding of N-alkyl sulfates to bovine serum albumin. *Biochemistry* **1970**, 9, 1232-1238.
80. Miller, R.; Alahverdijeva, V. S.; Fainerman, V. B., Thermodynamics and rheology of mixed protein-surfactant adsorption layers. *Soft Matter* **2008**, 4, 1141-1146.
81. Singh, R. B.; Mahanta, S.; Guchhait, N., Destructive and protective action of sodium dodecyl sulphate micelles on the native conformation of Bovine Serum Albumin: A study by extrinsic fluorescence probe 1-hydroxy-2-naphthaldehyde. *Chemical Physics Letters* **2008**, 463, 183-188.
82. Noskov, B. A.; Tikhonov, M. M., Effect of sodium dodecyl sulfate on dynamic surface properties of lysozyme solutions. *Colloid Journal* **2012**, 74, 248-253.
83. Tipping, E.; Jones, M. N.; Skinner, H. A., Enthalpy of interaction between some globular proteins and sodium n-dodecyl sulphate in aqueous solution. *Journal of the Chemical Society, Faraday Transactions 1: Physical Chemistry in Condensed Phases* **1974**, 70, 1306-1315.
84. Sun, M. L.; Tilton, R. D., Adsorption of protein/surfactant complexes at the air/aqueous interface. *Colloids and Surfaces B: Biointerfaces* **2001**, 20, 281-293.
85. Liu, Y.; Guo, R., Interaction between casein and sodium dodecyl sulfate. *Journal of Colloid and Interface Science* **2007**, 315, 685-692.
86. Seta, L.; Baldino, N.; Gabriele, D.; Lupi, F. R.; de Cindio, B., The effect of surfactant type on the rheology of ovalbumin layers at the air/water and oil/water interfaces. *Food Hydrocolloids* **2012**, 29, 247-257.
87. Fukushima, K.; Murata, Y.; Nishikido, N.; Sugihara, G.; Tanaka, M., The binding of sodium dodecyl sulfate to lysozyme in aqueous solutions. *Bulletin of the Chemical Society of Japan* **1981**, 54, 3122-3127.
88. Carrera Sánchez, C.; Rodríguez Patino, J. M., Surface shear rheology of WPI-monoglyceride mixed films spread at the air-water interface. *Colloids and Surfaces B: Biointerfaces* **2004**, 36, 57-69.
89. Jones, M.; Manley, P., Relationship between proton and surfactant binding to lysozyme in aqueous solution. *Journal of the Chemical Society, Faraday Transactions* **1981**, 1, 827-835.
90. Giroux, H. J.; Britten, M., Heat treatment of whey proteins in the presence of anionic surfactants. *Food Hydrocolloids* **2004**, 18, 685-692.
91. Lad, M. D.; Ledger, V. M.; Briggs, B.; Green, R. J.; Frazier, R. A., Analysis of the SDS-lysozyme binding isotherm. *Langmuir* **2003**, 19, 5098-5103.
92. Engelhardt, K.; Weichsel, U.; Kraft, E.; Segets, D.; Peukert, W.; Braunschweig, B., Mixed layers of β -lactoglobulin and SDS at air-water interfaces with tunable intermolecular interactions. *The Journal of Physical Chemistry B* **2014**, 118, 4098-4105.
93. Morén, A. K.; Khan, A., Phase equilibria of an anionic surfactant (sodium dodecyl sulfate) and an oppositely charged protein (lysozyme) in water. *Langmuir* **1995**, 11, 3636-3643.
94. Magdassi, S.; Vinetsky, Y.; Relkin, P., Formation and structural heat-stability of β -lactoglobulin/surfactant complexes. *Colloids and Surfaces B: Biointerfaces* **1996**, 6, 353-362.
95. Morén, A. K.; Khan, A., Surfactant hydrophobic effect on the phase behavior of oppositely charged protein and surfactant mixtures: Lysozyme and sodium alkyl sulfates. *Langmuir* **1998**, 14, 6818-6826.
96. Wilde, P. J.; Clark, D. C., The competitive displacement of β -lactoglobulin by Tween20 from oil-water and air-water interfaces. *Journal of Colloid and Interface Science* **1993**, 155, 48-54.
97. Pitt-Rivers, R.; Impiombato, F. A., The binding of sodium dodecyl sulphate to various proteins. *Biochemical Journal* **1968**, 109, 825.
98. Chakraborty, T.; Chakraborty, I.; Moulik, S. P.; Ghosh, S., Physicochemical and conformational studies on BSA-surfactant interaction in aqueous medium. *Langmuir* **2009**, 25, 3062-3074.
99. Hegg, P.-O., Precipitation of egg white proteins below their isoelectric points by sodium dodecyl sulphate and temperature. *Biochimica et Biophysica Acta (BBA) - Protein Structure* **1979**, 579, 73-87.
100. Ruiz-Garcia, J.; Gámez-Corralles, R.; Ivlev, B. I., Foam and cluster structure formation by latex particles at the air/water interface. *Physica A: Statistical Mechanics and its Applications* **1997**, 236, 97-104.
101. Mackie, A.; Wilde, P., The role of interactions in defining the structure of mixed protein-surfactant interfaces. *Advances in Colloid and Interface Science* **2005**, 117, 3-13.

Chapter 1

102. Santos, S. F.; Zanette, D.; Fischer, H.; Itri, R., A systematic study of bovine serum albumin (BSA) and sodium dodecyl sulfate (SDS) interactions by surface tension and small angle X-ray scattering. *Journal of Colloid and Interface Science* **2003**, *262*, 400-408.
103. Álvarez Gómez, J. M.; Pizones Ruiz Henestrosa, V.; Carrera Sánchez, C.; Rodríguez Patino, J. M., Role of static and dynamic characteristics of diglycerol esters and β -lactoglobulin mixed films foaming. 1. Dynamic phenomena at the air-water interface. *Food Hydrocolloids* **2008**, *22*, 1105-1116.
104. Zadmova, N. M.; Yampolskaya, G. P.; Filatova, L. Y., Interaction of bovine serum albumin with nonionic surfactant Tween 80 in aqueous solutions: Complexation and association. *Colloid Journal* **2006**, *68*, 162-172.
105. Dan, A.; Gochev, G.; Miller, R., Tensiometry and dilational rheology of mixed β -lactoglobulin/ionic surfactant adsorption layers at water/air and water/hexane interfaces. *Journal of Colloid and Interface Science* **2015**, *449*, 383-391.
106. Joshi, O.; McGuire, J., Adsorption behavior of lysozyme and Tween 80 at hydrophilic and hydrophobic silica-water interfaces. *Applied Biochemistry and Biotechnology* **2009**, *152*, 235-248.
107. Fernández, M. C.; Sánchez, C. C.; Niño, R. R.; Rodríguez Patino, J. M., Penetration of β -lactoglobulin into monoglyceride monolayers. Dynamics, interactions, and topography of mixed films. *The Journal of Physical Chemistry B* **2006**, *110*, 24212-24221.
108. Álvarez Gómez, J. M.; Ruíz Henestrosa, V. P.; Sánchez, C. C.; Rodríguez Patino, J. M., Role of static and dynamic characteristics of diglycerol esters and β -lactoglobulin mixed films on foaming, 2: Adsorption and foaming. *Food Hydrocolloids* **2008**, *22*, 1298-1309.
109. Fernández, M. C.; Carrera Sánchez, C.; Rodríguez Niño, M. R.; Rodríguez Patino, J. M., Monoglycerides and β -lactoglobulin adsorbed films at the air-water interface. Structure, microscopic imaging, and shear characteristics. *Langmuir* **2007**, *23*, 7178-7188.
110. Blomqvist, B. R.; Ridout, M. J.; Mackie, A. R.; Warnheim, T.; Claesson, P. M.; Wilde, P., Disruption of viscoelastic β -lactoglobulin surface layers at the air-water interface by nonionic polymeric surfactants. *Langmuir* **2004**, *20*, 10150-10158.
111. Krägel, J.; Wüstneck, R.; Husband, F.; Wilde, P. J.; Makievski, A. V.; Grigoriev, D. O.; Li, J. B., Properties of mixed protein/surfactant adsorption layers. *Colloids and Surfaces B: Biointerfaces* **1999**, *12*, 399-407.
112. Coke, M.; Wilde, P. J.; Russell, E. J.; Clark, D. C., The influence of surface composition and molecular diffusion on the stability of foams formed from protein/surfactant mixtures. *Journal of Colloid and Interface Science* **1990**, *138*, 489-504.
113. Krägel, J.; O'Neill, M.; Makievski, A. V.; Michel, M.; Leser, M. E.; Miller, R., Dynamics of mixed protein-surfactant layers adsorbed at the water/air and water/oil interface. *Colloids and Surfaces B: Biointerfaces* **2003**, *31*, 107-114.
114. Marin, I.; Relkin, P., Interaction properties of β -lactoglobulin and benzaldehyde and effect on foaming properties of β -lactoglobulin. *Food Chemistry* **2000**, *71*, 401-406.
115. Mackie, A. R.; Gunning, A. P.; Wilde, P. J.; Morris, V. J., Orogenic displacement of protein from the oil/water interface. *Langmuir* **2000**, *16*, 2242-2247.
116. Sarker, D. K.; Wilde, P. J.; Clark, D. C., Competitive adsorption of l- α -lysophosphatidylcholine/ β -lactoglobulin mixtures at the interfaces of foams and foam lamellae. *Colloids and Surfaces B: Biointerfaces* **1995**, *3*, 349-356.
117. Mackie, A. R.; Gunning, A. P.; Wilde, P. J.; Morris, V. J., Orogenic displacement of protein from the air/water interface by competitive adsorption. *Journal of Colloid and Interface Science* **1999**, *210*, 157-166.
118. Wei, X.; Chang, Z.; Liu, H., Influence of sodium dodecyl sulfate on the characteristics of bovine serum albumin solutions and foams. *Journal of Surfactants and Detergents* **2003**, *6*, 107-112.
119. Mikhailovskaya, A. A.; Noskov, B. A.; Lin, S. Y.; Loglio, G.; Miller, R., Formation of protein/surfactant adsorption layer at the air/water interface as studied by dilational surface rheology. *The Journal of Physical Chemistry B* **2011**, *115*, 9971-9979.
120. Alahverdijeva, V. S.; Khristov, K.; Exerova, D.; Miller, R., Correlation between adsorption isotherm, thin liquid films and foam properties of protein/surfactant mixtures: Lysozyme/ C_{10} DMPO and lysozyme/SDS. *Colloids and Surfaces A: Physicochemical and Engineering Aspects* **2008**, *323*, 132-138.
121. Mikhailovskaya, A. A.; Lin, S.-Y.; Loglio, G.; Miller, R.; Noskov, B. A., Effect of a cationic surfactant on protein unfolding at the air-solution interface. *Mendeleev Communications* **2011**, *21*, 341-343.

122. Sun, Y.; Filho, P.; Bozelli Jr, J.; Carvalho, J.; Schreier, S.; Oliveira, C. L. P., Unfolding and folding pathway of lysozyme induced by sodium dodecyl sulfate. *Soft Matter* **2015**, Advance Article, DOI: 10.1039/C5SM01231G.
123. Pradines, V.; Krägel, J.; Fainerman, V.; Miller, R., Interfacial properties of mixed β -lactoglobulin–SDS layers at the water/air and water/oil interface. *The Journal of Physical Chemistry B* **2009**, *113*, 745-751.
124. Rouimi, S.; Schorsch, C.; Valentini, C.; Vaslin, S., Foam stability and interfacial properties of milk protein-surfactant systems. *Food Hydrocolloids* **2005**, *19*, 467-478.
125. Rodríguez Patino, J. M.; Fernández, M. C.; Rodríguez Niño, M. R.; Sánchez, C. C., Self-assembly of monoglycerides in β -lactoglobulin adsorbed films at the air–water interface. Structural, topographical, and rheological consequences. *Biomacromolecules* **2006**, *7*, 2661-2670.
126. van Kempen, S. E. H. J.; Maas, K.; Schols, H. A.; van der Linden, E.; Sagis, L. M. C., Interfacial properties of air/water interfaces stabilized by oligofructose palmitic acid esters in the presence of whey protein isolate. *Food Hydrocolloids* **2013**, *32*, 162-171.
127. Loch, J. I.; Bonarek, P.; Polit, A.; Świątek, S.; Dziedzicka-Wasylewska, M.; Lewiński, K., The differences in binding 12-carbon aliphatic ligands by bovine β -lactoglobulin isoform A and B studied by isothermal titration calorimetry and X-ray crystallography. *Journal of Molecular Recognition* **2013**, *26*, 357-367.
128. Morén, A. K.; Khan, A., Phase behavior and phase structure of protein-surfactant-water systems. *Journal of Colloid and Interface Science* **1999**, *218*, 397-403.
129. Khan, J. M.; Chaturvedi, S. K.; Rahman, S. K.; Ishtikhar, M.; Qadeer, A.; Ahmad, E.; Khan, R. H., Protonation favors aggregation of lysozyme with SDS. *Soft Matter* **2014**, *10*, 2591-2599.
130. Lu, R.-C.; Cao, A.-N.; Lai, L.-H.; Xiao, J.-X., Interactions of β -lactoglobulin with sodium decylsulfonate, decyltriethylammonium bromide, and their mixtures. *Journal of Colloid and Interface Science* **2006**, *299*, 617-625.
131. Creamer, L. K., Effect of sodium dodecyl-sulphate and palmitic acid on the equilibrium unfolding of bovine β -lactoglobulin. *Biochemistry* **1995**, *34*, 7170-7176.
132. Schmitt, C.; Bovay, C.; Rouvet, M., Bulk self-aggregation drives foam stabilization properties of whey protein microgels. *Food Hydrocolloids* **2014**, *42*, 139-148.
133. Maldonado-Valderrama, J.; Patino, J. M. R., Interfacial rheology of protein-surfactant mixtures. *Current Opinion in Colloid and Interface Science* **2010**, *15*, 271-282.
134. Gunning, P. A.; Mackie, A. R.; Gunning, A. P.; Wilde, P. J.; Woodward, N. C.; Morris, V. J., The effect of surfactant type on protein displacement from the air-water interface. *Food Hydrocolloids* **2004**, *18*, 509-515.
135. Mackie, A. R.; Gunning, A. P.; Ridout, M. J.; Wilde, P. J.; Morris, V. J., Orogenic displacement in mixed β -lactoglobulin/ β -casein films at the air/water interface. *Langmuir* **2001**, *17*, 6593-6598.
136. Kotsmar, C.; Pradines, V.; Alahverdijeva, V. S.; Aksenenko, E. V.; Fainerman, V. B.; Kovalchuk, V. I.; Krägel, J.; Leser, M. E.; Noskov, B. A.; Miller, R., Thermodynamics, adsorption kinetics and rheology of mixed protein-surfactant interfacial layers. *Advances in Colloid and Interface Science* **2009**, *150*, 41-54.
137. Latnikova, A. V.; Lin, S. Y.; Noskov, B. A., Dynamic surface properties of the solutions of β -casein-surfactant complexes. **2009**, *71*, 208-218.
138. Gerasimova, A. T.; Angarska, J. K.; Tachev, K. D.; Yampolskaya, G. P., Drainage and critical thickness of foam films from mixed solutions of bovine serum albumin and n-dodecyl- β -D-maltoside. *Colloids and Surfaces A: Physicochemical and Engineering Aspects* **2013**, *438*, 4-12.
139. Kharlov, A.; Filatova, L.; Zadymova, N.; Yampol'skaya, G., Black foam films stabilized with the mixtures of bovine serum albumin and nonionic surfactant Tween 80. *Colloid Journal* **2007**, *69*, 117-123.
140. Bos, M. A.; van Vliet, T., Interfacial rheological properties of adsorbed protein layers and surfactants: a review. *Advances in Colloid and Interface Science* **2001**, *91*, 437-471.
141. Wilde, P.; Mackie, A.; Husband, F.; Gunning, P.; Morris, V., Proteins and emulsifiers at liquid interfaces. *Advances in Colloid and Interface Science* **2004**, *108-109*, 63-71.

2. Stability properties of surfactant free thin films at different ionic strengths: Measurements and modelling

Abstract

Foam lamellae are the smallest structural elements in foam. Such lamellae can experimentally be studied by analysis of thin liquid films in glass cells. These thin liquid films usually have to be stabilized against rupture by surface active substances, like proteins or low molecular weight surfactants. However, horizontal thin liquid films of pure water with a radius of 100 μm also show remarkable stability when created in closed Sheludko cells. To understand thin film stability of surfactant free films, the drainage behaviour and rupture times of films of water and NaCl solutions were determined. The drainage was modelled with an extended DLVO model, which combines DLVO and hydrophobic contributions. Good correspondence between experiment and theory is observed, when hydrophobic interactions are included, with fitted values for surface potential ($\psi_{0, \text{water}}$) of -60 ± 5 mV, hydrophobic strength ($B_{\text{hb, water}}$) of 0.22 ± 0.02 mJ m⁻² and a range of the hydrophobic interaction ($\lambda_{\text{hb, water}}$) of 15 ± 1 nm in thin liquid films. In addition, Vrij's rupture criterion was successfully applied to model the stability regions and rupture times of the films. The films of pure water are stable over long time scales (hours) and drain to final thickness > 40 nm if the concentration of electrolytes is low (resistivity 18.2 MQ). With increasing amounts of ions (NaCl) the thin films drain to < 40 nm thickness and the rupture stability of the films is reduced from hours to seconds.

Based on: Lech, F. J.; Wierenga, P. A.; Gruppen, H.; Meinders, M. B. J., Stability properties of surfactant-free thin films at different ionic strengths: Measurements and modeling. Langmuir 2015, 31, 2777-2782.

Introduction

An important aspect in the stability of foams is the life time of the thin liquid films that separate the gas bubbles in the foam¹. Usually, surface active materials, like proteins and low-molecular weight surfactants (LMW), are used to stabilize the films. The stability of LMW surfactant stabilized films has been studied extensively and was recently reviewed². Thin films of LMW can quantitatively be described by the DLVO³. In addition, Vrij developed a criterion to describe how the growth of small surface perturbations leads to spontaneous rupture of the film⁴. This criterion was used by others to determine the critical thickness in foam films⁵. Because it is impossible to make foam of pure water, it is expected that thin liquid water films are unstable. Still, horizontal thin liquid films of pure water and dilute NaCl solutions in closed Sheludko cells have been described by several authors⁶⁻⁸. The films described are usually very unstable since 90 % of the films ruptured immediately after creation⁶. However, stable, free standing (vertical) thin water films in small glass capillaries are also observed. The stability of the films is ascribed to ionizing x-ray photons, thereby inducing some charge between the two interfaces⁸. Wang and Yoon showed the possibility to create horizontal thin films of dilute NaCl solutions that were stable for minutes⁷. They argue that the stability of the films originates from equilibrium between hydrophobic and electrostatic forces that is mediated by the electrolytes in solution.

The electrostatic forces in the thin films are considered the result of a surface wall potential of the air-water interface. This surface wall potential was for instance shown using experiments where the electrophoretic mobility of air bubbles in an electric field was measured⁹. The origin, polarity and magnitude of the charge, however, is still under heavy debate. Several studies proposed the structuring of water layers close the hydrophobic interface as a source of the charge^{10, 11}. This structuring, however, would only be possible on short length scales up to 20 nm¹². The ordering of water over 40 nm is far shorter than the equilibrium thickness (120 nm) of the films reported⁷. Hence, it cannot explain the stability of the films by itself. For the stabilization of the films by structured water, the ordered layers should overlap to create repulsion. Other studies suggest that the surface charge of water could be due to the preferred adsorption of hydroxide ions to the interface¹³⁻¹⁵. Typical values for this surface potential, obtained by different experimental techniques (i.e. Volta potential difference measurements or calomel electrodes) and simulations, were recently summarized, and showed values ranging from -1.1 V to +0.5 V¹⁶. Next to the surface charge of the water interfaces, the repulsive hydration interaction has been suggested to attribute to the stabilization of a thin film of clean water.^{17, 18} Whether or not hydrophobic forces play a role in the stability of thin liquid films is still under debate^{19, 20}. The aim of this study is to gain a generic understanding of the drainage and stability of surfactant free thin liquid films. To achieve this, drainage behaviour and rupture times of surfactant free thin films, created in Sheludko cells, were described with a model using extended DLVO (including hydrophobic interactions) and the stability criterion of thin films⁴.

Experimental Section

Materials

Ultra-pure water (Millipore, EMD Millipore Corp., Billerica, MA, USA) with a surface tension of $72.6 \pm 0.3 \text{ mN m}^{-1}$ at 20°C stable over 1 hour, a resistivity of $18.6 \text{ M}\Omega \text{ cm}$ and residual total organic carbon of 3 ppb was used as is to make the films and the NaCl solutions. NaCl was purchased from Sigma Aldrich (Zwijndrecht, The Netherlands) and roasted at 700°C for three days to eliminate possible organic contaminants. A stock solution of 0.1 M NaCl was prepared and diluted to make solutions for the thin film experiments. The solutions were prepared on the day of the experiment and kept at the same temperature (20°C) as the experimental set up before making the thin film. All glassware was soaked in dilute (0.1 M) NaOH solution, thoroughly rinsed with ultra-pure water and dried in an oven at 60°C before use.

The total ionic strength of water and NaCl solutions is given by equation 1

$$(1) \quad I = \frac{1}{2} \sum_i \rho_{i\infty} z_i^2$$

where I is the sum of all ions i in the solution, $\rho_{i\infty}$ is the molar concentration of the ion in bulk at infinite distance from the interface and z is the valence of the ions. Note that this includes the OH^- and H^+ ions determining the pH of the water films, which was measured to be pH 5.6, for all experiments. The total ionic strength ($I_{\text{NaCl}} + I_{\text{pH } 5.6}$) of a 0.700 mM NaCl solution is 0.703 mM .

Methods

Thin liquid films (radius = $100 \mu\text{m}$) were made in a modified Sheludko cell as described elsewhere¹. A schematic drawing, including relevant dimensions of the setup is depicted in figure 2.1. The Sheludko cell is encased in glass, closed with a glass cover. The casing has a reservoir of water at the bottom to ensure a relative humidity of 100 % in the cell during the experiments.

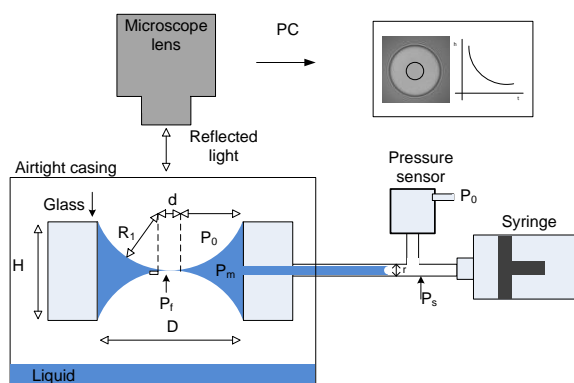


Figure 2.1: Schematic representation of a Sheludko cell with a thin liquid film. $D = H = 2.5 \text{ mm}$ and $d = 0.2 \text{ mm}$.

Chapter 2

The thickness of the thin films was determined by image analysis obtained by micro-interferometry using a microscope (Axio plan 01, Zeiss, Jena, Germany), in reflected light mode, equipped with a five mega pixel CCD camera (Mightex Systems, Pleasanton, CA, USA). Images of the thin films, recorded with the CCD camera, were processed by a software script (developed at the Laboratory of Food Chemistry) for Matlab (Software version 2013b, MathWorks, Natick, MA, USA). It calculated the average intensity of light in a defined area (at the centre) of the thin film. The area is typically $1963 \mu\text{m}^2$, which is ~6 % of total area of the thin film. The thickness h (nm) was calculated according to equation 2

$$(2) \quad h = \frac{\lambda}{2\pi n} [l\pi \pm \arcsin\sqrt{\Delta}]$$

where λ is the wavelength of the light (546 nm), n is the refractive index of water, l is the order of interference and Δ as $(I - I_{\min}) / (I_{\max} - I_{\min})$ where I is the average of the light intensity at each time point, I_{\min} , the minimum intensity (which is measured in the Sheludko cell without a water film present) and I_{\max} as the maximum intensity. The film thickness was measured from the moment it reaches a radius of $100 \mu\text{m}$ up to 1 hour of lifetime. If a film did not break within 1 hour, it was considered stable. In this case, the life time will be given as 1 hour. If the thin films ruptured during this time, at least 20 repetitions were used to calculate the average and standard deviation of the rupture time and thickness at which rupture occurred. The rupture time is the time from reaching a $200 \mu\text{m}$ wide film until the film breaks. In case of stable films, solutions were measured 4 times, in case of rupturing films; the experiment was repeated at least 20 times.

The whole setup, thin film cell, pure water and salt solution were equilibrated to room temperature (20°C) on the microscope table for at least 1 hour prior to the measurement. Liquid was drawn into the capillary by a syringe ($500 \mu\text{L}$, Hamilton, Reno, NV, USA) and left to equilibrate for 10 minutes before a thin film was made by drawing more solution into the capillary.

Modelling and theoretical background

Surface forces

When two bubbles come into contact, the thin liquid film between the bubbles will drain due to the capillary pressure, caused by the difference in curvature of the thin film and the adjacent meniscus (or Plateau border in foam). When the film thickness becomes smaller than about 100 nm , attractive and repulsive interactions between the interfaces of the film become important and determine the stability of the thin liquid film. Attractive interactions, enhancing film thinning and destabilizing the film, include long range dispersion forces summarized as van der Waals (vdW) forces. Repulsive interactions, acting against film thinning and thereby stabilizing the film, include electrostatic interactions (ES) between two similarly charged surfaces and steric interactions. The vdW and ES interactions are described quantitatively by the DLVO theory. Besides these DLVO forces, other interactions are recognized that might play a role in film stability. The interactions include steric repulsion (excluded volume), hydration, repulsive and attractive hydrophobic forces as well as oscillatory solvation forces^{2, 11, 18}. The sum of

these surface forces determine the disjoining pressure $\Pi(h)$, which depends on the film thickness.

The van der Waals contribution is calculated from equation 3

$$(3) \quad \Pi_{vw} = -\frac{A_H}{6\pi h^3}$$

where A_H is the compound Hamaker constant of a water film in air $A_H = 4 \cdot 10^{-20} \text{ J}^{18, 21}$. The contribution of the electrostatic interaction to the disjoining pressure is approximated by equation 4¹⁸

$$(4) \quad \Pi_{el} = 64k_B T \rho_{\infty} \gamma^2 e^{-\kappa h}$$

with

$$(5) \quad \gamma = \tanh\left(\frac{e\psi_0}{4k_B T}\right)$$

and

$$(6) \quad \kappa = \frac{\sqrt{\sum_i z_i^2 \rho_{i\infty} e}}{\epsilon_0 \epsilon_r k_B T}$$

κ is the inverse of the Debye screening length (m^{-1}) λ_D . Furthermore, $k_B = 1.38 \cdot 10^{-23} \text{ J K}^{-1}$ is the Boltzmann constant, T is the temperature (K), ρ_{∞} is the number density of ions in the bulk having valence z_i , $\rho_{\infty} = \sum \rho_{\infty} / n_i$, with n_i being the number of ions with same valence (m^{-3}), $e = 1.6 \cdot 10^{-19} \text{ C}$ is the electron charge, ψ_0 is the surface potential (mV) of the air/water interface, $\epsilon_0 = 8.54 \cdot 10^{-12} \text{ F m}^{-1}$ is the electric permittivity of vacuum and $\epsilon_r = 80$ is the relative dielectric constant of water.

Hydrophobic molecules can attract each other stronger than is expected from only the vdW attraction. Although not completely understood, this hydrophobic interaction is ascribed to the (de)wetting and solvation properties of water. The air can be considered hydrophobic.¹⁷ The attractive hydrophobic contribution (Π_{hb}) to the disjoining pressure can be approximated by equation 7²²

$$(7) \quad \Pi_{hb} = -\frac{B_{hb}}{\lambda_{hb}} \left(\coth^2\left(\frac{h}{2\lambda_{hb}}\right) - 1 \right)$$

where B_{hb} is a constant (mJ m^{-2}) and λ_{hb} is the decay length of the hydrophobic interaction (nm). The theoretical individual attractive and repulsive contributions for an air water interface as well as the resulting disjoining pressure as function of film thickness are calculated (figure 2.2).

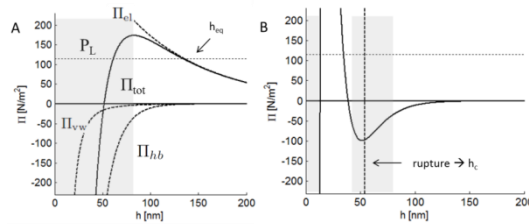


Figure 2.2: A) Calculated total disjoining pressure (Π) as function of the film thickness h as well as the individual contributions of the attractive van der Waals Π_{vw} and hydrophobic Π_{hb} as well as repulsive electrostatic interaction Π_{el} (dashed lines) of a water film. Ionic strength $I = 0.01 \text{ mM}$, $\text{pH} = 5.6$. The short dotted line corresponds to the capillary pressure $P_L = 2\sigma/R_m \sim 115 \text{ N}$. The shaded area indicates the unstable region according to the stability criterion of Vrij. Model parameters: $\psi_0 = -60 \text{ mV}$, $B_{hb} = 0.22 \text{ mJ m}^{-2}$, $\lambda_{hb} = 15 \text{ nm}$. B) Disjoining pressure curve for $I = 1 \text{ mM}$. The critical thickness at which the film ruptures is indicated by h_c .

Chapter 2

Film drainage

The drainage of the film is modelled by considering the flow between two circular plane-parallel plates^{23, 24}. The change of the film thickness h (m) with time t (s) was described by equation 8

$$(8) \quad \frac{dh}{dt} = -\frac{2c_f h^3}{3\mu R_f^2} \Delta P$$

where c_f is a factor that accounts for the interaction of the fluid with the interface. For an immobile interface, as we will consider here, $c_f = 1$. Furthermore, $\mu = 10^{-3} \text{ kg m}^{-1} \text{ s}^{-1}$ is the viscosity of the water phase, R_f is the radius (m) of the film (in our experimental set-up $R_f = 100 \text{ }\mu\text{m}$), and

$$(9) \quad \Delta P = \frac{2\sigma}{R_m} - \Pi$$

is the driving capillary pressure, where σ is the surface tension of the water-air interface (in the calculation we used $\sigma = 72 \text{ mN m}^{-1}$), $1/R_m$ is the (mean) curvature of the meniscus (m^{-1}) and Π is the total disjoining pressure ($\Pi = \Pi_{\text{vW}} + \Pi_{\text{el}} + \Pi_{\text{hb}}$) (N m^{-2}). $R_m \sim 1.25 \text{ mm}$, assuming complete wetting of the inner wall of the Sheludko cell (see figure 2.1).

Starting from an initial thick film with thickness h_0 , the film will drain. Depending on the precise shape of $\Pi(h)$, the film can drain to a stable equilibrium thickness where the disjoining pressure equals the capillary pressure (figure 2.2 B). If the disjoining pressure is smaller than the capillary pressure the thin film can rupture spontaneously.

Film rupture

Film rupture of surfactant stabilized films has successfully been described by the theory developed by Sheludko and Vrij^{4, 25}. They identified instability regions in the disjoining pressure over thickness curve. In these regions of instability, small spontaneous surface perturbations grow in time until both interfaces touch each other and the film ruptures. The unstable regions are given by the Vrij criterion (10)

$$(10) \quad \frac{\partial \Pi}{\partial h} < -\frac{\pi\sigma}{R_f^2}$$

where Π is the disjoining pressure, h is the thickness of the film, σ is the surface tension and R_f the radius of the thin film. In these regions, fluctuations in the film with a certain wavelength can grow exponentially in time, while in other regions all fluctuations will disappear. The fluctuation that grows fastest has a characteristic time given by equation 11

$$(11) \quad \tau_m = \frac{24\sigma\mu}{h_x^3} \left(\frac{\partial \Pi}{\partial h} \right)_{h_x}^{-1}$$

where h_x is the thickness of the film at which the fluctuation occurs. The time that both interfaces touch and the film will rupture corresponds to the rupture time t_b . Considering thermal fluctuations, Vrij derived the following estimation (equation 12).

$$(12) \quad \sqrt{\frac{2t_b}{\tau_m}} h_x^2 = \frac{k_B T}{2\sigma\sqrt{\pi}} e^{2t_b/\tau_m}$$

Equation 12 gives an estimation of the lower bound of the rupture time of a stationary film. When the film is draining, t_b has to be compared with the time the film is in the unstable region. This has been done using the graphical procedure described by Vrij, where the breaking time t_b and drainage time t are plotted in one figure. The life time of

the film then equals the minimum of $t+t_b^4$. These above described equations (3-12) were combined in the model, which is used to determine the equilibrium thickness of thin films as well as their stability.

Results and discussion

Thin films made of pure water ($I = 2 \cdot 10^{-6} \text{ M}$) are stable and drain to an equilibrium thickness of $126 \pm 5 \text{ nm}$. Micrographs show the difference in intensity as a function of the concentration (figure 2.3).

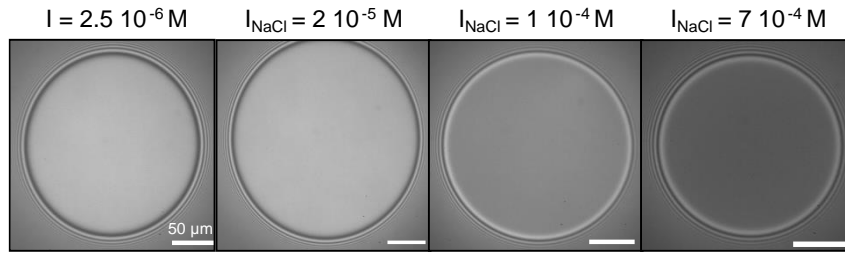


Figure 2.3: Typical micrographs of a thin water film ($I = 2.5 \cdot 10^{-6} \text{ M}$) and thin films of NaCl solution of different concentrations. Micrographs were obtained after 15 minutes. The scale bars in the bottom are $50 \mu\text{m}$.

In the presence of low concentrations of NaCl ($< 0.01 \text{ mM}$), the equilibrium thickness increases to $130 \text{ nm} \pm 1 \text{ nm}$. A further increase of the NaCl concentration to 0.7 mM results in a reduction of the equilibrium thickness to $39 \pm 7 \text{ nm}$ (figure 2.4 A). All films with NaCl concentrations $\leq 0.7 \text{ mM}$ were stable. Thin films with NaCl concentrations larger than 0.7 mM ruptured within a 1 hour period.

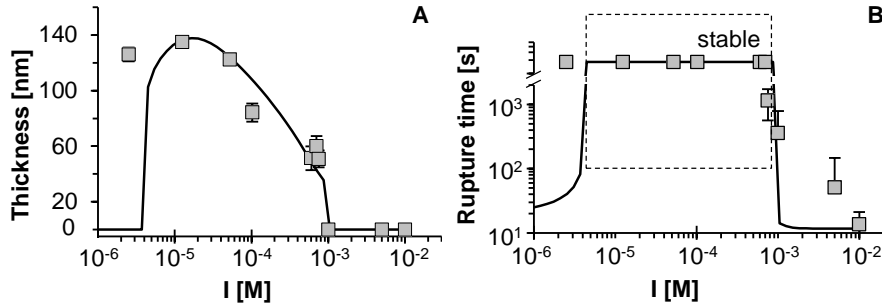


Figure 2.4: Experimental (■) and predicted values (solid lines) of A) equilibrium thickness and B) rupture times of thin liquid films of water ($I_{\text{ph5,6}} = 2 \cdot 10^{-6} \text{ M}$) and NaCl solutions as a function of the total ionic strength ($I = I_{\text{NaCl}} + I_{\text{ph5,6}}$). The predicted values were obtained by using the extended DLVO model that yields stability of thin films and equilibrium thickness of the films. Stable films are plotted as having rupture times of 1 hour, the stable region is indicated by the dashed line.

The rupture time decreases with increasing NaCl concentration from $1,150 \pm 588$ seconds at 0.75 M to 14 ± 1 seconds at 10 mM (figure 2.4 B). It has to be noted that also for the predicted values, rupture times larger than 1h are plotted as 1 hour. Comparable values

for film thickness of pure water films at similar pH values and NaCl concentrations have been reported earlier⁷. An exception being the reported life time < 750 seconds at 10^{-6} M NaCl, while in our study a stability > 1 h was reported for 10^{-6} - $7 \cdot 10^{-4}$ M NaCl solutions. The reasons for these differences are not completely clear. They might be due to differences in the experimental setup (different R_m and R_f), smaller Sheludko cell radius (1 mm instead of 1.25 mm), purity and/or pH of the water. Theoretical values of drainage curves ($h(t)$), rupture times (t_b), and equilibrium film thickness ($h(\infty)$), were calculated using the extended DLVO theory including hydrophobic interactions. In addition, the film rupture was calculated according to the theory of Vrij. Good correspondence is obtained between experimental and predicted drainage curves (figure 2.5) as well as values of equilibrium film thickness and film stability (figure 2.4 A and B).

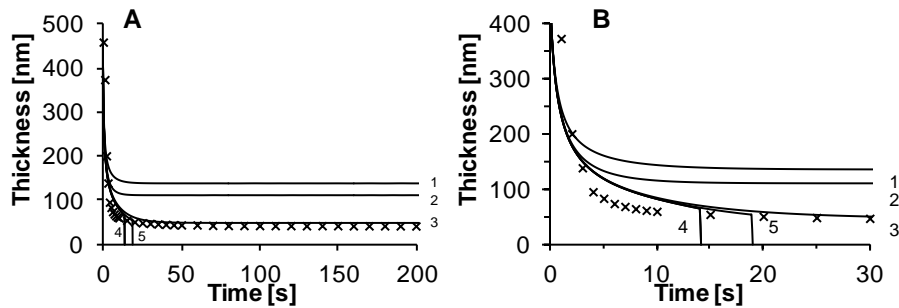


Figure 2.5: A) Predicted drainage curves of NaCl solutions of 0.01, 0.1, 0.7, 1, and 10 mM (lines 1-5 respectively). The predicted drainage curves were obtained by using the extended DLVO model, which is introduced in the modelling section that yields drainage curves of thin films. A typical experimental drainage curve of NaCl solution (0.7 mM) is included (x). B) Shows the first 30 seconds of drainage. The numbering for the lines is the same as in the panel A.

For solutions with ionic strengths below $5 \cdot 10^{-6}$ M, the model predicts unstable films. This however, was not found experimentally for thin films of pure water ($I = 2.5 \cdot 10^{-6}$ M). Still, the model is in line with literature where unstable films at low ionic strength were reported. The reported concentrations for stable films are between an ionic strength of 10^{-6} M and 10^{-3} M⁷. The reason for the discrepancy between the model and our experimental observation is yet unexplained. However, the model is very sensitive at low ionic strength and small underestimations of the ionic strength of pure water due to for instance dissolved CO_2 might be enough to shift the point of pure water ($I = 2.5 \cdot 10^{-6}$ M) towards higher ionic strength. This could explain the observation of stable thin films of water. The estimated values of the surface potential ($\psi_0 = -60 \pm 5$ mV) as well as hydrophobic strength ($B_{hb} = 0.22 \pm 0.02$ mJ m⁻²) and range ($\lambda_{hb} = 15 \pm 1$ nm) are similar as suggested by earlier studies with typical values for the air water interface^{7, 22, 24}. Additional to the vdW interaction, an attractive interaction is needed to accurately describe the thin film behaviour in a Sheludko cell. This (hydrophobic) interaction is about 2 orders of magnitude larger than the vdW interaction. At ionic strengths below 10^{-5} M, the electrostatic repulsion is too low to oppose the attractive interactions. Consequently, the film is unstable, resulting in rupture. At ionic strength, between 10^{-5} M and 10^{-3} M the electrostatic repulsion is larger than the attractive vdW and hydrophobic interaction and

the film is stable. At ionic strength, $> 10^{-3}$ M, the Debye screening length is short enough so that a second minimum in the disjoining pressure isotherm occurs, corresponding to a second instable region where film can rupture (figure 2.2 B). Additionally, while keeping the same parameters, it was possible to predict the stability and thickness of thin films with $I_{\text{NaCl}} = 10^{-5}$ M as function of pH (figure 2.6), reported by Wang and Yoon with our model.

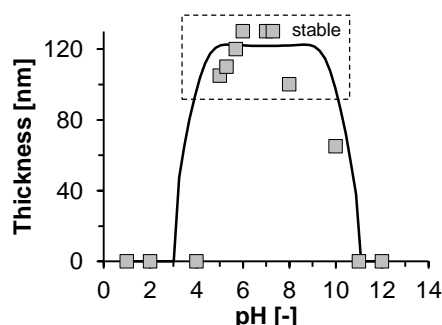


Figure 2.6: Predicted equilibrium film thickness of a water films as a function of pH with added NaCl $I_{\text{NaCl}} = 2 \cdot 10^{-5}$ M (solid line) using equations 8 and 10. Experimental data (■) from Wang and Yoon (2008)⁷ for a thin water film with $I_{\text{NaCl}} = 10^{-5}$ M. Model parameters were kept the same: $\psi_0 = -60$ mV, $B_{hb} = 0.22$ mJ m⁻², $\lambda_{hb} = 15$ nm, $R_f = 100$ μ m. $R_m = 1$ mm is equal to the radius of the Sheludko cell used by Wang and Yoon (2008)⁷.

This indicates the validity of the model and shows that the Vrij criterion can be used successfully to describe the stability (as expressed by rupture times) of surfactant free thin liquid films.

Conclusions

It was shown that surfactant free thin films are stable until a critical NaCl concentration (mM < 0.70 mM), which was confirmed by quantitative modelling. At higher NaCl concentrations, the surface charge is sufficiently screened, which ultimately leads to destabilization of the thin films. The combination of the extended DLVO model with the rupture criterion of Vrij, successfully describes the drainage and stability properties of surfactant free thin films. It has to be noted, that this special case of stability is unlikely to occur in any system containing surface active materials other than ions since in those cases, additional stabilization is caused by the layers of adsorbed material. The stabilizing forces of the absorbed layer exceed the (relatively) low electrostatic repulsion observed in pure water films.

References

1. Wierenga, P. A.; van Nor  l, L.; Basheva, E. S., Reconsidering the importance of interfacial properties in foam stability. *Colloids and Surfaces A: Physicochemical and Engineering Aspects* **2009**, *344*, 72-78.
2. Kralchevsky, P. A.; Danov, K. D.; Denkov, N. D., Chemical physics of colloid systems and interfaces. In *Handbook of Surface and Colloid Chemistry*, 3 ed.; Birdi, K. S., Ed. Elsevier: Boca Raton, FL, USA, **2008**; Vol. 7, pp 197-377.

Chapter 2

3. Tcholakova, S.; Denkov, N. D.; Lips, A., Comparison of solid particles, globular proteins and surfactants as emulsifiers. *Physical Chemistry Chemical Physics* **2008**, 10, 1608-1627.
4. Vrij, A., Possible mechanism for the spontaneous rupture of thin, free liquid films. *Discussions of the Faraday Society* **1966**, 42, 23-33.
5. Manev, E. D.; Angarska, J. K., Critical thickness of thin liquid films: comparison of theory and experiment. *Colloids and Surfaces A: Physicochemical and Engineering Aspects* **2005**, 263, 250-257.
6. Exerowa, D., Effect of adsorption, ionic strength and pH on potential of diffuse electric layer. *Kolloid Zeitschrift und Zeitschrift für Polymere* **1969**, 232, 703-710.
7. Wang, L.; Yoon, R.-H., Effect of pH and NaCl concentration on the stability of surfactant-free foam films. *Langmuir* **2008**, 25, 294-297.
8. Weon, B.; Je, J.; Hwu, Y.; Margaritondo, G., Stable freestanding thin films of pure water. *Applied Physics Letters* **2008**, 92, 104101-1 - 104101-2.
9. Graciaa, A.; Morel, G.; Saulner, P.; Lachaise, J.; Schechter, R. S., The ζ -potential of gas bubbles. *Journal of Colloid Interface Science* **1995**, 172, 131-136.
10. Besseling, N. A. M., Theory of hydration forces between surfaces. *Langmuir* **1997**, 13, 2113-2122.
11. Grasso, D.; Subramaniam, K.; Butkus, M.; Strevett, K.; Bergendahl, J., A review of non-DLVO interactions in environmental colloidal systems. *Reviews in Environmental Science and Bio/Technology* **2002**, 1, 17-38.
12. Forsman, J.; Jönsson, B.; Woodward, C. E.; Wennerström, H., Attractive Surface forces due to liquid density depression. *Journal of Physical Chemistry B* **1997**, 101, 4253-4259.
13. Creux, P.; Lachaise, J.; Graciaa, A.; Beattie, J. K.; Djerdjev, A. M., Strong specific hydroxide ion binding at the pristine oil/water and air/water interfaces. *Journal of Physical Chemistry B* **2009**, 113, 14146-14150.
14. Creux, P.; Lachaise, J.; Graciaa, A.; Beattie, J. K., Specific cation effects at the hydroxide-charged air/water interface. *Journal of Physical Chemistry B* **2007**, 111, 3753-3755.
15. Beattie, J. K.; Djerdjev, A. M., The pristine oil/water interface: Surfactant-free hydroxide-charged emulsions. *Angewandte Chemie International Edition* **2004**, 43, 3568-3571.
16. Parfenyuk, V. I., Surface potential at the gas-aqueous solution interface. **2002**, 64, 588-595.
17. van Oss, C. J.; Giese, R. F.; Docoslis, A., Hyperhydrophobicity of the water/air interface. *Journal of Dispersion Science and Technology* **2005**, 26, 585-590.
18. Israelachvili, J. N., *Intermolecular and surface forces*. 3 ed.; Academic Press (Elsevier): Santa Barbara, CA, USA, **2011**; p 674.
19. Stubenrauch, C.; Langevin, D.; Exerowa, D.; Manev, E.; Claesson, P. M.; Boinovich, L. B.; Klitzing, R. v., Comment on "hydrophobic forces in the foam films stabilized by sodium dodecyl sulfate: effect of electrolyte" and subsequent criticism. *Langmuir* **2007**, 23, 12457-12460.
20. Kralchevsky, P. A.; Danov, K. D.; Angarska, J. K., Reply to comment on "hydrophobic forces in the foam films stabilized by sodium dodecyl sulfate: Effect of electrolyte" and subsequent criticism. *Langmuir* **2008**, 24, 2953-2953.
21. Roth, C. M.; Neal, B. L.; Lenhoff, A. M., Van der Waals interactions involving proteins. *Biophysics Journal* **1996**, 70, 977-987.
22. Eriksson, J. C.; Ljunggren, S.; Claesson, P. M., A phenomenological theory of long-range hydrophobic attraction forces based on a square-gradient variational approach. *Journal of the Chemical Society, Faraday Transactions 2: Molecular and Chemical Physics* **1989**, 85, 163-176.
23. Bhakta, A.; Ruckenstein, E., Drainage and coalescence in standing foams. *Journal of Colloid Interface Science* **1997**, 191, 184-201.
24. Bhakta, A.; Ruckenstein, E., Decay of standing foams: drainage, coalescence and collapse. *Advances in Colloid and Interface Science* **1997**, 70, 1-124.
25. Sheludko, A. In *Certain peculiarities of foam lamellas, Parts I-III*, Proceedings of the Koninklijke Nederlandse Academie van Wetenschappen Series B: Physical Science, **1962**; pp 76-108.

3. Identification of critical concentrations determining foam ability and stability of β -lactoglobulin

Abstract

To understand the properties of protein stabilized foam, quantitative parameters, such as the concentration dependence of the foam properties need to be determined. Recently, a concept was proposed that predicts the emulsifying ability (i.e. the droplet size in emulsions) based on different parameters, including the protein concentration. The aim of the present study is to investigate whether a similar concept can be applied to describe the foam ability and stability of protein stabilized foams. To achieve this, the foam, thin film and molecular properties of β -lactoglobulin (BLG) were determined at different concentrations and different pH values (pH 3 - 7). At each pH, a certain critical concentration C_{FA} , could be identified above which the set foam volume was reached, while below that value the set volume was not reached. Furthermore, for all pH another critical concentration (C_{cr32}) at $C > C_{FA}$ was identified as the point where the bubble radius (measured at the end of foam formation) reached a minimal value. The foam ability increased with increasing pH (pH 3 - 7). The difference in foam ability as a function of pH was reflected in the adsorption rate (slope $\Pi/t^{0.5}$ curve) of BLG. The foam stability increased with increasing concentration at each pH value but even in the protein rich regime where $C > C_{cr32}$ different foam stabilities were observed, which were highest at pH 7.

Based on: Lech, F.J., Delahaije, R.J.B.M, Meinders, M.B.J., Gruppen, H., Wierenga, P.A. Submitted

Introduction

To understand of and control protein stabilised foams, quantitative parameters need to be identified that can be used to predict the foam properties based on parameters of the bulk solution. For this, the foam and interfacial properties of β -lactoglobulin (BLG) at different pH values and protein concentrations are determined. Furthermore, these properties are combined with pH dependent molecular properties, such as the protein structure, as well as with interfacial and thin film properties at different pH values to explain the different foam properties. In the case of proteins, the charge of the molecule is important for the protein structural stability, colloidal stability and techno-functional properties. For instance, the foam ability^{1, 2} and equilibrium surface tension³ of WPI were highest close to the iso-electric point of the main protein (BLG; pH 4.7, based on the amino acid sequence⁴). In addition, the quaternary structure, e.g. the association state of the protein, depends on the pH in solution. At pH 7, BLG occurs mainly as a dimer⁵. When the pH is lowered to the iso-electric point, most of the BLG is in the dimer state while some BLG octamers are formed⁵. Depending on the ionic strength at this pH, the octamers can form larger aggregates at low ionic strength (4.5 mM)⁶. Although some aggregates are formed, most of the BLG is still soluble (> 90 %⁷). The aggregation is reversible so that below the iso-electric point, mainly dimers are in solution⁶. If the pH is lowered further to pH < 3 the dimers separate into monomers⁸. Another pH dependent change is observed in the structural stability, indicated by the denaturation temperature (T_d), which increases with increasing pH from 72 °C at pH 7 to at 85 °C pH 3^{9, 10}.

In the case of protein stabilized emulsions, the droplet diameter after formation is used to characterize the emulsifying activity. The droplet size has been shown to strongly depend on the protein concentration^{11, 12}. Below a certain critical concentration, the so-called protein poor regime, the droplet diameter decreases with increasing protein concentration. Above this critical concentration, the protein rich regime, the droplet diameter is independent of the concentration. This has recently been extended by Delahaije *et al.*¹³ into a concept in which the droplet size in the emulsions is calculated based on the concentration, the relative exposed hydrophobicity of the protein, the volume fraction of oil, the adsorbed amount and a fitting parameter (equation 1).

$$(1) \quad d_{32} = \frac{F_S 6 \Phi_{oil} \Gamma_{mono,theory}}{(1 - \Phi_{oil}) Q_{HC}}$$

Although the conditions (e.g. shear) during emulsification are quite different from those during foam formation, it may be expected that a similar concept is also applicable to the description of foam. It is therefore hypothesised that for foams a critical concentration can be identified that separates a protein poor from a protein rich regime.

Materials and Methods

Materials

β -Lactoglobulin (BLG, L0130, Lot #SLBF4545V) was bought from Sigma Aldrich (Zwijndrecht, The Netherlands). The preparation had a protein content of 90 % as determined by DUMAS method (N*6.33 based on the amino acid sequence⁴), and was

Identification of critical concentrations determining foam ability and stability

composed of 80 % genetic variant A and 20 % genetic variant B (determined by electro spray ionization mass spectrometry, similar ionization for both variants was assumed; no other proteins were present). All chemicals used were of analytical grade. McIlvaine buffers (pH 3-8) were made by mixing appropriate amounts of 10 mM citric acid and 20 mM Na₂HPO₄. The water used to prepare the buffer solutions was filtered through MilliQ filtration unit (Millipore, EMD Millipore, Billerica, MA, USA) with resistivity of 18.2 MΩ cm, 3 ppb total organic carbon and a surface tension of 72.5 ±0.5 mN m⁻¹ at 20 °C.

Sample preparation

BLG powder was dissolved in the buffer solutions (pH 3 - 8) by trickling the powder onto the surface of the solution and letting it dissolve by itself. After the powder was dissolved (which was generally after 10 minutes), the solutions were stirred slowly for 10 minutes. The pH was subsequently checked and adjusted to the original pH using 1 M citric acid or 1 M Na₂HPO₄ if the value deviated by >0.1 pH unit from the desired value. Finally, the protein solutions were left to equilibrate for 1 hour 20 °C before they were used. The protein concentration of solutions used in the experiments was 0.5 mg mL⁻¹ (27.2 μM, checked by UV absorbance at 280 nm with an extinction coefficient of 15,164 L mol⁻¹ cm⁻¹ determined at pH 7.0) except when mentioned otherwise. The procedure for sample preparation was the same throughout the study except when it is mentioned otherwise.

Determination of foam properties

Foam was made by sparging N₂ through a metal frit in a closed foam cell of an automated foaming device (Foamscan, Teclis IT-Concept, Longessaigne, France) as described elsewhere¹⁴. The foaming cylinder had a diameter of 60 mm, gas flow rate was set to 400 cm³ min⁻¹, the volume of the solution was 60 mL and the maximum foam volume was 400 cm³ in each experiment. The temperature of the foam cylinder was set to 24 °C and controlled using a water bath. Samples were placed in the foam tube by an automatic dosing device (Teclis IT-Concept) and were equilibrated for 15 minutes prior to generating the foam. The relative foam ability (FA) of the BLG solutions was determined by relating the foam volume obtained after 60 seconds $V_{i,60s}$ (cm³) for each sample to the maximum obtainable foam volume after 60 seconds $V_{max, 60s}$ (cm³) (equation 2)

$$(2) \quad FA = \frac{V_{i,60s}}{V_{max,60s}}$$

with the set parameters of the FoamScan, $V_{max,60s} = 348$ cm³, which was obtained using a 10 % SDS solution. The Sauter radius (r_{32} , (mm)) of the bubbles and the relative bubble radius distributions were determined by image analysis from pictures taken at the end of the sparging. The pictures were analysed using a custom Matlab (Version 13b for Windows 7 OS, MathWorks, Natick, MA, USA) script. The script used the open DIPlib and DIPimage image analysis package for Matlab (version 2.51, developed at the Quantitative Imaging group, Delft University of Technology, Delft, The Netherlands). The grey values of the images were stretched by assigning the lowest intensity value of a pixel in the picture to 0 and the highest value to 255. Then, a background picture (Gaussian blurred image with a 25 pixel radius) was subtracted from the image to enhance the contrast. The threshold between black and white for the analysis of images with the bubbles were

Chapter 3

automatically applied using the OTSU algorithm (part of the DIPlib image analysis package) and afterwards the thresholded image was segmented to extract the bubble size distribution. A metal ball with known diameter was used to calibrate the image analysis software. To determine the foam stability, the foam of BLG of 0.5 mg mL⁻¹ (pH 3 - 8) and 0.25, 5, 10 and 20 mg mL⁻¹ at pH 3, 5 and 7 were allowed to collapse while it was monitored by a camera and analysed by image analysis. The foam stability was characterized using the half-life time $t_{1/2}$ of the foam volume, which is the time at which 50 % of the initial foam volume has collapsed.

The FA as a function of the concentration was fitted with a least square fitting of a fitting parameter a (equation 3)

$$(3) \quad FA(C)_{fit} = 1 - \frac{1}{aC}$$

where FA is the foam ability (-), C is the concentration (mg mL⁻¹) and a is a fitting parameter (mL mg⁻¹). The r_{32} was fitted with equation 4 adapted from Delhaije *et al.*¹³

$$(4) \quad r_{32}(C)_{fit} = \frac{1}{bC}$$

where r_{32} is the Sauter mean bubble radius (mm), b is a constant (m² g⁻¹) and C is the protein concentration (mg mL⁻¹). The R² obtained was used to indicate how well the model fits the data. For a better comparison in figure 3.3 and 3.10, the FA and r_{32} , are both normalized using equations 5 and 6

$$(5) \quad FA_{norm} = \frac{FA_i - FA_{min}}{FA_{max} - FA_{min}}$$

where FA_{norm} is the normalized FA, FA_i is the measured value and FA_{min} and FA_{max} are the minimum and maximum measured values under that condition.

$$(6) \quad r_{32,norm} = \frac{r_{32,i} - r_{32,min}}{r_{32,max} - r_{32,min}}$$

where $r_{32,norm}$ is the normalized r_{32} , $r_{32,i}$ is the measured value and $r_{32,min}$ and $r_{32,max}$ are the minimum and maximum measured values under that condition.

Reported values of $t_{1/2}$, FA and r_{32} are averages of at least five individual foam experiments.

Determination of interfacial properties

Interfacial tension measurements were performed using an automated drop tensiometer (ADT) (Tracker, Teclis IT-Concept, Longessaigne, France) at 20 °C as described elsewhere¹⁴. A bubble of 5 µL of air was formed by a computer controlled syringe on the tip of a curved needle in solutions containing 0.5 mg mL⁻¹ BLG at different pH values. The interfacial tension was calculated by analysis of the shape of the air bubble performed by software provided with the ADT. Adsorption of proteins results in a decrease of the surface tension. The surface pressure was calculated from the surface tension of the buffer (at the respective pH) and the surface tension of each BLG solution (equation 7).

$$(7) \quad \Pi = \gamma_{buffer} - \gamma_{BLG \text{ solution}}$$

where Π is the surface pressure (mN m⁻¹), γ_{buffer} is the surface tension of buffer (mN m⁻¹) and $\gamma_{BLG \text{ solution}}$ is the surface tension of the BLG solution (mN m⁻¹). To describe the adsorption rate of BLG, the slope of the linear part of the $\Pi(t^{0.5})$ curve was used. The complex dilatational elastic modulus (E_d) was measured by subjecting a bubble to a 5 % relative change in interfacial area ($dA/A = 5 \%$) with a frequency of 0.1 Hz for a cycle of

Identification of critical concentrations determining foam ability and stability

50 seconds followed by a rest period of 50 seconds over a period of 1 hour. $E_d = E' + iE''$ is the complex viscoelastic modulus (mN m^{-1}), consisting of a storage modulus and a loss modulus, E' and E'' respectively¹⁵. The detection limit for surface tension measurements was 0.06 mN m^{-1} . From this, the detection limit of the complex dilatational elastic modulus was calculated to be 0.44 mNm^{-1} ($d\Pi/dA = 0.06 \text{ mN m}^{-1}/0.135$). Experiments were performed in duplicate and values of the elastic modulus are expressed as mean of the duplicates. Standard deviations between replicates for surface pressure experiments were less than $\pm 0.5 \text{ mN m}^{-1}$ and of E_d less than $\pm 1.5 \text{ mN m}^{-1}$.

Determination of protein ζ -potential

The ζ -potential of BLG molecules at different pH values was determined in solutions of 10 mg mL^{-1} on a Zeta Sizer Nano ZSP (Malvern Instruments, Malvern, UK) as was described elsewhere¹⁶. The measurements were performed at 20°C and 40 V . The ζ -potential was calculated using Henry's equation (equation 8) and values taken from Jachimska *et al.*¹⁷

$$(8) \quad \zeta = \frac{3\eta \cdot \mu_e}{2\varepsilon F(\kappa\alpha)}$$

where $\eta = 1.002 \cdot 10^{-3}$ (Pa s) is the liquid viscosity at 20°C ¹⁸, μ_e is the electrophoretic mobility ($\text{m}^2 \text{ V}^{-1} \text{ s}^{-1}$), ε is the dielectric constant of the medium ($7.1 \cdot 10^{-10} \text{ C}^2 \text{ J}^{-1} \text{ m}^{-1}$)¹⁸ and $F(\kappa\alpha)$ is the dimensionless Henry's function of the Debye length κ^{-1} and the dimensions of the protein (α), which equals 1.5 in the Smoluchowski approximation¹⁸. The ζ -potential was determined in triplicate with a minimum of 25 individual measurements per determination and the reported values are the average values of the triplicates.

Determination of protein structure

Circular dichroism (CD) spectra of BLG at different pH values were determined using a spectropolarimeter (J-715, Jasco, Easton, MD, USA) as described elsewhere¹⁴. The concentrations used for far-UV and near UV CD were 0.1 and 1 mg mL^{-1} respectively. The optical path length for far-UV and near-UV CD were 1 mm and 10 mm , respectively. Sixteen spectra were averaged and corrected for the corresponding buffer solution. For comparison with literature, the molar ellipticity Θ_{mol} ($\text{mdeg cm}^2 \text{ dmol}^{-1}$) was calculated using equation 9

$$(9) \quad \Theta_{\text{mol}} = \frac{100\Theta_{\text{obs}}}{d \cdot m}$$

where Θ_{obs} is the measured ellipticity (deg), d the path length of the cuvette (cm) and m the molar concentration of BLG (mol L^{-1}).

Determination of adsorbed amount

A BLG stock solution of 16.5 mg mL^{-1} was prepared by dissolving powder in buffer of the desired pH. The ellipsometric angles (Δ and ψ) of the respective buffer were determined over a period of 1 hour on a multiscope ellipsometer (Optrel, Sinzig, Germany) using a monochromatic laser (632.8 nm at an angle of incidence 50°) as described elsewhere¹⁶. Then, the BLG stock solution was injected into the buffer to yield a final concentration of 0.5 mg mL^{-1} . After 24 hours of adsorption, the ellipsometric angles of the protein solutions were determined over a period of 1 hour. The adsorbed amount Γ (mg m^{-2}) was fitted

Chapter 3

from the change in ellipsometric angles between buffer and protein solution using a two phase model from the software that was provided with the ellipsometer as described by Delhaije *et al.*¹⁶. The fitting parameters of the model were the refractive indices of air ($n_{\text{air}} = 1$) and buffer ($n_{\text{buffer}} \approx n_{\text{water}} = 1.333$) and $dn/dc = 0.185 \text{ mL g}^{-1}$, which is typical for globular proteins¹⁹.

Determination of equilibrium thin film thickness

Aliquots of BLG solution (0.5 mg mL^{-1}) at the respective pH values were placed in a glass Sheludko cell with a radius of 1.25 mm and equilibrated for 15 minutes. Then liquid was drawn into the capillary of the Sheludko cell to make a film of $200 \mu\text{m}$ diameter. The Sheludko cell was fixed to a microscope (Axio Plan 01, Zeiss, Jena, Germany) that was equipped with a five mega pixel CCD camera (Mightex Systems, Pleasanton, CA. USA). The thickness of the thin films of BLG was determined using a microinterferometric method as described elsewhere²⁰. For this, the light intensity of an area of $1963 \mu\text{m}^2$ within the plane parallel part of the film was measured and averaged and the thickness was calculated using equation 10

$$(10) \quad h = \frac{\lambda}{2\pi n} [l\pi \pm \arcsin\sqrt{\Delta}]$$

where h is the thickness (nm), $\lambda = 546 \text{ nm}$ is the wavelength of the used light, $n=1.333$ is the refractive index of the solution, l is the order of interference and $\Delta=(I-I_{\text{min}})/(I_{\text{max}}/I_{\text{min}})$ in which I , I_{min} and I_{max} are the average, minimum, and maximum light intensity.

Results and discussion

Foam ability

The relative foam ability (FA) of BLG at pH 7 increases with increasing concentration (figure 3.1).

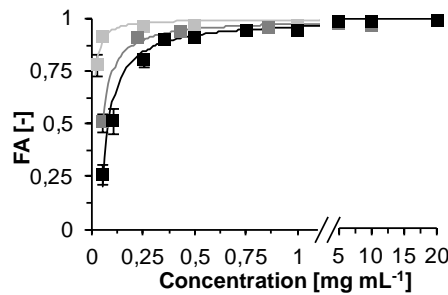


Figure 3.1: Relative foam ability of BLG solutions at pH 3 (■), 5 (■) and 7 (■). The lines represent the fit of the data and were calculated using equation 3 and the fitting parameter a shown in table 3.1. Error bars indicate the standard deviation, which decreases with increasing concentration and can be smaller than the marker used.

The curve of FA over the concentration for pH 7 levels off at about 0.25 mg mL^{-1} . Similar to the curve of pH 7, the FA curves of BLG at pH 5 and 3 increase with concentration, but in these cases the curve level off at a concentration of about 0.45 mg mL^{-1} and 0.75 mg mL^{-1} .

Identification of critical concentrations determining foam ability and stability

mL^{-1} , respectively. These concentration at which the foam ability becomes independent of the concentration is denoted the critical concentration (C_{crFA}) for foam ability. The data were fitted with equation 3 and the values are shown in table 3.1. The calculated R^2 values indicate a good fit (R^2 was 0.89, 0.98 and 0.97 for FA at pH 7, pH 5 and pH 3, respectively). BLG at pH 7 has the lowest C_{crFA} , which means that the highest FA was reached at a lower concentration than pH 5 and pH 3. In other studies it was observed that the emulsifying ability index²¹ increases with increasing pH^{22, 23}, similar to the observation of FA in this study.

Table 3.1: Critical concentration, fitting parameters (a and b) and fitted FA and r_{32} for pH 3, 5 and 7.

	pH 3	pH 5	pH7
$C_{\text{crFA}} [\text{mg mL}^{-1}]$	0.75	0.45	0.25
$C_{\text{cr32}} [\text{mg mL}^{-1}]$	-	10	1
a	25.1	40.0	187.0
b	2.2	4.0	21.7
FA_{fit}	0.95	0.94	0.98
$R_{32,\text{fit}} [\text{mm}]$	-	0.025	0.046

Similar to the FA over concentration curve, the r_{32} curves for each pH value level off and become independent of concentration (figure 3.2). The Sauter bubble radius (r_{32}) decreases with increasing concentration for pH 7 until the r_{32} curve levels off at a critical concentration (C_{cr32}) of 1 mg mL^{-1} with a minimum bubble size of 0.08 mm.

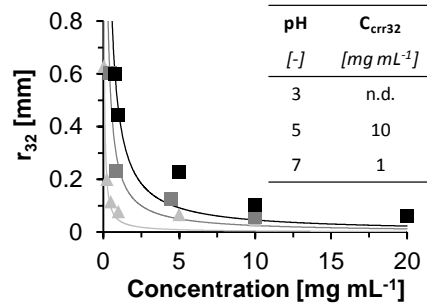


Figure 3.2: Bubble radius (r_{32}) as a function of the concentration of BLG at pH 3(■), 5(■) and 7(▲). The lines represent the fit of the data calculated with equation 4 and the fitting parameter b shown in table 3.1. Error bars indicate the standard deviation between replicate experiments.

For pH 5 the curve followed a similar trend but levelled off at 10 mg mL^{-1} with 0.07 mm. The r_{32} curve of pH 3 only showed a decrease and no levelling off was observed until 20 mg mL^{-1} . The r_{32} at 20 mg mL^{-1} (0.06 mm) was similar to the minimum r_{32} values at the other pH values, which suggests that for pH 3, 20 mg mL^{-1} is the C_{cr32} of BLG. The r_{32} data were fitted with equation 4, which resulted in less good fit than in the case of the fitted FA with an R^2 of 0.62 for the fitted pH 7, 0.94 for fitted pH 5 and 0.79 for fitted pH 3 (table 3.1). This indicates that, similar to the FA, the concentration dependence of r_{32} in

Chapter 3

foam follows a similar trend as observed for the formation of emulsion droplets. In the protein rich regime where $C > C_{\text{cr}32}$, the FA and r_{32} of all studied solutions are similar. $C_{\text{cr}32}$ is comparable to the critical concentration that is reported for emulsions, which separates the curve of the Sauter droplet size over concentration into a protein rich and protein poor regime^{11, 13}. To compare the foam stability of different foams, both critical concentrations need to be taken into account (figure 3.3). At concentrations $C < C_{\text{crFA}}$, $\text{FA} < \text{FA}_{\text{max}}$ and $r_{32} > r_{32\text{min}}$.

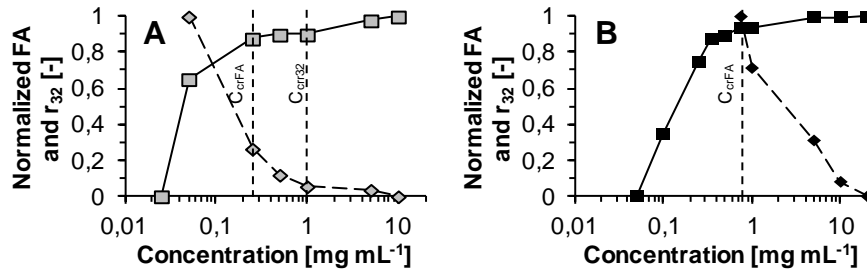


Figure 3.3: Normalized FA (■ and ■) and r_{32} (◆ and ◆) for BLG at pH 7 (A) and pH 3 (B). Critical concentrations indicated by dotted lines. FA and r_{32} were normalized according to equation 5 and 6.

This concentration regime can be defined as the protein poor regime. At $C > C_{\text{crFA}}$, $\text{FA} = \text{FA}_{\text{max}}$ and $r_{32} > r_{32\text{min}}$ (figure 3.3), which indicates different bubble size distributions that will affect the drainage and the foam stability (figure 3.4).

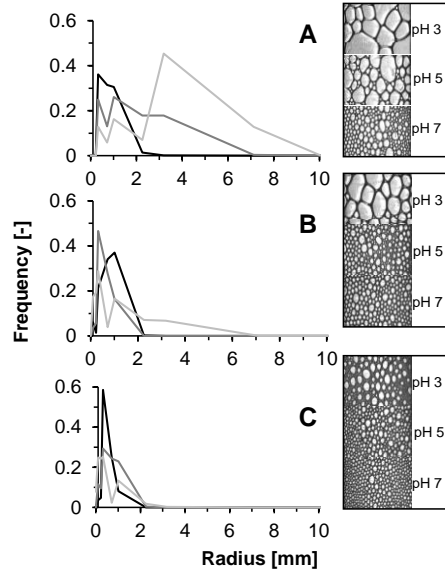


Figure 3.4: Relative bubble size distribution of BLG solutions at three different concentrations 1 mg mL⁻¹ (A), 5 mg mL⁻¹ (B) and 10 mg mL⁻¹ (C) for pH 3 (---), pH 5 (—) and pH 7 (—).

Identification of critical concentrations determining foam ability and stability

This concentration regime can be defined as the intermediate regime. At $C > C_{\text{crr}32}$, both $FA = FA_{\text{max}}$ and $r_{32} = r_{32\text{max}}$. The concentration range above $C_{\text{crr}32}$ can be defined as the protein rich regime. Consequently, to make a fair comparison of the foam stability of different samples, the concentration in each sample should be above the $C_{\text{crr}32}$ to ensure similar bubbles size distributions. It should be noted that the r_{32} should be determined preferably within a short time (i.e. 1 second) after foam formation has stopped to exclude effects from coalescence and disproportionation.

Interfacial properties

The value of E_d increased with increasing Π from 5.1 mN m^{-1} at $\Pi = 1.5 \text{ mN m}^{-1}$ at pH 3 up to 96 mN at $\Pi = 23 \text{ mN m}^{-1}$ at pH 4.5 (figure 3.5 A).

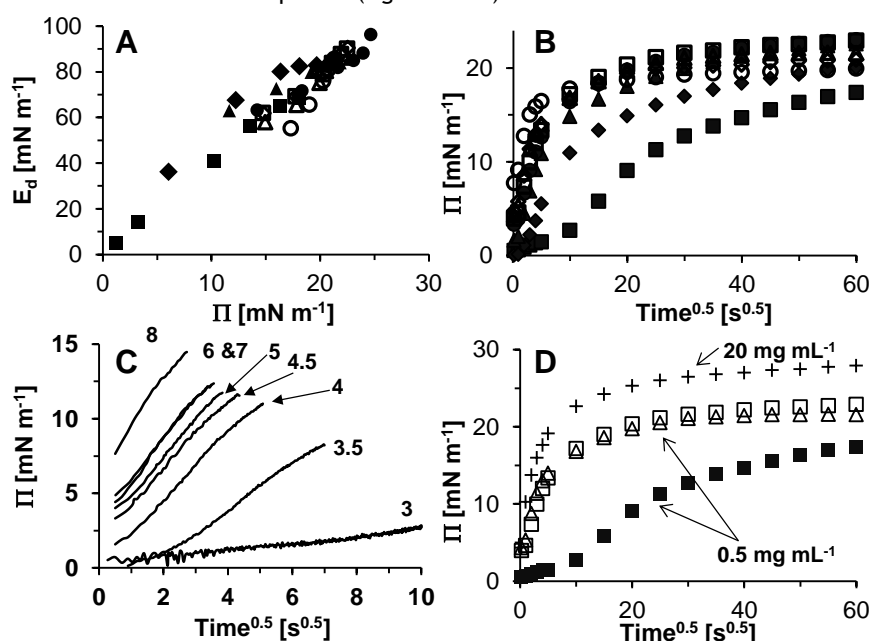


Figure 3.5: A) The E_d over Π of BLG solutions at pH 3 (■), 3.5 (◆), 4 (▲), 4.5 (●), 5 (□), 6 (◇), 7 (△), 8 (○). B) $\Pi(t^{0.5})$, the marker symbols are the same as in panel A. C) shows the initial part of the curves from panel B, which was used to determine the slope of the curves. D) $\Pi(t^{0.5})$ curve for BLG (0.5 mg mL⁻¹) at pH 3 (■), 5 (□) and 7 (△) and BLG (20 mg mL⁻¹) pH 3 (+). Note that in D, the curves of pH 3 belong to two different concentrations (0.5 mg mL⁻¹ and 20 mg mL⁻¹) as indicated in the figure. Standard error between replicates < 5 %.

The highest E_d and Π values were observed at pH values around the iso-electric point of BLG (pH 4.7-5). This maximum of Π around pH 5 has been attributed to the fact that around the iso-electric point the absorbed amount of BLG is higher than at other pH values^{3, 7}. The differences in FA and r_{32} with pH and concentration could not be linked to the values of Π or E_d after longer adsorption time (1 hour). The $E_d(\Pi)$ curves of BLG for all studied pH values collapse onto the same master curve, which indicates a similar equation of state of adsorption for BLG at different pH values²⁴. This allows the interpretation of

differences of the curve of Π versus time as differences in adsorption kinetics. The adsorption rate of BLG increased with increasing pH from pH 3 to 8 (figure 3.5 B and C), which was reflected in increased foam ability and reduced bubble radius. Similarly, an increase in concentration led to an increase of the adsorption kinetics (figure 3.5 D), which in turn led to increased foam ability and reduced bubble radius e.g. for pH 3 at 20 mg mL⁻¹.

Foam stability

The foam stability, expressed as foam half-life $t_{1/2}$ as a function of pH, was compared at 0.5 mg mL⁻¹ (figure 3.6 A). The highest $t_{1/2}$ were observed at pH 7 and 8. Around the iso-electric point, the lowest foam stability was found.

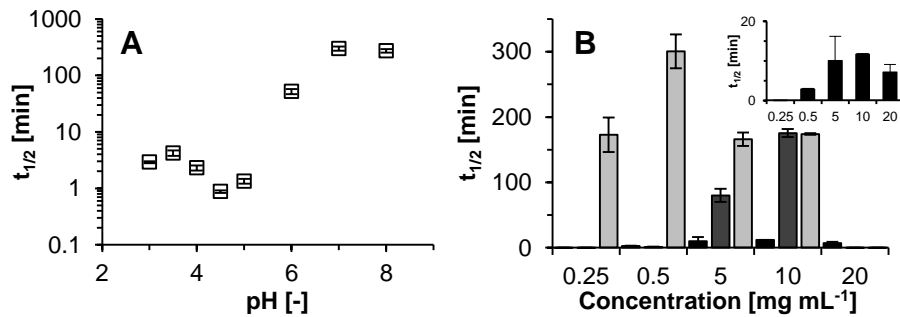


Figure 3.6: A) Foam stability as a function of the pH at 0.5 mg mL⁻¹. B) Foam stability of BLG at pH 3 (■), 5 (■) and 7 (■) for different concentrations. For pH 3 and 5 at 0.25 mg mL⁻¹, not enough foam was created to determine the $t_{1/2}$. The inset in shows scaled view of the foam stability at pH 3. Error bars indicate standard deviation between experiments.

Below the iso-electric point, the $t_{1/2}$ increases somewhat but not to the values observed for pH 7-8. However, it must be noted that the sample at pH 7 is in the protein rich regime, while samples at pH 5 and 3 are in the protein poor regime as discussed above. Therefore, at pH 3, 5 and 7, another set of experiments with increasing concentration was conducted (figure 3.6 B). With increased concentration, at concentrations above C_{crFA} , a transition to increased foam stabilities was identified at each pH. The $t_{1/2}$ of BLG ($C_{crFA} = 0.25$ mg mL⁻¹), at pH 7 at 0.25 mg mL⁻¹ is 173 ± 10 minutes and increases to a maximum of 300 ± 26 minutes at 0.5 mg mL⁻¹. At pH 5 ($C_{crFA} = 0.45$ mg mL⁻¹) the $t_{1/2}$ shows an increase from 1.3 minutes at 0.5 mg mL⁻¹ to 80 ± 10 minutes at 5 mg mL⁻¹. In samples at pH 3 ($C_{crFA} = 0.75$ mg mL⁻¹) $t_{1/2}$ increases from 3 ± 0.1 minutes until 12 ± 1 minutes at 10 mg mL⁻¹. In the intermediate regime ($C_{crFA} < C < C_{cr32}$), the $t_{1/2}$ of BLG at pH 5 (at 10 mg mL⁻¹) was similar to that at pH 7 (0.25 mg mL⁻¹). This shows that the comparison of the foam stability of samples at constant concentration is hindered by the fact that not all samples are in the intermediate or protein rich regime. For $C > C_{cr32}$ the adsorption kinetics is not limiting, leading to a similar initial foam structure (bubble size distribution). However, there are two unexpected observations that are worthwhile mentioning. Firstly, at pH 7 and 3 remarkable maxima of $t_{1/2}$ as a function of concentration were observed. For pH 7 $t_{1/2}$ changed from 170 to 300 to 170 minutes and for pH 3 from 3 to 11 to 7 minutes. Similar maxima have been reported for apo α -lactalbumin²⁵, which indicates that this is a

Identification of critical concentrations determining foam ability and stability

typical trend for the concentration dependence of the foam stability. However, this is not well understood yet. Secondly, even in the intermediate/protein rich regime, the values of the foam stability of BLG at pH 3 (10 and 20 mg mL⁻¹) were remarkably lower than that at pH 5 and 7.

Link of the critical concentrations to molecular properties

In order to identify the reason for the different foam ability and foam stability at pH 7 and 3, physicochemical properties of BLG are determined. Using circular dichroism (figure 3.7 A and B) it was found that there were no differences between the far UV and near UV spectra of BLG at different pH values were observed.

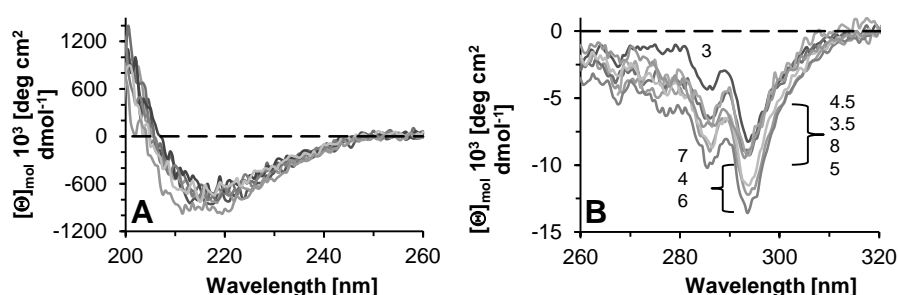


Figure 3.7: Far-UV (A) and near UV (B) circular dichroism spectra of BLG at different pH values.

This means that the pH had no noticeable influence on the secondary and tertiary structure. The ζ -potential of BLG decreases from 10 mV at pH 3 to -10 mV at pH 6 where it levels off (figure 3.8).

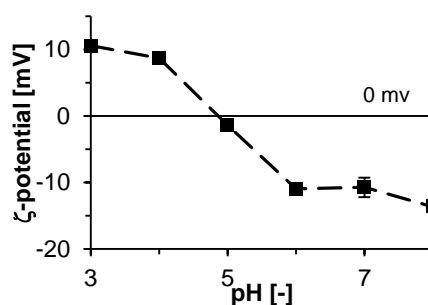


Figure 3.8: ζ -potential of BLG solutions (10 mg mL⁻¹) as a function of the pH. Error bars indicate the standard deviation between replicate experiments. The solid line indicates 0 mV and the dashed line is to guide the eye.

The lowest absolute charge (0 mV) is reached at pH 4.9, which is in line with previous data²⁶. Overall, the ζ -potential curve is symmetric, which means that it does not explain the different foam stabilities at pH 3 and pH 7. The equilibrium adsorbed amounts (Γ after 24 hours, figure 3.9 A) were also similar for pH 7 and pH 3: 1.4 and 1.5 mg m⁻², respectively. At pH 5 Γ was 2.5 mg m⁻².

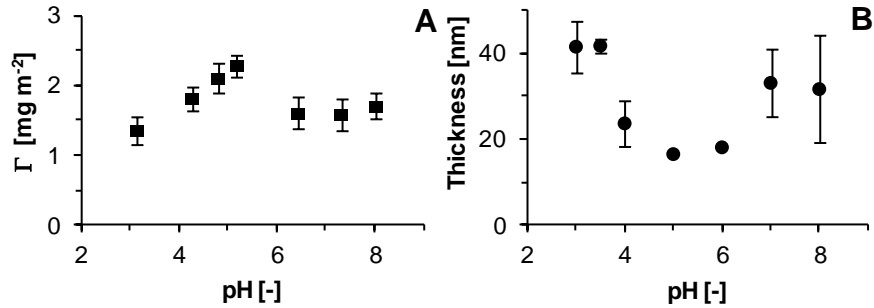


Figure 3.9: A) Adsorbed amount (after 24 hours adsorption) of BLG at different pH values. The standard deviation is the deviation in the measured signal averaged over the 1 hour measurement of per sample. B) Thickness of thin liquid films of BLG solution as a function of the pH. Error bars indicate the standard deviation between experiments.

This indicates that the adsorption properties after longer adsorption time are not related to the foam ability or stability. Hence it is postulated that the differences in foam properties are reflected in the thickness of the thin liquid films of BLG (0.5 mg mL⁻¹) (figure 3.9 B). The equilibrium thicknesses of BLG at pH 3 and pH 7 were comparable within the error of the experiment 40 ± 5 nm at pH 3 and 30 ± 8 nm at pH 7. The lowest thickness, 17 nm, was observed at pH 5. Such a low thickness indicates a low repulsive charge²⁷. The thickness is in part determined by the disjoining pressure, which is related to the charge of the interface. The similar equilibrium thickness of the thin films at pH 3 and 7 is, therefore, in agreement with the ζ -potential of the proteins at these pH values. However, the equilibrium thickness does not explain the difference in foam stability of BLG at pH 3 and pH 7. Thin liquid films at all pH values were stable enough to determine the equilibrium thickness, except for pH 5 and 6 where only single measurements could be obtained due to instable films. Summarizing: Under these conditions, parameters such as the Π , E_d , adsorbed amount and the thickness of thin films are similar for BLG at pH 3 and 7.

The C_{crFA} and C_{cr32} were identified as critical parameters, separating the protein poor and protein rich regime for foam ability. This separation is also reflected in foam stability, which for each sample increases at $C > C_{cr32}$ (figure 3.10).

To compare the foam stability in different samples, one should take care that the samples have a concentration $C > C_{cr32}$. The differences in $t_{1/2}$ at ($C > C_{cr32}$) between BLG at pH 3 and 7 remain to be explained.

Identification of critical concentrations determining foam ability and stability

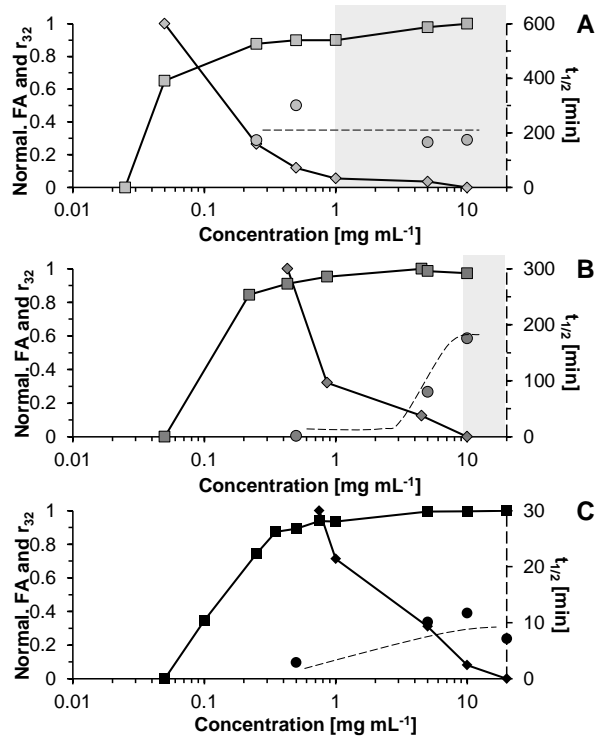


Figure 3.10: Normalized FA (■) and r_{32} (◆) as well as $t_{1/2}$ (●) for BLG at pH 7 (A), pH 5 (B) and pH 3 (C). FA and r_{32} were normalized according to equation 5 and 6. The protein rich regime is indicated by the grey area.

Conclusions

This study has shown the strong dependence of the foam ability on the protein concentration C , which is characterized by two critical concentrations, C_{FA} and C_{cr32} . C_{FA} separates a protein poor regime from an intermediate regime while C_{cr32} separates the intermediate from a protein rich regime. Such regimes were also identified in emulsions, which show that foam ability and the ability to create a stable emulsion can be described by the same concept. In the case of BLG, the critical concentrations depend on the pH of the solution, which was strongly reflected by the adsorption kinetics of the protein. When $C > C_{cr32}$ the foam ability and bubble size at $t = 60s$ are independent the concentration, which allows a fair comparison of the foam properties.

References

1. Zhang, Z.; Dagleish, D. G.; Goff, H. D., Effect of pH and ionic strength on competitive protein adsorption to air/water interfaces in aqueous foams made with mixed milk proteins. *Colloids and Surfaces B: Biointerfaces* **2004**, 34, 113-121.
2. Phillips, L. G.; Schulman, W.; Kinsella, J. E., pH and heat treatment effects on foaming of whey protein isolate. *Journal of Food Science* **1990**, 55, 1116-1119.

Chapter 3

3. Waniska, R. D.; Kinsella, J. E., Surface properties of β -lactoglobulin: Adsorption and rearrangement during film formation. *Journal of Agricultural and Food Chemistry* **1985**, 33, 1143-1148.
4. Uniprot P02754 (LACB_BOVIN) Reviewed, UniProtKB/Swiss-Prot. <http://www.uniprot.org/uniprot/P02754> (03.06.2014),
5. Casal, H. L.; Köhler, U.; Mantsch, H. H., Structural and conformational changes of β -lactoglobulin B: an infrared spectroscopic study of the effect of pH and temperature. *Biochimica et Biophysica Acta (BBA) - Protein Structure and Molecular Enzymology* **1988**, 957, 11-20.
6. Majhi, P. R.; Ganta, R. R.; Vanam, R. P.; Seyrek, E.; Giger, K.; Dubin, P. L., Electrostatically driven protein aggregation: β -Lactoglobulin at low ionic strength. *Langmuir* **2006**, 22, 9150-9159.
7. Schwenzfeier, A.; Lech, F.; Wierenga, P. A.; Eppink, M. H. M.; Gruppen, H., Foam properties of algae soluble protein isolate: Effect of pH and ionic strength. *Food Hydrocolloids* **2013**, 33, 111-117.
8. Townend, R.; Weinberger, L.; Timasheff, S. N., Molecular interactions in β -lactoglobulin. IV: The dissociation of β -lactoglobulin below pH 3.52. *Journal of the American Chemical Society* **1960**, 82, 3175-3179.
9. Verheul, M.; Roefs, S. P. F. M.; de Kruif, K. G., Kinetics of heat-induced aggregation of β -lactoglobulin. *Journal of Agricultural and Food Chemistry* **1998**, 46, 896-903.
10. Haug, I. J.; Skar, H. M.; Vegarud, G. E.; Langsrud, T.; Draget, K. I., Electrostatic effects on β -lactoglobulin transitions during heat denaturation as studied by differential scanning calorimetry. *Food Hydrocolloids* **2009**, 23, 2287-2293.
11. Tcholakova, S.; Denkov, N. D.; Lips, A., Comparison of solid particles, globular proteins and surfactants as emulsifiers. *Physical Chemistry Chemical Physics* **2008**, 10, 1608-1627.
12. Tcholakova, S.; Denkov, N. D.; Ivanov, I. B.; Campbell, B., Coalescence in β -lactoglobulin-stabilized emulsions: Effects of protein adsorption and drop size. *Langmuir* **2002**, 18, 8960-8971.
13. Delahaije, R. J. B. M.; Gruppen, H.; Giuseppin, M. L. F.; Wierenga, P. A., Towards predicting the stability of protein-stabilized emulsions. *Advances in Colloid and Interface Science* **2015**, 219, 1-9.
14. Lech, F. J.; Steltenpool, P.; Meinders, M. B. J.; Sforza, S.; Gruppen, H.; Wierenga, P. A., Identifying changes in chemical, interfacial and foam properties of β -lactoglobulin-sodium dodecyl sulphate mixtures. *Colloids and Surfaces A: Physicochemical and Engineering Aspects* **2014**, 462, 34-44.
15. Benjamins, J.; Cagna, A.; Lucassen-Reynders, E. H., Viscoelastic properties of triacylglycerol/water interfaces covered by proteins. *Colloids and Surfaces A: Physicochemical and Engineering Aspects* **1996**, 114, 245-254.
16. Delahaije, R. J. B. M.; Wierenga, P. A.; Giuseppin, M. L. F.; Gruppen, H., Improved emulsion stability by succinylation of patatin is caused by partial unfolding rather than charge effects. *Journal of Colloid and Interface Science* **2014**, 430, 69-77.
17. Jachimska, B.; Wasilewska, M.; Adamczyk, Z., Characterization of globular protein solutions by dynamic light scattering, electrophoretic mobility, and viscosity measurements. *Langmuir* **2008**, 24, 6866-6872.
18. Walstra, P.; Appendix H: Physical properties of water at 0°C to 100°C. In *Physical Chemistry of Foods*, Marcel Dekker: New York, NY, USA, **2009**; p 807.
19. De Feijter, J. A.; Benjamins, J.; Veer, F. A., Ellipsometry as a tool to study the adsorption behavior of synthetic and biopolymers at the air-water interface. *Biopolymers* **1978**, 17, 1759-1772.
20. Lech, F. J.; Wierenga, P. A.; Gruppen, H.; Meinders, M. B. J., Stability properties of surfactant-free thin films at different ionic strengths: Measurements and modeling. *Langmuir* **2015**, 31, 2777-2782.
21. Pearce, K. N.; Kinsella, J. E., Emulsifying properties of proteins: evaluation of a turbidimetric technique. *Journal of Agricultural and Food Chemistry* **1978**, 26, 716-723.
22. Shimizu, M.; Saito, M.; Yamauchi, K., Emulsifying and structural properties of β -lactoglobulin at different pHs. *Agricultural and Biological Chemistry* **1985**, 49, 189-194.
23. Huang, X. L.; Catignani, G. L.; Swaisgood, H. E., Improved emulsifying properties of β -barrel domain peptides obtained by membrane-fractionation of a limited tryptic hydrolysate of β -lactoglobulin. *Journal of Agricultural and Food Chemistry* **1996**, 44, 3437-3443.

Identification of critical concentrations determining foam ability and stability

24. Wierenga, P. A.; Meinders, M. B. J.; Egmond, M. R.; Voragen, A. G. J.; de Jongh, H. H. J., Quantitative description of the relation between protein net charge and protein adsorption to air–water interfaces. *The Journal of Physical Chemistry B* **2005**, 109, 16946-16952.
25. Dhayal, S. K., *Mesoscale structure and techno-functional properties of enzymatically cross-linked α -lactalbumin nanoparticles*, PhD thesis, Wageningen University: Wageningen, The Netherlands, **2015**; p 162.
26. Engelhardt, K.; Lexis, M.; Gochev, G.; Konnerth, C.; Miller, R.; Willenbacher, N.; Peukert, W.; Braunschweig, B., pH effects on the molecular structure of β -lactoglobulin modified air-water interfaces and its impact on foam rheology. *Langmuir* **2013**, 29, 11646-11655.
27. Gochev, G.; Retzlaff, I.; Exerowa, D.; Miller, R., Electrostatic stabilization of foam films from β -lactoglobulin solutions. *Colloids and Surfaces A: Physicochemical and Engineering Aspects* **2014**, 460, 272-279.

4. Identifying changes in chemical, interfacial and foam properties of β -lactoglobulin-sodium dodecyl sulphate mixtures

Abstract

Techno functional properties of proteins, such as foam stability, can be affected by the presence of low-molecular weight surfactants. In order to understand and control the foam properties of such protein-surfactant mixtures, a thorough characterization of foam and interfacial properties needs to be supplemented by a detailed analysis of the structural changes of the protein and possible complexation with the surfactant. In this study, β -lactoglobulin (BLG) was mixed with sodium dodecyl sulphate (SDS) in different molar ratios (MR). The foam half-life time of BLG-SDS mixtures decreased from that of pure BLG (315 minutes at MR 0) to 44 minutes at MR 20, which is close to the half-life of SDS at the respective concentration. With a further increase of the MR, the foam stability of the mixture increased, similar to the stability of SDS, to 250 minutes at the highest MR (MR 100). The minimum in the foam stability curve was not reflected in the interfacial properties (Π_{1h} and E_{d1h}). Π_{1h} decreased and E_{d1h} increased continuously with increasing MR from values close to those of protein towards values typically found in pure surfactant solutions. The results show no clear correlation between the interfacial and foaming properties. In addition, it was shown by isothermal titration calorimetry and by mass spectrometry that SDS molecules bind to the BLG. This leads to the formation of BLG-SDS complexes. These complexes have large influence on the foam properties in the mixture. The combination of analytical methods that were used, give insights about protein complexation and the resulting change of foam properties of the mixture.

Based on: Lech, F. J.; Steltenpool, P.; Meinders, M. B. J.; Sforza, S.; Gruppen, H.; Wierenga, P. A., *Identifying changes in chemical, interfacial and foam properties of β -lactoglobulin-sodium dodecyl sulphate mixtures. Colloids and Surfaces A: Physicochemical and Engineering Aspects* **2014**, 462, 34-44.

Introduction

When investigating foam properties, a general rule of thumb is that the foam properties will improve with increasing amount of surface active substances. However, when mixtures of the latter of different types of surfactants are used, this observation may change. For mixtures of low molecular weight surfactants (LMWS) and proteins it has, under certain conditions, been observed that the foam stability of the mixture is lower than of the protein alone¹. This could be explained by assuming an interaction between the proteins and the surfactant as mentioned in literature². This shows that the foam properties of protein surfactant mixtures are not simply explained by a weighted average of the contributions of the individual compounds. One reason for this effect could be the different mechanisms of foam stabilization of proteins and LMWS or the interaction of the material in the bulk solution. The aim of this study is to describe the effect of protein surfactant interaction on functional properties of the protein by using chemical (bulk interaction etc.) as well as the physical (interfacial properties, foam etc.) techniques. Combining these techniques leads to a more detailed understanding of the functional properties of the protein surfactant mixture. The current literature on mixed proteins and LMWS shows a broad separation into two major categories (figure 4.1).

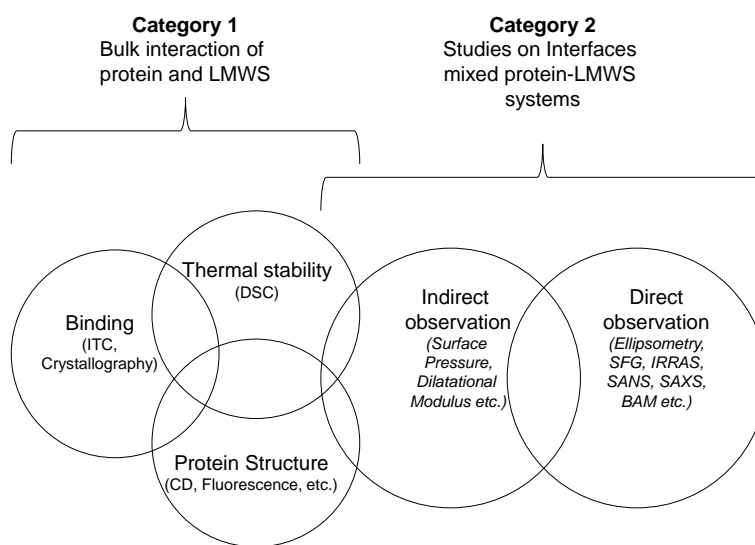


Figure 4.1: Segmentation of studies dealing with mixed protein-surfactant systems. Venn diagram of literature shows sets of studies with similar experimental approach dealing with protein surfactant interaction.

One research category focuses on bulk interactions between proteins and LMWS, while the other category focuses on the interfacial and foam properties of mixed protein-surfactant solutions. The next section of the review focusses mainly on studies, which use BLG and SDS as examples. The approach in the first category (figure 4.1 category 1) is to determine specific aspects such as the binding of LMWS to protein. Further studies in this field

Identifying changes in chemical, interfacial and foam properties of BLG-SDS mixtures

determine the effects of binding on changes of the protein structure³. For instance, isothermal titration calorimetry (ITC) was used to show that one mole of sodium dodecyl sulphate (SDS) binds to one molecule of β -lactoglobulin (BLG), which is a molar ratio (MR) of 1⁴. The binding of SDS to BLG was also shown by X-ray diffraction analysis of BLG-SDS crystals⁵. The binding site is a cavity formed by nine β -sheets (calyx), is located on the inside of the BLG molecule. Another study, found no changes of the secondary structure of BLG up to a concentration of 5 mM SDS (which corresponds to a molar ratio (MR) of 91 in this study) using circular dichroism (CD). At higher MR (between MR 100 and 200; concentrations are above the critical micelle concentration (CMC) of SDS in this case), however, the predominantly β -sheet rich secondary structure of BLG changed into a more helical structure. Simultaneously, unfolding of to the tertiary structure occurred in the range of MR 18 up to 91⁶. Surprisingly, the binding to LMWS increases the heat stability of BLG against denaturation from 80 °C at MR 0 to 88 °C at MR 1. The research on interfacial behaviour of mixed systems (figure 4.1, category 2) has been reviewed extensively e.g. by^{7, 8}. The reviews emphasize the important improvement of foam properties that mixing proteins and LMWS can have. They also indicate the lack of quantitative understanding on the relation between foam stability and interfacial rheology of the protein-surfactant mixtures. The adsorption of molecules at the air-water interface can be studied directly (i.e. using ellipsometry, infrared reflection-adsorption spectroscopy (IRRAS) or Brewster angle microscopy (BAM)) or indirectly, from the measured interfacial properties (surface pressure (Π) and dilatational elasticity (E_d)). The direct studies are used to investigate the interfacial composition and structure of molecules adsorbed at the interface. The methods to study adsorbed monolayers are described in reviews⁹⁻¹². The composition of interfacial layers, is also studied using atomic force microscopy on Langmuir Blodgett (LB) films¹³. In such studies, first a protein adsorption layer is made, and sequentially LMWS are added to the bulk solution. Then, an LB film is made by transferring the adsorbed layer unto a solid surface. Results of sequential adsorption studies indicate the expulsion of proteins from the interface at high surfactant concentration, which is explained by the orogenic displacement model¹³. However, the observations of protein displacement is not generally true but depend on the type of protein and surfactant, the respective concentrations and on the experimental procedure, since for instance HFBII hydrophobin cannot be displaced from the interface¹⁴. Other studies characterise air/water interfaces indirectly, e.g. by determining the interfacial tension or complex dilatation elastic modulus of protein-surfactant mixtures. Proteins and LMWS stabilize interfaces in two counteracting mechanisms. Protein form elastic networks¹⁵, while surfactant interfaces are stabilized by the *Marangoni mechanism*¹⁶. Those different ways of stabilizing are, for instance, reflected in different interfacial properties, such as the surface pressure (Π) and the complex dilatational modulus (E_d). Π is related to adsorption of material onto the interface by the equation of state¹⁷, while the dilatational modulus is related to interfacial interactions between molecules in the interface as well as to the adsorption and desorption of material from the interface¹⁸. Studies investigating these parameters are usually related to adsorption of the mixtures and to the interfacial interactions between the protein and surfactant molecules^{19, 20}. These indirect methods are usually

applied in competitive adsorption studies. In these studies, proteins and LMWS are combined and both can adsorb to the interface at the same time. However, the only common conclusions among these studies are related to high MR, when the concentration of LMWS is higher than the CMC and proteins seem to be completely removed from the interface²¹. Another possibility to use indirect techniques is to determine the change of interfacial properties during or after sub-phase exchange with buffer. The buffer displaces the surfactant solution from the bulk of the droplet, resulting in desorption from the interface. A comparison of the interfacial properties before and after exchange gives insight about the initial interfacial composition¹⁹. The occurrence of changes in chemical properties of proteins after mixing with LMWS is generally accepted by researchers from the first category. Only recently, the researches belonging to the second category are beginning to consider this. The common picture on protein surfactant mixtures at the interface can be summarized by picturing two models (figure 4.2 A and B).

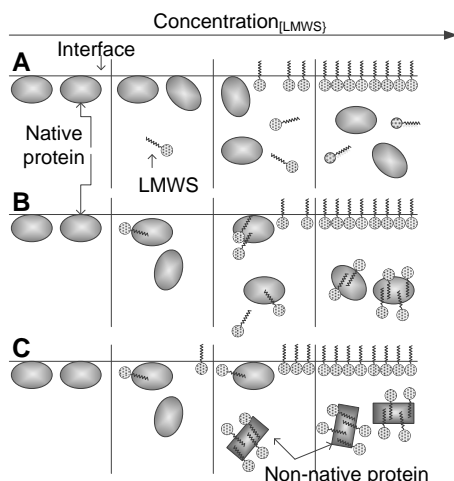


Figure 4.2: Two models of interfacial composition for mixed systems of proteins and LMWS at different bulk concentrations of LMWS. A) No interaction between protein and LMWS. Proteins and surfactant are treated as separate non interacting entities. B) Formation of protein surfactant complexes with different degrees of modification. Complexes are competing with LMWS to adsorb at the interface. No complexes in the interface at high surfactant concentrations. Modified from^{7, 19, 21-24}. C) Proposed adaptation of model B including structural changes of the protein.

In model (A), the simplest model of a mixture of any protein and surfactant, both substances are considered as separate, non-interacting entities. With increasing concentration, the LMWS displace the proteins from the interface and determine the interfacial properties of the mixture (figure 4.2 A). Since for certain systems (e.g. BLG-SDS) it is known that there is an interaction between both substances, an alternative model (B) has been described. In this model the proteins and LMWS are considered to form complexes. With increasing surfactant concentration, more LMWS bind to the protein. At concentrations higher than a critical concentration, the interface is mostly covered by LMWS while the influence of the protein-surfactant complexes on the interfacial

Identifying changes in chemical, interfacial and foam properties of BLG-SDS mixtures

properties decreases (figure 4.2 B). Both research categories investigate similar types of LMWS and proteins. However, their focus as well the used mixing ratios in their studies are different. Studies from the interface category are performed with SDS concentrations ranging from 10^{-9} mol L⁻¹ up to concentrations of 10^{-1} mol L⁻¹, which is above the critical micelle concentration ($8 \cdot 10^{-3}$ mol L⁻¹). Usually, the largest changes in interfacial properties, such as the surface tension, are observed between MR 10 and 100, after which the interfacial properties of the mixed system become similar to those of the pure surfactant²⁵. A few of the above mentioned studies from both categories use experimental similar techniques. These studies however, mainly combine interfacial properties with interactions in bulk solution, but only a minority extends their approach towards functional properties such as the foam stability of the mixed systems^{22, 26, 27}. Since most studies on protein-surfactant mixtures focus either on the bulk or the interfacial aspects, this study improves the understanding of the techno-functional properties (foam) of protein surfactant mixtures by combining aspects of bulk interaction as well as interfacial properties.

Material and Methods

Materials

β -Lactoglobulin (BLG) (Lot number 030M7025V, containing 90 % protein based on DUMAS (N x 6.33 based on amino acids sequence from Uniprot database sequence P02754²⁸) was purchased from Sigma Aldrich (Zwijndrecht, The Netherlands). Sodium dodecyl sulphate (SDS) was obtained from Merck (Schiphol-Rijk, The Netherlands). MilliQ grade water (Millipore, EMD Millipore Corp., Billerica, MA, USA), free of surface active contaminants was used in all experiments (resistivity 18.6 M Ω cm, total organic carbon 3 ppb and surface tension 72.5 ± 0.5 mN m⁻¹ at 20 °C).

Sample preparation

Stock solutions of BLG (0.109 mM) and SDS (10.9 mM) were made by separately dissolving BLG and SDS in sodium phosphate buffer (pH 7.0, 10 mM), respectively. Solutions were prepared 30 - 120 minutes before use by mixing both stock solutions and buffer, while stirring slowly (without foaming) for 15 minutes at room temperature. The final protein concentrations of the solutions were 1 mg mL⁻¹ (54.5 μ M) BLG with different MR of SDS. The pH of the solutions was controlled and adjusted to pH 7.0 by adding aliquots of 1 M NaOH or 1 M H₃PO₄ to the solution. In all experiments, the concentration of BLG was kept constant at 1 mg mL⁻¹ (54.5 μ M), unless stated otherwise. Sample solutions were named according to the molar ratio of SDS to BLG. This is denoted as MR X, where X is the ratio of the SDS concentration (μ M) over a fixed BLG concentration at a (54.5 μ M). The solutions containing pure SDS are named for the concentration of SDS, equivalent to the SDS-BLG mixtures (EC). This is denoted as EC W, where W is the ratio of the SDS concentration (μ M) divided by 54.5 μ M. The MRs were chosen in a way that all concentrations of SDS used in the experiments were below the critical micelle concentration of SDS at 20 °C ($8 \cdot 10^{-3}$ M).

Chapter 4

Foam experiments

Foam of BLG-SDS solutions (1 mg mL⁻¹ protein concentration, 10 mM sodium phosphate buffer pH 7.0) was prepared by sparging nitrogen through a metal frit (60 mm diameter, pore size 27 ± 2 µm, 100 µm distance between centres of pores, square lattice) in an automated foaming device (Foamscan, Teclis IT-Concept, Longessaigne, France). The flow rate of gas was 400 mL min⁻¹ and the maximum foam volume was 600 cm³. The decay of the foam was monitored by a camera and the foam volume was calculated from image analysis performed by software provided with the Foamscan. The time it took the foam to decay to half of the initial volume was used as an indicator for the foam stability; denoted the foam half-life or $t_{1/2}$. Reported values of $t_{1/2}$ are averages of at least six individual foam measurements. Foam experiments were performed at 20 °C.

Drop tensiometry

Interfacial tension measurements were performed using an automated drop tensiometer (ADT) (Tracker, Teclis, Longessaigne, France) at 20 °C²⁹. A bubble of air (5 µL) was formed by a computer controlled syringe on the tip of a curved needle in solutions containing BLG (1 mg mL⁻¹) and corresponding amounts of SDS. The interfacial tension was calculated by analysis of the shape of the air bubble performed by software provided with the ADT. Changes of the surface tension are expressed as surface pressure, which is the surface tension (mN m⁻¹) of sodium phosphate buffer (pH 7, 10 mM, 71.8 ± 0.5 mN m at 20 °C) minus surface tension of each sample solution ($\Pi = \gamma_{\text{buffer}} - \gamma_{\text{BLG-SDS solution}}$) (mN m⁻¹).

The complex dilatational modulus (E_d) was measured by subjecting a bubble to a change in interfacial area ($dA/A = 10\%$) with a frequency of 0.1 Hz for a cycle of 50 seconds followed by a rest period of 50 seconds over a period of 1 hour. E_d is the complex viscoelastic modulus (mN m⁻¹), which consists of a storage modulus (E') and a loss modulus (E'') as described by³⁰. The moduli can be calculated from the complex modulus with equation 1 and 2.

$$(1) \quad E' = E_d \cdot \cos(\delta)$$

and

$$(2) \quad E'' = E_d \cdot \sin(\delta)$$

To investigate the dependence of interfacial and bulk composition, bulk exchange experiments were performed. Similar bulk exchange experiments have been described elsewhere^{19, 31}. In this case, a drop of 9 µL of BLG (1 mg mL⁻¹) or SDS or BLG-SDS mixtures was formed at the end of a coaxial double capillary needle. The droplet was equilibrated for 3600 s, while interfacial tension and dilatational elastic modulus were measured. After the equilibration, the bulk liquid of the droplet was exchanged with 1 mL of fresh sodium phosphate buffer (pH 7, 10 mM). The buffer was introduced through the inner part of the double capillary needle. At the same time, the injected volume was removed through the outer part of the needle. In this way, the total surface area of the droplet was kept within 10 % of the initial surface area. After the bulk exchange, the interfacial tension and dilatational elastic modulus were determined again. The detection limits for surface pressure measurements were 0.06 mN m. The detection limit of complex dilatational moduli with a minimum $1/AdA$ 0.135 was 0.44 mN m⁻¹. Π and E_d values after 1 hour of adsorption are denoted as Π_{1h} and E_{d1h} . Experiments were performed in duplicate and

Identifying changes in chemical, interfacial and foam properties of BLG-SDS mixtures

values of the complex dilatation elastic modulus are expressed as mean of the duplicates. Standard deviations between replicates for surface pressure experiments were less than ± 0.5 mN m and for the complex dilatational modulus less than ± 1.5 mN m.

Mass spectrometry

SDS and BLG were dissolved in water (MilliQ grade) and combined to yield a protein concentration of 2 mg mL^{-1} and molar ratios MR 0.5, 1, 1.5 and 2. The protein concentration was increased from 1 mg mL^{-1} as used in other experiments, to 2 mg mL^{-1} to amplify the signal intensity in the mass spectrometer. The solutions were directly infused into the ionization source of a Synapt mass spectrometer (ESI-TOF-MS, Waters, Elstree, UK) at a flow rate of $5 \mu\text{L min}^{-1}$. The sample was analysed in positive ion mode with a cone voltage of 2.95 kV, a source temperature of 120°C and a desolvation gas (Argon) flow rate of 800 L h^{-1} . The time of flight detector was calibrated with sodium iodide. Accurate mass of the protein parent ion was determined by a maximum entropy deconvolution algorithm, assuming a Gaussian distribution of ions. For clarity, displayed curves have been smoothed (mean of ten points, 10 times) after deconvolution.

Isothermal titration calorimetry

Binding of SDS to BLG was investigated by isothermal titration calorimetry (ITC) according to a modified protocol of Bohin *et al.*³². A microcalorimeter (ITC₂₀₀, GE Healthcare, Piscataway, NJ, USA) was used to titrate SDS solution (5.45 mM in 10 mM sodium phosphate buffer, pH 7.0) stepwise into BLG at 20°C . The BLG solution ($54.5 \mu\text{M}$) in the cell was stirred at 600 rpm to ensure optimal mixing of the SDS in the measuring cell. The first titration was $0.8 \mu\text{L}$ of SDS solution, each titration afterwards was $1.2 \mu\text{L}$ SDS solution was injected, followed by an equilibration period of 120 seconds until the final concentration of SDS was reached corresponding to an MR of 2. The area under the heat flow curve was integrated to obtain the total enthalpy change (ΔH) per injection. Each experiment was corrected with respective titration of SDS solution into buffer. A model assuming one set of identical (non-interacting) binding sites was fit to the integrated curve with a non-linear regression procedure with ITC data analysis software add in (GE Healthcare, Piscataway, NJ, USA) for the Origin software suite (Origin 7.0, OriginLab Corp., Northampton, MA, USA)^{33, 34}. The model used the theoretical stoichiometry ($n [-]$), which corresponds to the number of binding sites, the binding constant ($K [\text{M}^{-1}]$), and the binding enthalpy ($\Delta H [\text{kJ mol}^{-1}]$) as fitting parameters.

Circular dichroism

Sample solutions containing BLG and/or SDS were prepared and diluted for far UV CD and near UV CD with sodium phosphate buffer (pH 7.0, 10 mM) to yield a protein concentration of 0.1 mg mL^{-1} and 1 mg mL^{-1} and SDS at different MR, respectively. Sample solutions were placed in a cuvette of 1 mm and 10 mm path length for far UV and near UV CD respectively. The far and near UV CD spectra were recorded from 260 nm to 190 nm and from 350 nm to 280 nm respectively. 32 spectra were recorded in a spectropolarimeter (J 715, Jasco, Easton, MD, USA) at a scan rate of 100 nm min^{-1} , 0.2 nm

Chapter 4

resolution and 1 nm bandwidth. The recorded spectra were averaged and corrected for blank spectra of cuvettes containing buffer and corresponding amounts of SDS.

Secondary structural elements of the protein estimated from far UV CD spectra by using a non-linear least squares fitting procedure with reference spectra as described elsewhere³⁵.

The ellipticity signal from the spectropolarimeter was converted to molar ellipticity Θ_{mol} (mdeg cm² dmol⁻¹) (equation 3)

$$(3) \quad \Theta_{mol} = \frac{100 \Theta_{obs}}{d m}$$

where Θ_{obs} is the observed ellipticity (deg), d is the path length of the cuvette (cm) and m is the protein concentration (mol L⁻¹).

Determination of unfolding temperature

A temperature trace was performed from 20 °C to 106 °C at a heating rate of 2 °C min⁻¹ at a wavelength of 205 nm sample solutions of BLG and SDS (C_{prot} = 0.1 mg mL⁻¹ in sodium phosphate buffer pH 7.0, 10 mM) were measured during heating. Cuvettes (path length 0.1cm) containing the sample solutions were heated in the spectropolarimeter (J 715, Jasco). A normal distribution model was fitted to the obtained data and the average was used as indicator for the unfolding temperature of the protein (T_D).

Calculation of the weighted average of foam and interfacial properties

In the absence of interaction effects (synergistic or antagonistic), the foam stability of a mixed systems is expected to be described by the weighted average of the contribution of both compounds in the mixture. The weighted average (\overline{WA}) of foam stability as well as the interfacial properties Π and E_d was calculated as with equation 4

$$(4) \quad \overline{WA} = \frac{MR \cdot R_{SDS} + R_{BLG}}{MR + 1}$$

where MR is the molar ratio and R_{SDS} and R_{BLG} are the response (e.g. $t_{1/2}$, Π or E_d) for pure SDS or BLG, respectively.

Results and discussion

Foam stability of BLG-SDS mixtures

The foam stability of the pure BLG solution (1 mg mL⁻¹, MR 0) is the highest of all experiments with a foam half-life $t_{1/2}$ = 315 ±65 minutes (figure 4.3 A). For pure SDS solutions of EC 1 and EC 2, the sparged bubbles directly coalesced after formation. Hence, no foam was formed. The lowest concentration that produced the desired foam volume was EC 5 with a $t_{1/2}$ = 9.8 ±1.5 minutes. The foam half-life of pure SDS solutions further increased linearly with increasing EC (SDS concentration) to $t_{1/2}$ = 28.2 ±4.4 minutes at EC 20 and $t_{1/2}$ = 218.7 ±32.2 minutes at EC 100. The foam stability of BLG-SDS mixtures already shows a strong decrease at the lowest investigated MR 0.5, compared to that of pure BLG. With increasing MR, $t_{1/2}$ decreases drastically from $t_{1/2}$ = 217 ±53.3 minutes at MR 0.5 to $t_{1/2}$ = 44.2 ±3.7 minutes at MR = 20, where the lowest foam stability is reached.

Identifying changes in chemical, interfacial and foam properties of BLG-SDS mixtures

For $MR > 20$, the foam stability increases with increasing MR to $t_{1/2} = 250.1 \pm 77$ minutes at MR 100.

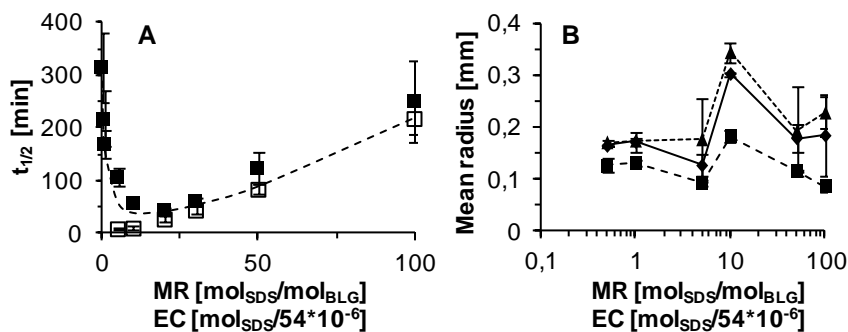


Figure 4.3: A) Foam half-life time ($t_{1/2}$) over MR for mixtures of BLG-SDS (■) and concentrations of SDS EC (□). The dashed line is the weighted average of foam stability of BLG-SDS mixtures and SDS. Error bars show deviation from mean for $N = 6$. B) Mean bubble radius after 1 (■), 5 (◆) and 10 (▲) minutes. The dashed lines are guides for the eye. Error bars indicate standard deviation between replicates.

The decrease of the stability from MR 0 to MR 10 is also represented by a sudden increase in mean bubble radius. Increasing MR further leads to a decrease in mean bubble radius (figure 4.3 B). In contrast to the linear increase of foam stability of SDS, the foam stability of BLG-SDS mixtures shows a minimum of $t_{1/2}$ at MR 20. If a basic, non-interacting model is used to explain this observation, this minimum is surprising since the overall concentration of surface active compounds is increasing. The deviation from a continuous increase in foam stability with increasing surface active material hints at molecular interaction between the protein and the surfactant. From $MR > 20$ the foam stability of the mixtures follows the same trend as the foam stability of pure SDS at corresponding EC. A similar minimum of the foam stability as a function of concentration of mixed solutions of other proteins with Tween 20, a non-ionic surfactant, has been reported before¹. In mixed systems of BLG, α -lactalbumin and Tween 20 similar minima were observed at MR 2 and MR 5, respectively. These minima occur at lower MR than the MR that is found in this study. Tween 20, is a non-ionic surfactant, which could explain the different numerical values of the minimum in foam stability.

Interfacial properties of BLG-SDS mixtures

The surface pressure (Π_1) of BLG increases over time and reaches a plateau value of 19.5 mN m^{-1} after an adsorption time of 3600 seconds (figure 4.4 A dashed line). The Π_{1h} value of SDS increases with increasing SDS concentration from 3 mN m^{-1} at EC 1 until Π_{1h} levels off at 38.8 mN m^{-1} at EC 50. Further increase to EC 100, which is 68 % of the concentration of the CMC of SDS, increases the surface pressure only slightly. This levelling off has previously been reported³⁶. The Π_{1h} - MR curve of the mixtures shows an increase from 22 mN m^{-1} up to 34 mN m^{-1} between MR 0.5-10. A plateau of the Π_{1h} - MR curve is observed between MR 10 and MR 20. With increasing MR, the curve increases slightly from 34 mN m^{-1} at MR 20 until 38.5 mN m^{-1} at MR 100. The largest increase of Π_{1h}

in SDS-BLG mixtures occurs at low MR, between MR 0.5 and MR 5, which is denoted by the steepest increase of $d\Pi_{1h}/dMR$.

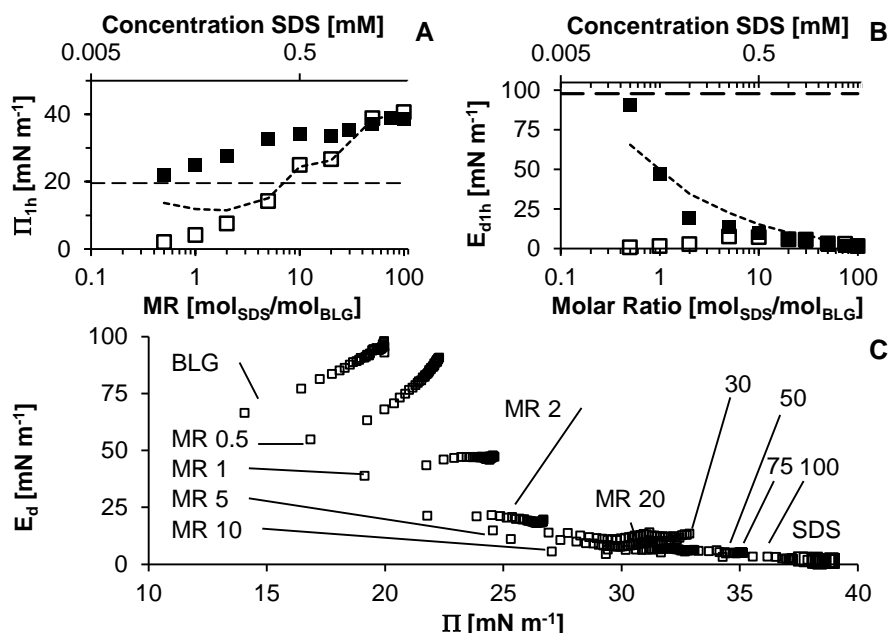


Figure 4.4: A) Π_{1h} as a function of the MR for BLG-SDS mixtures (■) and as a function of the EC for SDS (□). B) E_{d1h} as a function of the MR for BLG-SDS mixtures (■) and a function of the EC for SDS (□). Dashed lines indicate Π_{1h} and E_{d1h} of pure BLG, respectively and are a guide to the eye. Dotted lines are the calculated weighted average (WA) of BLG and SDS data. C) E_d over Π curve. Data points are the mean of two measurements and deviated <0.5

Such an increase of Π_{1h} with MR as measured here has also been observed before for BLG-SDS²⁷, and WPI-SDS²⁶ mixtures. Because of the high Π_{1h} values at MR 100, it is likely that almost exclusively SDS adsorbs at the interface. This observation is confirmed by another study the interfacial rheology of BLG-SDS mixtures³⁶. A recent study on the interfacial composition of BLG-SDS mixtures confirms the hypothesis. They report that from MR 1.7 onwards competitive adsorption of a BLG-SDS complex and SDS occurs, while at higher SDS concentrations the surface is entirely covered by SDS²². The results show a continuous increase of Π_{1h} for BLG-SDS mixtures over the whole range of molar ratios, while the foam stability shows a minimum at MR 20. This is in contrast to the general assumption that increasing Π_{1h} values are positively correlated with foam stability and indicates that Π alone is not an adequate predictor for foam stability. To quantify this change of interfacial interaction, the complex dilatation elastic modulus after 1 hour adsorption (E_{d1h}) is determined (figure 4.4 B). The sample containing pure BLG (MR 0) shows a continuous increase of E_{d1h} over time until it reaches a value 98 mN m⁻¹ after 1 hour (figure 4.4 B, dashed line). The SDS solution EC 100 has a low E_{d1h} 1.5 mN m⁻¹. The BLG-SDS mixtures show a decrease of E_d with increasing MR. The values start close to those of pure BLG, and then decrease to values typically observed for SDS covered interfaces. The

Identifying changes in chemical, interfacial and foam properties of BLG-SDS mixtures

curve of E_{d1h} over MR of the mixtures is initially characterized by a steep decrease of E_{d1h} with MR from E_d 91 mN m⁻¹ at MR 0.5 to an E_{d1h} of 6 mN m⁻¹ at MR 20. From MR 20 to MR 100, E_{d1h} is slowly decreasing, from 5 mN m⁻¹ to 1 mN m⁻¹, which is similar to the values observed for SDS alone. The continuous decrease of E_{d1h} with increasing MR seems to be a typical behaviour of protein surfactant systems and has been described earlier for BLG-SDS systems^{37, 38} as well as for SDS-ovalbumin³⁹ and Do-TAB- β -casein⁴⁰. The low E_{d1h} at high surfactant concentration (MR 50+) is usually explained by the gradual displacement of proteins from the interface^{36, 41}. A further analysis of E' and E'' (table 4.1) confirmed the conclusions based on the behaviour of the complex modulus. The phase angle (δ) increases from 4° at MR 0 up a maximum of 76° at MR 50 (table 4.1). A further increase of the MR results in a decrease of the δ to 53° at MR 100. The low δ below MR 10 indicates a predominantly elastic behaviour of the interface, which is typical for protein dominated interfaces⁴⁰. At higher MR where δ is larger than 45° the interface behaves more viscous, which is typical for surfactant covered interfaces⁴¹.

Table 4.1: Summary of values for interfacial rheology for BLG-SDS mixtures at different MR

Molar ratio	MR	mol_{SDS}/mol_{BLG}	0	0.5	1	2	5	10
Complex modulus	E_{d1h}	mN m ⁻¹	99	101	47	19	12	10
Phase angle	δ	°	4	4	8	12	24	10
Storage modulus	E'	mN m ⁻¹	99	101	47	19	11	10
Loss modulus	E''	mN m ⁻¹	7	7	7	4	5	2
Molar ratio	MR	mol_{SDS}/mol_{BLG}	20	30	50	75	100	SDS
Complex modulus	E_{d1h}	mN m ⁻¹	6	5	2	1	1	1
Phase angle	δ	°	61	37	76	72	53	49
Storage modulus	E'	mN m ⁻¹	3	4	1	0	1	1
Loss modulus	E''	mN m ⁻¹	5	3	2	1	1	1

The change from elastic behaviour towards viscous behaviour with increasing MR is an indication that the interfacial composition is changing from a protein or protein-surfactant covered interface towards an interface covered solely by LMWS. The change of interfacial composition from a protein solution towards a surfactant solution is clearly depicted in the E_{d1h} over Π_{1h} curve (figure 4.4 C). For MR 0 the curve shows typical protein like behaviour of correlated increase of surface pressure and complex dilatation elastic modulus. With increasing MR, the curves change from protein to a mixed interface. Here, both proteins and LMWS are present. The shape of the curves in the intermediate MR could also be attributed to unfolded protein interface⁴². At MR > 50 the E_{d1h} over Π_{1h} curves of the mixtures are similar to pure surfactant solutions, which show large increase of Π_{1h} and almost static E_{d1h} . The data on interfacial properties supports a model that includes interactions and binding of SDS to BLG as well as co-adsorption of both substances at low MR and a surfactant covered interface at high MR (figure 4.2 B).

Individual contributions of proteins and LMWS

The most basic model to describe the foam stability and interfacial properties of protein-surfactant mixtures is to assume that the system consists of two non-interacting species (figure 4.2 A). In such a system, the observations would be colligative and correlated to the used molar ratio between the compounds. This would mean that the observed properties could be predicted by the combination of the individual contributions of pure SDS and BLG. Therefore, the weighted average (WA, dotted lines in figure 4.3 and 4.4 A and B) of the foam properties as well as that of the interfacial properties of the BLG-SDS mixtures were calculated based on the foam and interfacial properties of pure BLG and SDS, for each molar ratio. The WA of foam stability of the protein-surfactant mixtures is quite close to the observed foam stability of the mixture (figure 4.3 A, dotted line). This may indicate that indeed the foam properties of the mixture can be predicted as an addition of the individual contribution of the LMWS and the proteins. For the interfacial properties (Π_{1h} and E_{d1h}), the WA does not correspond to the observations (figure 4.4 A and B, dotted lines). This shows that the intermolecular interactions have an influence on the interfacial properties of the mixture (i.e. of the complexes), as described in the second interfacial model (figure 4.2 B). The importance of the changes in interfacial properties, due to the interactions is not directly clear. Specifically, when the foam stability is plotted against the interfacial properties Π_{1h} and E_{d1h} (figure 4.5 A and B), no linear correlation is observed. In addition, since the foam stability was found to be closely approximated by the WA of foam stability, this can be taken as an indication that additional factors, other than the interfacial properties, influence the foam stability.

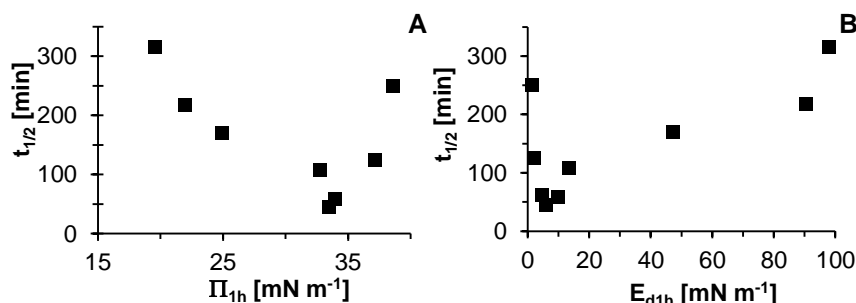


Figure 4.5: Correlation of foam stability with Π_{1h} (A) and E_{d1h} (B) of BLG-SDS mixtures.

For other systems, it has previously been described that foam stability was not only due to interfacial properties, but also due to contributions from non-adsorbed molecules⁴³.

Interaction of BLG and SDS in bulk solution

The non-covalent binding of SDS to BLG is analysed by direct infusion mass spectrometry. MR 0 analysed in negative ionization mode showed, after deconvolution, the accurate masses of BLG to be 18355.9 ± 1.9 Da and 18269.8 ± 1.9 Da for the genetic variants A and B, respectively (no further data shown). In the m/z spectrum of BLG solutions in positive mode, the nine charged ion is the most abundant species of ions. The spectrum of the 9

charged ion shows the native protein in an m/z range from 2050 until 2124 (figure 4.6 A). The onset of the pure BLG peak at 2050.8 corresponds to the mass of BLG with 5 Na^+ adducts. The most abundant peak in the m/z range for pure BLG is a 15 times sodiated ion at m/z 2076. The m/z spectra of mixed BLG-SDS solutions show peaks in the region of BLG (2050-2124 m/z).

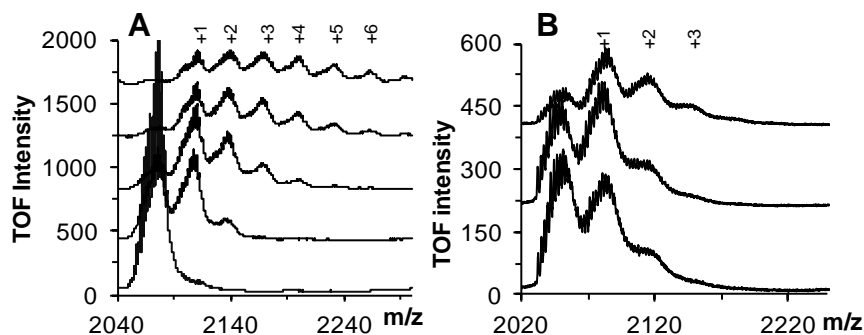


Figure 4.6: A) Mass spectra of the 9 charged ion of BLG-SDS at different MR. Each successive MR curve is displayed with an offset of 500 units. B) Mass spectra of 9 charged ion of dialysed BLG-SDS complexes at different MR after dialysis. Each successive MR curve is displayed with an offset of 200 units. The modification of BLG by n molecules of SDS is indicated as $+n$ above the respective peak.

Additionally, the spectrum shows two peaks in the range from 2090 to 2115 and from 2124 until 2148 m/z . Those two peaks correspond to the mass of BLG with added SDS (M_w SDS = 288 Da). Solutions of higher MR show more peaks of BLG-SDS adducts. In sample MR 1, three different BLG-SDS peaks and in MR 1.5 and 2, up to four SDS molecules were identified binding to BLG. The amount of unmodified BLG decreases with increasing MR from MR 0.5 onwards and at MR 1 the peak of unmodified BLG is barely visible. The increasing number of identified peaks correlates with weakening of the TOF intensity, which could be caused by the suppression ionization due to unbound SDS in positive ionization mode. The weakened intensity limits the detection range of mixed BLG-SDS solutions to a MR of up to MR 2. To avoid the suppressing effect of unbound SDS molecules, dialysed BLG-SDS mixtures were analysed under the same conditions (figure 6 B). In the dialysed samples, a similar pattern to non-dialysed BLG-SDS mixtures is seen, confirming that the SDS does indeed bind to BLG in solution. To supplement the findings on the binding of multiple SDS molecules per BLG molecule, the heat flow during titration of SDS into BLG solution was measured by ITC. Each injection of SDS titrated in BLG (figure 4.7 A, black line) produces a peak. A model with one type of binding site was fitted to the integrated data (figure 4.7 B). It yielded a binding stoichiometry of 0.76 ± 0.005 and a total heat change (ΔH) of $-1.4 \cdot 10^4 \text{ J mol}^{-1}$. The affinity of binding ($K = 6.9 \cdot 10^5 \text{ mol}^{-1}$) is derived from the slope of the steep part of the binding isotherm.

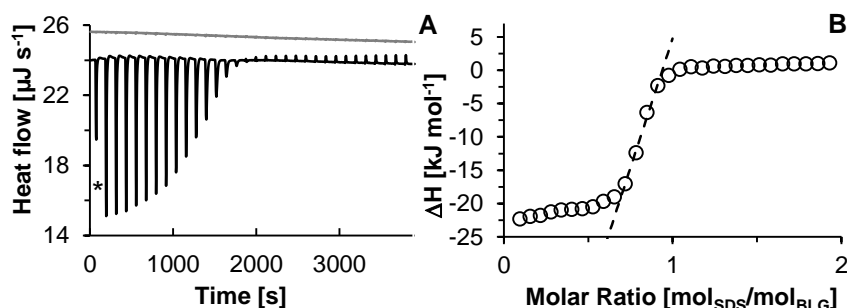


Figure 4.7: A) Heat flow after addition of SDS into BLG (black line) and into buffer (grey line). The peaks correspond to injections of 1.2 μL SDS (5.45 mM) into BLG or buffer. The injected volume of the first injection was 50 % less than the rest of the injections. The corresponding peak is denoted by an *. B) Integrated binding isotherm of SDS titrated in BLG solution. The dotted line is a guide for the eye to illustrate the affinity constant of SDS towards BLG.

At molar ratios above 1.1, saturation of the high affinity binding site is indicated by the diminishing heat change. The observed binding stoichiometry and affinity constant of BLG towards SDS fit well with values reported in other studies under similar conditions (pH 7, 15-25 °C)^{22, 44}. The total heat change of $1.4 \cdot 10^4 \text{ kJ mol}^{-1}$ shows that the interaction energy is below the energy needed for covalent interaction and should be related to either hydrophobic or electrostatic interaction. These are roughly of the same order of magnitude at the used temperature and cannot be distinguished⁴⁵. Studies investigating the binding of LMWS to BLG as ligands usually report that the LMWS are bound to the hydrophobic calyx at low MR. This binding to the calyx might not be true for all LMWS however. It has been shown that dodecyl trimethyl ammonium bromide binding to BLG did not hinder the binding of retinol to BLG⁴⁶. Their results showed that BLG could bind two different ligands at the same time; one ligand inside the hydrophobic calyx, the other ligand to another binding site on the outside. In the case of BLG and SDS, it would allow binding of more than one SDS molecule. At this moment, it is unclear, why in the ITC only one binding site shows a high binding affinity while the others are not detected. Based on these results we conclude the presence of attractive interactions between BLG and SDS leading to binding of several SDS molecules to BLG. At the same time, the amount of free BLG is decreasing. One of those bound SDS molecules binds to a high affinity binding site, which could be the hydrophobic calyx. The presence of multiple, discretely modified BLG-SDS peaks, indicates a distribution of differently modified BLG molecules with up to six (identifiable) SDS molecules attached. These findings support an interfacial model, which includes the interaction of proteins and LMWS (figure 4.2 B).

Changes of protein structure at different MR

Structure of BLG mixed with SDS

To determine the effects of SDS binding on BLG, far and near UV CD spectra were recorded at different MR. The far UV CD spectra of BLG at different MR all show the same crossing of the x-axis at 204 nm and a minimum at 215 nm (figure 4.8 A). The dominant

structural elements in BLG are in β -sheets (60 %) and random coil (25 %). These spectra are typical features of native BLG^{46, 47}. The effect of SDS on the tertiary structure of BLG mixed with SDS was investigated by near UV CD (figure 4.8 B). The spectrum of MR 0 shows a negative Θ_{mol} in the region commonly associated with the tryptophan residues (290-300 nm). The spectra of MR 20 - 50 show an increase of Θ_{mol} in the tryptophan region from -5 to 0. At MR to 50 or 100, no further effect on Θ_{mol} could be seen in the spectra.

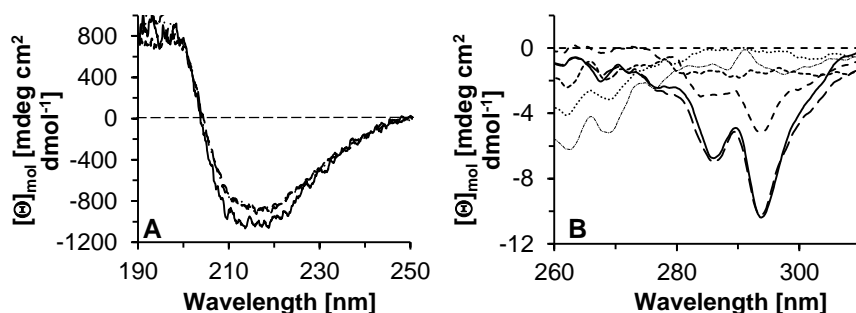


Figure 4.8: Far (A) and near (B) UV circular dichroism spectra of BLG mixed with SDS MR 0 (—), MR 10 (---), MR 20 (-----), MR 30 (.....), MR 50 (.....) and MR 100 (-----).

This increase is associated to change in polarity of the environment, which is caused by changes in the tertiary structure. A negative Θ_{mol} in the tryptophan region is typical for pure BLG and has been reported before⁶. The change of Θ_{mol} hints at changes in tertiary structure of the BLG molecule resulting in exposure of hydrophobic amino acids to a polar solvent. Similar unfolding of tertiary structure with increasing MR up to the total loss tertiary structure at MR < 100 have been observed before⁶. Overall, binding of SDS to BLG shows no change of secondary structural composition of BLG in the investigated MR region, while tertiary structure unfolding occurs between MR 20 and MR 50.

Thermal stability of BLG

In order to investigate whether the modification of BLG by SDS had an effect on structural stability, the unfolding temperatures of BLG in presence of SDS was determined by measuring the circular dichroism while heating the sample to 106 °C. The midpoint of unfolding (T_D) increased with increasing MR from 68.1 °C at MR 0 up to 89.8 °C at MR 50 (table 4.2). The T_D of MR 0 is lower than expected, since in literature the unfolding temperature BLG (determined by DSC) is between 70 °C and 75 °C^{27, 48}.

Chapter 4

Table 4.2: Unfolding temperatures (T_D) of BLG at different MR.

MR	T_D	MR	T_D
$[mol_{SDS}/mol_{BLG}]$	$[^{\circ}C]$	$[mol_{SDS}/mol_{BLG}]$	$[^{\circ}C]$
0	68.1	10	83.6
0.5	70.4	20	84.4
1	74.2	50	89.8
2	79.8	100	89.5
5	81.0	-	-

The difference between the results of this study and literature values originates in the difference between DSC and CD heat trace. While DSC measures changes in secondary and tertiary structure of the molecule the CD heat trace measures shifts in secondary structure only. This discrepancy between unfolding temperatures obtained by DSC and heat trace CD has been described previously⁴⁷. Although changes in the tertiary structure occur with increasing MR, T_D is increasing as well indicating a stabilizing effect of SDS on its host molecule BLG. The data on structural changes as function of the MR indicates that the earlier mentioned model (figure 4.2 B) in which BLG is bound to SDS but keeps its structure has to be revised. The fact that the tertiary structure of BLG is unfolding with increasing MR should be included in the interfacial model: BLG molecules which are present in the interface at those MR are not in their native globular form but are modified or even unfolded.

Composition of the air/water interface of BLG-SDS mixtures

Some studies suggest that the interfacial composition of protein-surfactant mixtures depend on the MR e.g.^{20, 49}. Surface pressure values close to that of pure surfactant indicated that only surfactant molecules are adsorbed and no protein or protein-surfactant complexes would be present. To investigate the interfacial composition, the interfacial properties (Π_{1h} and E_{d1h}) were measured before and after exchanging the bulk liquid of a droplet of the BLG-SDS mixtures, BLG and SDS respectively. During the exchange, the bulk liquid is removed while fresh, surfactant free, buffer is introduced into the droplet. This liquid exchange step should eliminate all free LMWS from the bulk of the droplet and show the interfacial properties of the adsorbed layer alone. Π_{1h} and E_{d1h} values of pure BLG (MR 0) were not significantly influenced by the exchange step (figure 4.9 A and B). This shows that BLG is irreversibly adsorbed to the air-water interface, at least when decreasing the protein concentration in the bulk solution. After the exchange, the pure SDS solution without protein shows the lowest surface pressure (6 mN m^{-1}). This shows that most of the SDS was removed from the interface.

Identifying changes in chemical, interfacial and foam properties of BLG-SDS mixtures

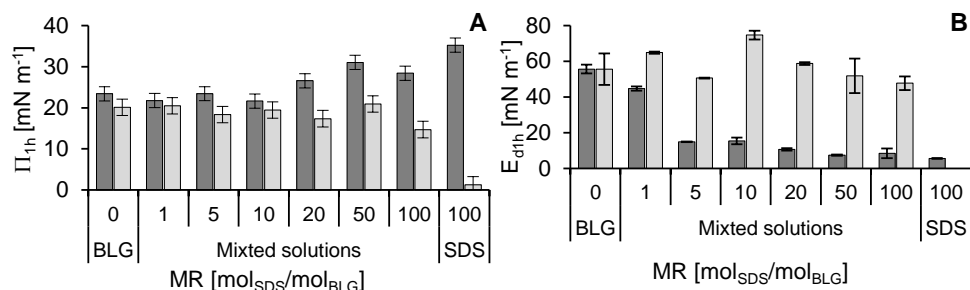


Figure 4.9: Π_{1h} (A) and E_{d1h} (B) of the air/water interface of BLG-SDS solutions before (dark grey) and after (light grey) replacing the solution inside the droplet by buffer. Error bars indicate deviation between replicates.

The desorption of LMWS and subsequent removal from the bulk liquid of the droplet has been reported elsewhere⁵⁰. After the exchange, E_{d1h} values of the SDS sample could not be determined, confirming the desorption of the LMWS. For BLG-SDS mixtures up to MR 10, Π_{1h} stays unchanged by the exchange, which shows that the interface is mainly covered in protein and protein-surfactant complexes. Π_{1h} is expectedly higher at higher molar ratios (MR 20, MR 50 and MR 100) before the exchange than Π_{1h} at MR 0. After the exchange, Π_{1h} drop to values similar to those for MR 0. This shows the effectiveness of the exchange as well as that the remaining adsorbed material is proteinaceous. The E_{d1h} of BLG-SDS mixtures before the exchange decreases with increasing MR. At MR higher than 10 the E_{d1h} values before the exchange plateau at a value between 10 and 5 mN m⁻¹, while after the exchange, E_{1h} values increase and reach values similar to MR 0. This is another indication that the exchange removed free surfactant and the residual absorbed material are protein and protein-surfactant complexes. From these findings, it is deduced that proteins are not displaced from the interface during the exchange since interfacial interactions between these proteins still take place. At high molar ratios, the huge amounts of free SDS suppress the interfacial properties of the protein, so that they are drowned out by the effect of the LMWS. The effect of SDS on the E_{d1h} of BLG at higher MR explains the correlation of the foam stability of BLG-SDS mixtures at MR >20, which is similar to that of pure surfactant.

Adapting the model of protein surfactant interaction in foam and interface

When combining measurements on the bulk, the interface and the foam of BLG-SDS mixtures, it became apparent that an increase in the surfactant concentration leads to changes at different MR (table 4.3). At molar ratios around MR 1, the largest changes of bulk properties (binding and change of unfolding temperature) were observed. When increasing the surfactant concentration to MR 20, the presence of differently modified BLG-SDS complexes were identified. In the MR range up to MR 20, the largest changes were observed in the interfacial and foam properties of the mixtures. At MR > 20, where

Chapter 4

also protein unfolding was observed, the interfacial properties of the mixtures cannot be distinguished from those of pure surfactant.

Table 4.3: Table summarizing key molar ratios on foam, bulk and interfacial properties of BLG-SDS mixtures

	Molar Ratio	Experiment	Observation
Foam	0.5	Foam	Largest $dt_{1/2}/dMR$
	10	Foam	Lowest foam stability
Bulk interaction	0.8	ITC	Reaction stoichiometry
	1	ITC	Saturation
	2	CD 3rd	Largest dT_D/dMR
	20	CD 3rd	Begin change
Interfacial properties	1	E_{d1h}	Largest dE_d/dMR
	5	Π_{1h}	Largest $d\Pi/dMR$
	50	Π_{1h}	No difference between mixture and surfactant
	50	E_{d1h}	No difference between mixture and surfactant

Although the interfacial pressure continuously increases with increasing MR, the resulting foam of the protein-surfactant mixture is less stable than the foam of pure protein. The foam stability depends strongly on the MR, especially below MR 20. It is proposed that in the range from MR 1 to MR 20, the protein molecules are saturated and that from MR 20, the interface is mainly covered by the surfactant. From these observations, it becomes clear that the interaction and subsequent structural changes in protein structure need to be taken into account when describing the properties of protein-surfactant mixtures. Consequently, the previously discussed models (figures 4.2 A and B) need to be adjusted to these observations. It is proposed that a model about functional properties of protein-surfactant mixtures should include (1) protein-LMWS complexation, (2) changes of protein structure with increased MR and (3) the presence of protein and or protein-surfactant complexes at the interface at MR > 20 (figure 4.2 C). In this view, the behaviour of the system does not depend on the total concentration of surfactant or MR, but should be related to the degree of saturation of the protein by LMWS. It is expected that this view leads to better comparability and understanding of protein-surfactant mixtures in respect of the used LMWS.

References

1. Coke, M.; Wilde, P. J.; Russell, E. J.; Clark, D. C., The influence of surface composition and molecular diffusion on the stability of foams formed from protein/surfactant mixtures. *Journal of Colloid and Interface Science* **1990**, 138, 489-504.
2. Saint-Jalmes, A.; Peugeot, M. L.; Ferraz, H.; Langevin, D., Differences between protein and surfactant foams: Microscopic properties, stability and coarsening. *Colloids and Surfaces A: Physicochemical and Engineering Aspects* **2005**, 263, 219-225.

Identifying changes in chemical, interfacial and foam properties of BLG-SDS mixtures

3. Otzen, D., Protein-surfactant interactions: A tale of many states. *Biochimica et Biophysica Acta (BBA) - Proteins and Proteomics* **2011**, 1814, 562-591.
4. Hansted, J. G.; Wejse, P. L.; Bertelsen, H.; Otzen, D. E., Effect of protein-surfactant interactions on aggregation of β -lactoglobulin. *Biochimica et Biophysica Acta (BBA) - Proteins and Proteomics* **2011**, 1814, 713-723.
5. Loch, J. I.; Polit, A.; Bonarek, P.; Olszewska, D.; Kurpiewska, K.; Dziedzicka-Wasylewska, M.; Lewiński, K., Structural and thermodynamic studies of binding saturated fatty acids to bovine β -lactoglobulin. *International Journal of Biological Macromolecules* **2012**, 50, 1095-1102.
6. Lu, R.-C.; Cao, A.-N.; Lai, L.-H.; Xiao, J.-X., Interactions of β -lactoglobulin with sodium decylsulfonate, decyltriethylammonium bromide, and their mixtures. *Journal of Colloid and Interface Science* **2006**, 299, 617-625.
7. Maldonado-Valderrama, J.; Patino, J. M. R., Interfacial rheology of protein-surfactant mixtures. *Current Opinion in Colloid and Interface Science* **2010**, 15, 271-282.
8. Rodríguez Patino, J. M.; Rodríguez Niño, M. R.; Sánchez, C. C., Protein-emulsifier interactions at the air-water interface. *Current Opinion in Colloid and Interface Science* **2003**, 8, 387-395.
9. Engelhardt, K.; Peukert, W.; Braunschweig, B., Vibrational sum-frequency generation at protein modified air-water interfaces: Effects of molecular structure and surface charging. *Current Opinion in Colloid and Interface Science* **2014**, 19, 207-215.
10. Stefaniu, C.; Brezesinski, G., X-ray investigation of monolayers formed at the soft air/water interface. *Current Opinion in Colloid and Interface Science* **2014**, 19, 216-227.
11. Penfold, J.; Thomas, R. K., Neutron reflectivity and small angle neutron scattering: An introduction and perspective on recent progress. *Current Opinion in Colloid and Interface Science* **2014**, 19, 198-206.
12. Vollhardt, D., Brewster angle microscopy: A preferential method for mesoscopic characterization of monolayers at the air/water interface. *Current Opinion in Colloid and Interface Science* **2014**, 19, 183-197.
13. Mackie, A. R.; Gunning, A. P.; Wilde, P. J.; Morris, V. J., Orogenic displacement of protein from the air/water interface by competitive adsorption. *Journal of Colloid and Interface Science* **1999**, 210, 157-166.
14. Stanimirova, R. D.; Marinova, K. G.; Danov, K. D.; Kralchevsky, P. A.; Basheva, E. S.; Stoyanov, S. D.; Pelan, E. G., Competitive adsorption of the protein hydrophobin and an ionic surfactant: Parallel vs sequential adsorption and dilatational rheology. *Colloids and Surfaces A: Physicochemical and Engineering Aspects* **2014**, 457, 307-317.
15. Dickinson, E., Adsorbed protein layers at fluid interfaces: interactions, structure and surface rheology. *Colloids and Surfaces B: Biointerfaces* **1999**, 15, 161-176.
16. Wilde, P.; Mackie, A.; Husband, F.; Gunning, P.; Morris, V., Proteins and emulsifiers at liquid interfaces. *Advances in Colloid and Interface Science* **2004**, 108-109, 63-71.
17. Wierenga, P. A.; Gruppen, H., New views on foams from protein solutions. *Current Opinion in Colloid and Interface Science* **2010**, 15, 365-373.
18. Walstra, P., Surface Phenomena. In *Physical Chemistry of Foods*, Marcel Dekker, Inc.: New York, NY, USA, **2003**; pp 316-396.
19. Dan, A.; Kotsmar, C.; Ferri, J. K.; Javadi, A.; Karbaschi, M.; Kragel, J.; Wustneck, R.; Miller, R., Mixed protein-surfactant adsorption layers formed in a sequential and simultaneous way at water-air and water-oil interfaces. *Soft Matter* **2012**, 8, 6057-6065.
20. Noskov, B. A.; Tikhonov, M. M., Effect of sodium dodecyl sulfate on dynamic surface properties of lysozyme solutions. *Colloid Journal* **2012**, 74, 248-253.
21. Dan, A.; Wüstneck, R.; Krägel, J.; Aksenenko, E. V.; Fainerman, V. B.; Miller, R., Adsorption and dilatational rheology of mixed β -casein/DoTAB layers formed by sequential and simultaneous adsorption at the water/hexane interface. *Langmuir* **2013**, 29, 2233-2241.
22. Engelhardt, K.; Weichsel, U.; Kraft, E.; Segets, D.; Peukert, W.; Braunschweig, B., Mixed layers of β -lactoglobulin and SDS at air-water interfaces with tunable intermolecular interactions. *The Journal of Physical Chemistry B* **2014**, 118, 4098-4105.
23. Fernández, M. C.; Sánchez, C. C.; Niño, R. R.; Rodríguez Patino, J. M., Penetration of β -lactoglobulin into monoglyceride monolayers. Dynamics, interactions, and topography of mixed films. *The Journal of Physical Chemistry B* **2006**, 110, 24212-24221.
24. Miller, R.; Alahverdijeva, V. S.; Fainerman, V. B., Thermodynamics and rheology of mixed protein-surfactant adsorption layers. *Soft Matter* **2008**, 4, 1141-1146.

Chapter 4

25. Blomqvist, B. R.; Ridout, M. J.; Mackie, A. R.; Warnheim, T.; Claesson, P. M.; Wilde, P., Disruption of viscoelastic β -lactoglobulin surface layers at the air-water interface by nonionic polymeric surfactants. *Langmuir* **2004**, *20*, 10150-10158.
26. Giroux, H. J.; Britten, M., Heat treatment of whey proteins in the presence of anionic surfactants. *Food Hydrocolloids* **2004**, *18*, 685-692.
27. Magdassi, S.; Vinetsky, Y.; Relkin, P., Formation and structural heat-stability of β -lactoglobulin/surfactant complexes. *Colloids and Surfaces B: Biointerfaces* **1996**, *6*, 353-362.
28. Uniprot P02754 (LACB_BOVIN) Reviewed, UniProtKB/Swiss-Prot. <http://www.uniprot.org/uniprot/P02754> (03.06.2014),
29. Wierenga, P. A.; Meinders, M. B. J.; Egmond, M. R.; Voragen, A. G. J.; de Jongh, H. H. J., Quantitative description of the relation between protein net charge and protein adsorption to air-water interfaces. *The Journal of Physical Chemistry B* **2005**, *109*, 16946-16952.
30. Benjamins, J.; Cagna, A.; Lucassen-Reynders, E. H., Viscoelastic properties of triacylglycerol/water interfaces covered by proteins. *Colloids and Surfaces A: Physicochemical and Engineering Aspects* **1996**, *114*, 245-254.
31. Miller, R.; Grigoriev, D. O.; Krägel, J.; Makievski, A. V.; Maldonado-Valderrama, J.; Leser, M.; Michel, M.; Fainerman, V. B., Experimental studies on the desorption of adsorbed proteins from liquid interfaces. *Food Hydrocolloids* **2005**, *19*, 479-483.
32. Bohin, M. C.; Vincken, J.-P.; van der Hijden, H. T. W. M.; Gruppen, H., Efficacy of food proteins as carriers for flavonoids. *Journal of Agricultural and Food Chemistry* **2012**, *60*, 4136-4143.
33. Ladbury, J. E.; Chowdhry, B. Z., Sensing the heat: the application of isothermal titration calorimetry to thermodynamic studies of biomolecular interactions. *Chemistry & Biology* **1996**, *3*, 791-801.
34. Freyer, M. W.; Lewis, E. A.; Correia, J.; Detrich, III, H., Isothermal titration calorimetry: Experimental design, data Analysis, and probing macromolecule/ligand binding and kinetic interactions. In *Methods in Cell Biology*, J., C.; Detrich, III, H., Eds. Academic Press: Waltham, MA, USA, **2008**; Vol. Volume 84, pp 79-113.
35. de Jongh, H. H.; Goormaghtigh, E.; Killian, J. A., Analysis of circular dichroism spectra of oriented protein-lipid complexes: toward a general application. *Biochemistry* **1994**, *33*, 14521-14528.
36. Pradines, V.; Krägel, J.; Fainerman, V.; Miller, R., Interfacial properties of mixed β -lactoglobulin-SDS layers at the water/air and water/oil interface. *The Journal of Physical Chemistry B* **2009**, *113*, 745-751.
37. Mackie, A. R.; Gunning, A. P.; Wilde, P. J.; Morris, V. J., Competitive displacement of β -lactoglobulin from the air/water interface by sodium dodecyl sulfate. *Langmuir* **2000**, *16*, 8176-8181.
38. Krägel, J.; O'Neill, M.; Makievski, A. V.; Michel, M.; Leser, M. E.; Miller, R., Dynamics of mixed protein-surfactant layers adsorbed at the water/air and water/oil interface. *Colloids and Surfaces B: Biointerfaces* **2003**, *31*, 107-114.
39. Seta, L.; Baldino, N.; Gabriele, D.; Lupi, F. R.; de Cindio, B., The effect of surfactant type on the rheology of ovalbumin layers at the air/water and oil/water interfaces. *Food Hydrocolloids* **2012**, *29*, 247-257.
40. Dan, A.; Gochev, G.; Krägel, J.; Aksenenko, E. V.; Fainerman, V. B.; Miller, R., Interfacial rheology of mixed layers of food proteins and surfactants. *Current Opinion in Colloid and Interface Science* **2013**, *18*, 302-310.
41. Wei, X.; Chang, Z.; Liu, H., Influence of sodium dodecyl sulfate on the characteristics of bovine serum albumin solutions and foams. *Journal of Surfactants and Detergents* **2003**, *6*, 107-112.
42. Noskov, B. A., Protein conformational transitions at the liquid-gas interface as studied by dilational surface rheology. *Advances in Colloid and Interface Science* **2014**, *206*, 222-238.
43. Wierenga, P. A.; van Norél, L.; Basheva, E. S., Reconsidering the importance of interfacial properties in foam stability. *Colloids and Surfaces A: Physicochemical and Engineering Aspects* **2009**, *344*, 72-78.
44. Gutiérrez-Magdaleno, G.; Bello, M.; Portillo-Téllez, M. C.; Rodríguez-Romero, A.; García-Hernández, E., Ligand binding and self-association cooperativity of β -lactoglobulin. *Journal of Molecular Recognition* **2012**, *26*, 67-75.
45. Israelachvili, J. N., *Intermolecular and surface forces*. 3 ed.; Academic Press (Elsevier): Santa Barbara, CA, USA, **2011**; p 674.
46. Taheri-Kafrani, A.; Asgari-Mobarakeh, E.; Bordbar, A.-K.; Haertlé, T., Structure-function relationship of β -lactoglobulin in the presence of dodecyltrimethyl ammonium bromide. *Colloids and Surfaces B: Biointerfaces* **2010**, *75*, 268-274.

Identifying changes in chemical, interfacial and foam properties of BLG-SDS mixtures

47. Broersen, K.; Voragen, A. G. J.; Hamer, R. J.; de Jongh, H. H. J., Glycoforms of β -lactoglobulin with improved thermostability and preserved structural packing. *Biotechnology and Bioengineering* **2004**, *86*, 78-87.
48. Wanninge, R.; Paulsson, M.; Nylander, T.; Ninham, B.; Sellers, P., Binding of sodium dodecyl sulphate and dodecyl trimethyl ammonium chloride to β -lactoglobulin: A calorimetric study. *International Dairy Journal* **1998**, *8*, 141-148.
49. Green, R. J.; Su, T. J.; Joy, H.; Lu, J. R., Interaction of lysozyme and sodium dodecyl sulfate at the air-liquid interface. *Langmuir* **2000**, *16*, 5797-5805.
50. Fainerman, V. B.; Leser, M. E.; Michel, M.; Lucassen-Reynders, E. H.; Miller, R., Kinetics of the desorption of surfactants and proteins from adsorption layers at the solution/air interface. *The Journal of Physical Chemistry B* **2005**, *109*, 9672-9677.

5. Comparing foam and interfacial properties of similarly charged mixtures of protein and low molecular weight surfactants

Abstract

The foam stability of protein-low molecular weight surfactant (LMWS) mixtures strongly depends on the charge of the protein and the LMWS, as well as on their mixing ratio. Depending on the conditions, the mixtures will contain free proteins, free LMWS and/or protein- LMWS complexes. To be able to compare different protein- LMWS mixtures, generic knowledge about the occurrence of each of these states and their relative contribution to foam stability is essential. In this work, the foam stability and interfacial properties of bovine serum albumin (BSA) mixed with sodium dodecyl sulphate (SDS) as well the binding of SDS to BSA as are studied at different molar ratios (MR). A comparison is made with β -lactoglobulin (BLG) mixed with SDS. Both proteins and SDS are negatively charged at pH 7. The foam stability in the presence of small amounts (up to MR 1) of SDS is half the value of the pure protein solutions. The foam stability for both protein LMWS mixtures reaches a minimum at MR 20. A further increase of the MR leads to an increase of foam stability. The foam stability of BLG-SDS at MR >20 follows the foam stability of pure SDS solutions at equivalent concentrations, while BSA-SDS mixtures have an offset and begin to increase from MR >50. This behaviour was also reflected in the surface pressure and complex dilatational elastic moduli, and could be linked to the binding of the LMWS to the proteins. Both proteins bind SDS at high and low affinity binding sites. BSA's high affinity binding sites have a binding stoichiometry of $5.5 \text{ mol}_{\text{SDS}}/\text{mol}_{\text{protein}}$, and BLG's high affinity binding site has a stoichiometry of $0.8 \text{ mol}_{\text{SDS}}/\text{mol}_{\text{protein}}$ (determined by isothermal titration calorimetry). Binding to the low affinity binding sites, occurs with a binding ratio, leading to an accumulation of free LMWS. While the basic mechanisms underlying the foam properties of mixed systems are not explained in detail by this approach, the foam stability plots of both protein-LMWS mixtures could be superimposed using the concentration of free SDS.

Based on: Lech, F. J.; Meinders, M. B. J.; Wierenga, P. A.; Gruppen, H., Comparing foam and interfacial properties of similarly charged protein-surfactant mixtures. Colloids and Surfaces A: Physicochemical and Engineering Aspects 2015, 476, 18-23.

Introduction

For similarly charged mixtures of proteins and LMWS it is well-known that the LMWS binds to the proteins, which in return changes the foam properties of the mixtures depending on molar ratio ($MR = \text{mol}_{\text{LMWS}}/\text{mol}_{\text{protein}}$). Recently, it was shown that the foam stability of different BLG-SDS mixtures can be understood in terms of the MR and consequently the amount of bound and unbound LMWS in the mixtures (**chapter 4**)¹. Additional quantitative data on foam stability for similarly charged protein LMWS mixtures is lacking, however earlier work indicated the importance of free LMWS in relation to the foam properties. If indeed the binding of the LMWS to the protein determines the foam properties, a comparison of different systems, e.g. different proteins and the same LMWS, can be obtained by accounting for the number of bound LMWS molecules per protein. Hence, the hypothesis is that the foam stability of similarly charged protein-LMWS mixtures can be described in terms of the amount of bound and free LMWS. To investigate this, two proteins with different binding capacities are used in the present study. Both proteins used, bovine serum albumin (BSA) and β -lactoglobulin (BLG) are known to bind LMWS, such as sodium dodecyl sulphate (SDS). They have both been used in studies on the effect of mixing on bulk interaction (BSA-SDS^{2, 3}, BLG-SDS⁴⁻⁶), showing the binding of SDS to the proteins. Typically, at low MR, a small number of SDS molecules is bound to high affinity binding sites, while at higher MR more SDS will be bound in non-specific sites. A detailed discussion on the effect of LMWS binding on protein structure and conformation of the resulting complex was previously published⁷. Next to the effect of mixing on the bulk properties, interfacial properties and foam properties of those protein LMWS mixtures have been studied. It was shown that BSA and SDS cooperatively adsorb and cover the interface⁸ and that the formation of protein LMWS complexes is reflected by changes in the interfacial tension of the mixtures⁹. Similar observations of coexistence of protein-LMWS complexes as well as free LMWS have been reported for BLG-SDS mixtures^{10, 11}. The foam ability of BSA-SDS mixtures increases with concentration of SDS¹². However, the foam stability of this mixture has not been reported. In case of BLG-SDS, the foam stability first decreases upon increased SDS concentration until (MR 20) and starts to increase from that MR onwards¹.

Although both proteins are commonly used model proteins, only one study compared BSA- and BLG LMWS mixtures directly, finding co-adsorption of proteins and LMWS as well as destruction of protein structure at SDS concentration higher than 1 mM in case of BLG-SDS and 3 mM in case of BSA SDS¹³. In the present study, results on BSA-SDS mixtures are complemented with prior results of BLG-SDS mixtures¹. The quantitative link between the two protein-LMWS mixtures and the free LMWS results in a broader description of foam stability of similarly charged mixtures.

Materials and Methods

Materials

Bovine serum albumin (BSA) (Lot number 041M1801V, containing 91 % protein based on DUMAS (N x 6.07¹⁴ and molecular mass of 66.46 kDa determined by electrospray ionization

Comparing foam properties of similarly charged protein-LMWS mixtures

mass spectrometry) and β -Lactoglobulin (BLG) (Lot number 030M7025V, containing 90 % protein based on DUMAS ($N \times 6.33^{14}$, molecular mass 18.35 kDa determined by electrospray ionization mass spectrometry) were purchased from Sigma Aldrich (Zwijndrecht, The Netherlands). Sodium dodecyl sulphate (SDS, 288.99 Da) was obtained from Merck (Schiphol-Rijk, The Netherlands). MilliQ grade water (Millipore, EMD Millipore Corp., Billerica, MA, USA), free of surface active contaminants was used in all experiments (resistivity 18.6 M Ω cm, total organic carbon 3 ppb and surface tension 72.5 \pm 0.5 mN m $^{-1}$ at 20 $^{\circ}$ C).

Sample preparation

Stock solutions of BSA (6.56 mg mL $^{-1}$) and BLG (1.8 mg mL $^{-1}$) with a protein concentration of 0.89 mM and SDS concentration of 10.9 mM for solution MR 0 -100 and 54.5 mM for solutions MR 100 - 500 were made by separately dissolving protein powder and SDS in sodium phosphate buffer (pH 7.0, 10 mM). Solutions were prepared 30 - 120 minutes before use by mixing the stock solutions and buffer, while stirring slowly (without foaming) for 15 minutes at room temperature. The protein concentrations for solutions of different MR, after mixing with different amounts of stock solution of SDS and buffer, were always 49 μ M for BSA and BLG, respectively, unless stated otherwise. The pH of the solutions after mixing was adjusted to pH 7.0 by adding 1 M NaOH or 1 M H $_3$ PO $_4$.

Sample solutions were named according to the molar ratio of LMWS to protein. This is denoted as MR X, where X is the ratio of the SDS concentration (μ M) over the protein concentration (μ M). For each mixed solution of a MR, a similar pure SDS solution at an equivalent concentration of SDS ($EC = [SDS]/49 \cdot 10^{-6}$) was used as a reference. The MRs below MR 125 were below the assumed critical micelle concentration of SDS at 20 $^{\circ}$ C ($8 \cdot 10^{-3}$ M) 15 .

Isothermal titration calorimetry (ITC)

A microcalorimeter (ITC $_{200}$, GE Healthcare, Piscataway, NJ, USA) was used to titrate SDS solution (in 10 mM sodium phosphate buffer, pH 7.0) stepwise into the above described protein solutions at 20 $^{\circ}$ C. The LMWS concentrations were 10.9 mM SDS for titration into BSA and 5.45 mM SDS for titration into BLG. The solutions in the titration vessels were stirred at 600 rpm to ensure optimal mixing of the SDS in the measuring cell. In each titration step, 1.4 μ L, or 1.2 μ L SDS solution were injected into the BSA or BLG solution, respectively, followed by an equilibration period of 120 seconds until the final concentration of SDS was reached corresponding to an MR of 20 (BSA) and 2 (BLG). The area under the heat flow curve was integrated to obtain the total enthalpy change (ΔH) per injection. Each experiment was corrected with respective titration of SDS solution into buffer. A model assuming one set of identical (non-interacting) binding sites was fit to the integrated curve with a non-linear regression procedure with ITC data analysis software add in (GE Healthcare) for the Origin software suite (Origin 7.0, OriginLab Corp., Northampton, MA, USA). A more detailed description of the model and its theory can be found elsewhere 16 . The model used the theoretical stoichiometry (n (-)), which corresponds to the number of binding sites, the binding constant (K (M $^{-1}$)), and the binding enthalpy (ΔH (kJ mol $^{-1}$)) as fitting parameters.

Chapter 5

Foam experiments

Foam (from solutions described above) was prepared by sparging nitrogen through a metal frit (60 mm diameter, pore size $27 \pm 2 \mu\text{m}$, $100 \mu\text{m}$ distance between centres of pores, square lattice) in an automated foaming device (Foamsan, Teclis IT-Concept, Longessaigne, France). The flow rate of gas was 400 mL min^{-1} and the maximum foam volume was 600 cm^3 . The decay of the foam was monitored by a camera and the foam volume was determined by image analysis performed by software provided with the Foamsan. The time it took the foam to decay to half of the initial volume (foam half-life or $t_{1/2}$) was used as an indicator for the foam stability.

Reported values of $t_{1/2}$ are averages of at least six individual foam measurements and the coefficient of variation was usually <0.1 . Foam experiments were performed at 20°C .

Drop tensiometry

Interfacial tension measurements were performed using an automated drop tensiometer (ADT) (Tracker, Teclis IT-Concept) at 20°C as previously described elsewhere¹⁷. A bubble of air ($5 \mu\text{L}$) was formed by a computer controlled syringe on the tip of a curved needle in the solution (prepared as described above). The interfacial tension was calculated by analysis of the shape of the air bubble performed by software provided with the ADT. Changes of the surface tension are expressed as surface pressure, which is the surface tension of sodium phosphate buffer (pH 7, 10 mM, $71.8 \pm 0.5 \text{ mN m}^{-1}$ at 20°C) minus the surface tension of the measured solution at certain time point (equation 1)

$$(1) \quad \Pi = \gamma_{\text{buffer}} - \gamma_{\text{solution}}$$

where Π is the surface pressure (mN m^{-1}), γ_{buffer} is the surface tension of buffer and γ_{solution} is the surface tension of the solution (mN m^{-1}). The complex dilatational modulus (E_d) was measured by subjecting a bubble to a change in interfacial area ($dA/A = 10\%$) with a frequency of 0.1 Hz for a cycle of 50 seconds followed by a rest period of 50 seconds over a period of 1 hour. These settings are within the linear viscoelastic regime as was reported elsewhere¹⁸. E_d is the complex viscoelastic modulus (mN m^{-1}), which consists of a storage modulus (E') and a loss modulus (E'') as described by¹⁹. The moduli can be calculated from the complex modulus with equation 2 and 3.

$$(2) \quad E' = E_d \cdot \cos(\delta)$$

and

$$(3) \quad E'' = E_d \cdot \sin(\delta)$$

The detection limits for surface pressure measurements (0.06 mN m^{-1}) were determined from the standard deviation of a measurement of pure water. The detection limit for complex dilatational moduli using these conditions with a minimum $1/AdA = 0.135$ was 0.44 mN m^{-1} as determined with pure water. Π and E_d values after 1 hour of adsorption are denoted as Π_{1h} and E_{d1h} . Experiments were performed in duplicate and values of the complex dilatational elastic modulus are expressed as mean of the duplicates. Standard deviations between replicates for surface pressure experiments were less than $\pm 0.5 \text{ mN m}^{-1}$ and for the complex dilatational modulus less than $\pm 1.5 \text{ mN m}^{-1}$.

Calculation of the weighted average of foam properties

For a binary system of non-interacting compounds, the response of the mixture could in first order approximation be described by the weighted average of the response of the individual compounds. Therefore, as a reference, the weighted average (\bar{R}) of foam stability was calculated using equation 4.

$$(4) \quad \bar{R} = \frac{[SDS] \cdot R_{SDS} + [protein] \cdot R_{protein}}{[SDS] + [protein]}$$

Where \bar{R} is the weighted average, [SDS] is the total concentration of SDS (mM), [protein] is the concentration of protein, and R_{SDS} and $R_{protein}$ are the responses (foam half-life $t_{1/2}$), for pure SDS and protein (BSA or BLG), respectively.

Results & Discussion

Foam stability of protein-LMWS mixtures

The foam stability of BSA and BSA-SDS mixtures, expressed by the foam half-life time ($t_{1/2}$) are shown in figure 5.1.

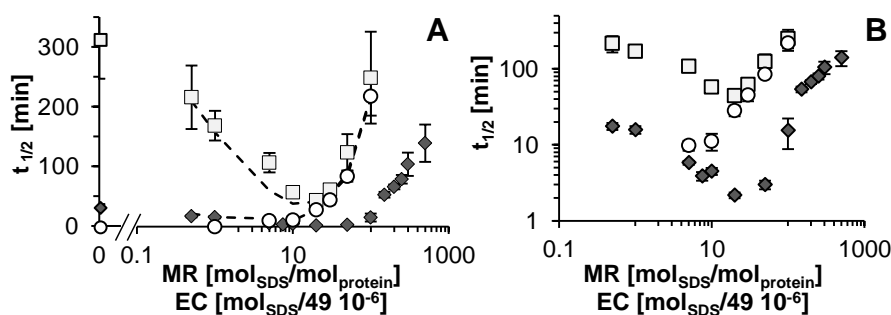


Figure 5.1: A) Foam stability ($t_{1/2}$) of BLG-SDS (■) and BSA-SDS (◆) mixtures and pure SDS (○) over the MR (protein-LMWS mixtures) and EC (SDS). The dashed lines are the weighted average (calculated with equation 4) for BSA-SDS and BLG-SDS respectively. The error bars indicate the standard deviation between replicates. Panel B shows a log-log plot of $t_{1/2}$. The symbols are the same as in panel A.

The foam stability of the pure BSA solution ($t_{1/2}$ 32 minutes) is much lower than that of the pure BLG solution ($t_{1/2}$ 315 minutes). The foam stability of SDS increases with increasing EC (reaching 216 minutes at EC 100). Upon addition of low amounts of LMWS (MR < 20) to the protein solution, for both proteins the foam stability decreases in a similar way. At higher MR (MR > 20) the protein-LMWS mixtures show an increase in foam stability. For BSA-SDS, the foam stability remains low until ~MR 50, where the $t_{1/2}$ is 4 minutes. Above MR 100 a strong increase in foam stability is observed. This increase of the foam stability follows the same trend as the foam stability of pure SDS. For the BLG-SDS mixture, the foam stability approximates that of the pure SDS at corresponding EC after MR 20. It was previously observed that the foam stability of BLG-SDS mixtures closely corresponds to the weighted average foam stability calculated using equation 4¹. This however, seems not to be a generic observation, since in case of BSA-SDS, the weighted average does not follow the experimental data. Still, for BSA-SDS and the overall trend of

Chapter 5

the foam stability is similar to the trend of BLG-SDS (figure 5.1 B). Beyond a certain MR, the foam stability of the protein-LMWS mixtures coincides with the foam stability of pure SDS. This indicates that above that MR, the foam stability of the mixtures is due to a sufficiently high free LMWS concentration. For BSA-SDS the point at which the concentration of free LMWS is sufficiently high is reached at MR 50, while for BLG-SDS mixtures, this point is reached at MR 20.

Typically, the stability of foams made by LMWS and proteins are explained by two different and incompatible mechanisms. In case of LMWS, the interfaces should be stabilized by Marangoni flow that counteracts gradients in surface tension. For proteins, the stability is attributed to the formation of a viscoelastic network at the interface. Mixtures of proteins and LMWS should therefore not be stable. It is expected that these mechanism are reflected by dramatic changes in the interfacial properties that are caused by a transition from a proteinaceous towards a LMWS-like interface.

Interfacial properties protein-LMWS mixtures

The surface pressure after 1 hour (Π_{1h}) of the pure protein solutions is 17 mN m⁻¹ and 20 mN m⁻¹ for BSA and BLG, respectively (figure 5.2 A). The Π_{1h} of SDS increases with the increase of EC, reaching 40 mN m⁻¹ at EC 100. For BLG-SDS mixtures, Π_{1h} and E_{d1h} values after 1 hour of adsorption are denoted as Π_{1h} and E_{d1h} vs MR increases and coincides with that of pure SDS at MR >20. When MR>20, the curve levels off. For BSA-SDS mixtures, the slope of the Π_{1h} vs. MR has a lower absolute value than that of the BLG-SDS mixtures. However, a final increase and levelling-off of the curve similar to BLG-SDS and pure SDS is observed from MR 100 onwards. It has to be noted that the Π_{1h} does not reach the same values as pure SDS or BLG-SDS mixtures respectively.

These observations suggest that at high MR (> 100 for BSA-SDS and > 20 for BLG-SDS) the interface is primarily covered by free LMWS. This is further supported by the plot of E_{d1h} vs. MR, which shows a decrease in E_{d1h} from 67 for BSA and from 100 for pure BLG to the values of the pure SDS solutions (figure 5.2 B). The E_{d1h} of BLG-SDS and BSA-SDS mixtures decrease with an increase of the MR and coinciding with the curve of pure SDS at MR >20 (BLG-SDS) and MR >100 (BSA-SDS). In case of E_{d1h} , both the values for both mixtures reach the same value as pure LMWS.

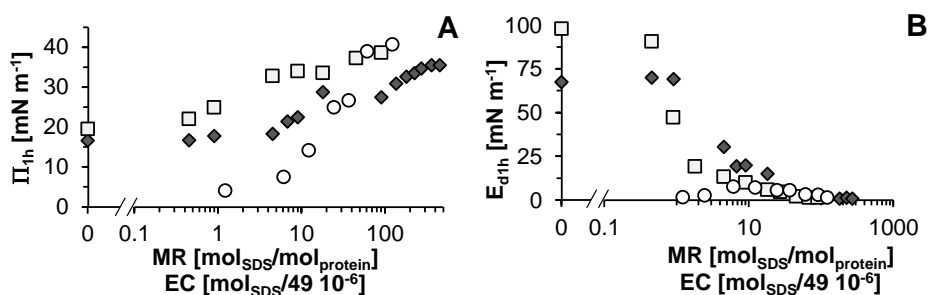


Figure 5.2: A) Surface pressure (Π_{1h}) and B) complex dilatational elastic modulus (E_{d1h}) as function of the MR for BLG-SDS (■) and BSA-SDS (◆) mixtures and EC for SDS (○). Variation between replications was < 0.5 mN m⁻¹.

Comparing foam properties of similarly charged protein-LMWS mixtures

The change from a protein covered interface via an interface covered by protein-LMWS complexes towards an interface that is mainly covered by LMWS is also indicated in the change of the curve of E_d over Π (figure 5.3 A and B). The curves at low MR (MR 0.46 - MR 4.6 for BSA-SDS and MR 0.45 for BLG-SDS) show an increase of E_d with increased Π , which is typically found for protein covered interfaces. At high MR (MR > 100 for BSA and > 20 for BLG), no change of E_d over Π is observed, which is typical behaviour of LMWS covered interfaces. Such a gradual change from protein to LMWS covered interface has been proposed in literature for interacting protein LMWS mixtures²⁰.

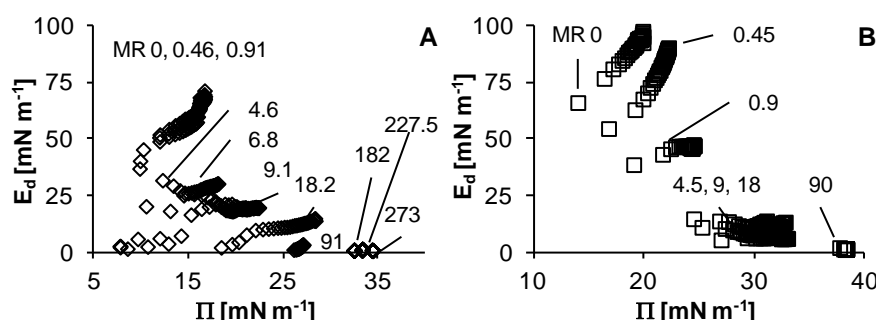


Figure 5.3: The complex dilatational elastic modulus (E_d) as function of the surface pressure (Π) for BLG-SDS (A) and BSA-SDS (B) mixtures for different MR. Variations between replications were < 0.5 mN m⁻¹.

The results obtained for foam stability as well as the correlation between Π_{1h} and E_{d1h} of the protein LMWS mixtures show that the behaviour of the mixtures gradually changes from protein covered interfaces towards LMWS-like systems. Such a gradual change is expected if the interfacial properties of the proteins are changed by interaction with the LMWS. Therefore, the binding of LMWS to proteins is determined.

Protein binding and the effect of free LMWS

The binding of SDS to BSA and BLG was determined by isothermal titration calorimetry (figure 5.4). The heat flow curves in the samples show endothermic peaks, that are decreasing in height upon addition of SDS (figure 5.4 A). For both proteins, a high affinity binding is observed, indicated by the steep slope in the enthalpogram (figure 5.4 B and C). The fitting of a model assuming one type of binding site yields high affinity sites for BSA with a total heat change (ΔH) of -33 kJ mol⁻¹, a binding stoichiometry for high affinity binding of 5.5 ± 0.11 and saturation at MR 10. For BLG the model yields one type of high affinity binding site with a binding stoichiometry for high affinity binding of 0.78 ± 0.11 , a total heat change of -14 kJ mol⁻¹ and saturation at MR 1.

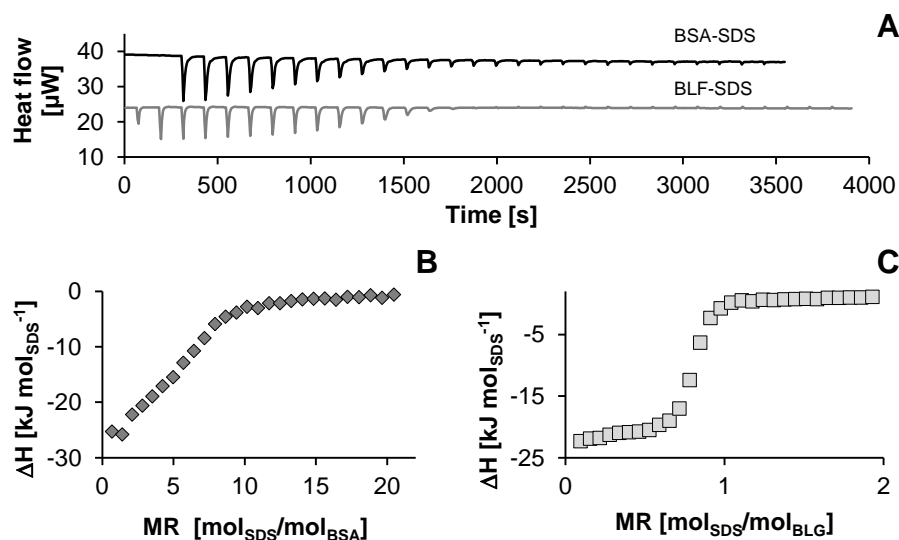


Figure 5.4: A) Heat flow during isothermal titration calorimetry of SDS into protein solutions with a protein concentration of 49 μM. The injected volume of SDS was 1.2 μL (BLG-SDS) and 1.4 μL (BSA-SDS). Integrated binding isotherm of SDS titrated into BSA (B) and BLG (C).

The values obtained for binding stoichiometry and total heat change are in close agreement with data reported on the binding of SDS to BSA^{2, 21, 22} and BLG^{5, 10, 23}. In case of the titration of SDS in BSA solution, the concentration of SDS in the syringe was slightly above the CMC (10.9 mM). The demicellisation of SDS is endothermic ($-0.024 \text{ kJ mol}^{-1}$ at 25 °C in water²⁴) and contributes minutely to the signal of ITC. The contribution is small compared to the total binding enthalpy of -33 kJ mol^{-1} of the LMWS protein interaction.

The ITC results presented in this study on binding of SDS to proteins cover only a small range of MR, excluding any possible binding to low affinity sites at higher MR. Earlier research on BLG-SDS interaction showed binding of up to 7 SDS molecules to BLG (at MR 2) and changes of the tertiary structure of the BLG molecules were observed at MR >20¹. Other studies on LMWS binding in BSA-SDS mixtures showed that BSA is able to bind 160-300 SDS molecules^{25, 26}. Also, the additional binding of SDS has been linked to changes in protein conformation^{8, 13}. From that, it was concluded that in case of BSA and BLG at least two different types of LMWS binding occur. One type is the binding of SDS to high affinity binding sites, while the other type of binding occurs at non-specific sites that could be related to structural changes or even unfolding of the protein. This additional binding cannot be accurately determined by ITC, but can be estimated from binding isotherms of BSA-SDS mixtures. From studies reporting these isotherms, we estimated that at MR above the saturation of the high affinity binding sites, is ~81 % of the total SDS (at any MR below complete saturation of the protein) is bound by low affinity binding sites of BSA. The studies report values of values of 80 %²⁶, 90 %²⁵, and 75 %²⁷. This binding ratio however does not include the binding of SDS to high affinity binding sites, which should be included to calculate the total concentration of bound SDS. To include the high affinity

Comparing foam properties of similarly charged protein-LMWS mixtures

binding, the binding ratio is modified with a term including the SDS bound to high affinity binding sites. The total amount of bound SDS molecules equals

$$(5) \quad [\text{SDS}]_{\text{bound}} = [\text{SDS}]_{\text{HAB}} + [\text{SDS}]_{\text{LAB}}$$

where the amount of SDS that is bound to the high affinity sites equals

$$(6) \quad [\text{SDS}]_{\text{HAB}} = [\text{protein}] \times N$$

where $[\text{protein}]$ is the protein concentration and N is the number of binding sites per protein molecule, which equals the stoichiometry of the high affinity binding site.

The amount of SDS that is bound to the low affinity sites corresponds to

$$(7) \quad [\text{SDS}]_{\text{LAB}} = X \times ([\text{SDS}] - [\text{SDS}]_{\text{HAB}})$$

Where $[\text{SDS}]$ is the total SDS concentration and X as the protein specific binding ratio of SDS. It is noted that the values for X reported in literature correspond to $[\text{SDS}]_{\text{bound}}/[\text{SDS}]$, thereby treating the high affinity sites equal to the low affinity sites. Here we distinguish both affinities, which lead to equation 5.

Hence two binding regimes follow

$$(8) \quad [\text{SDS}]_{\text{bound}} = \begin{cases} [\text{SDS}] & \text{when } [\text{SDS}] < N \times [\text{protein}] \\ N \times [\text{protein}] + X \times ([\text{SDS}] - N \times [\text{protein}]) & \text{when } [\text{SDS}] \geq N \times [\text{protein}] \end{cases}$$

This equation can be rewritten to obtain an expression for the concentration of free SDS, since the $[\text{SDS}]_{\text{Free}} = [\text{SDS}] - [\text{SDS}]_{\text{bound}}$

$$(9) \quad [\text{SDS}]_{\text{Free}} = \begin{cases} 0 & \text{when } [\text{SDS}] < N \times [\text{protein}] \\ (1 - X) \times ([\text{SDS}] - N \times [\text{protein}]) & \text{when } [\text{SDS}] \geq N \times [\text{protein}] \end{cases}$$

In the case of BLG, no values for X are available in literature, as far as we know. Assuming that the amount of low-affinity binding sites scales with the molecular mass of the protein, the number of low affinity sites for BLG can be estimated using equation 10

$$(10) \quad X_{\text{BLG}} = \frac{N_{\text{BLG}}}{N_{\text{BSA}}} \times X_{\text{BSA}}$$

where X_{BLG} is the number of low affinity binding sites, X_{BSA} as the number of low affinity sites of BSA and N_{BLG} and N_{BSA} as the number of high affinity sites of BLG and BSA, respectively. Using equation 9, the concentration of free SDS in BSA-SDS mixtures (and equation 10 for BLG-SDS) as a function of the total SDS concentration was calculated (figure 5.5).

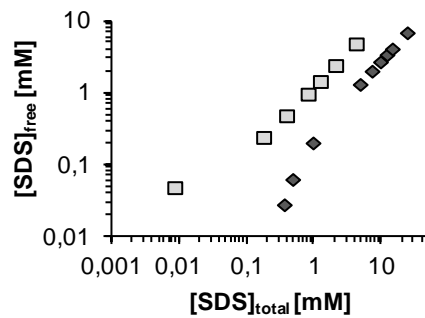


Figure 5.5: Concentration of free SDS as function of the total concentration of SDS for BSA-SDS (◆) and BLG-SDS (■) mixtures, calculated using equations 9 and 10.

These calculations were used to make a plot of the foam stability, surface pressure and complex dilatational modulus versus the calculated concentration of free SDS (figure 5.6).

Chapter 5

For foam stability, it is clear that the behaviour of both protein-LMWS mixtures (i.e. BSA-SDS and BLG-SDS) almost coincide with the plot of pure SDS. In the rescaled plots of Π_{1h} , the protein LMWS mixtures coincide with the plot of pure LMWS at concentrations higher than 1 and 2 mM SDS for BSA and BLG, respectively. This implies that when the x-axis is rescaled to free SDS, the adsorption isotherms of the protein-LMWS mixtures cannot be distinguished from the adsorption isotherm of SDS in the absence of protein from 1 mM onwards.

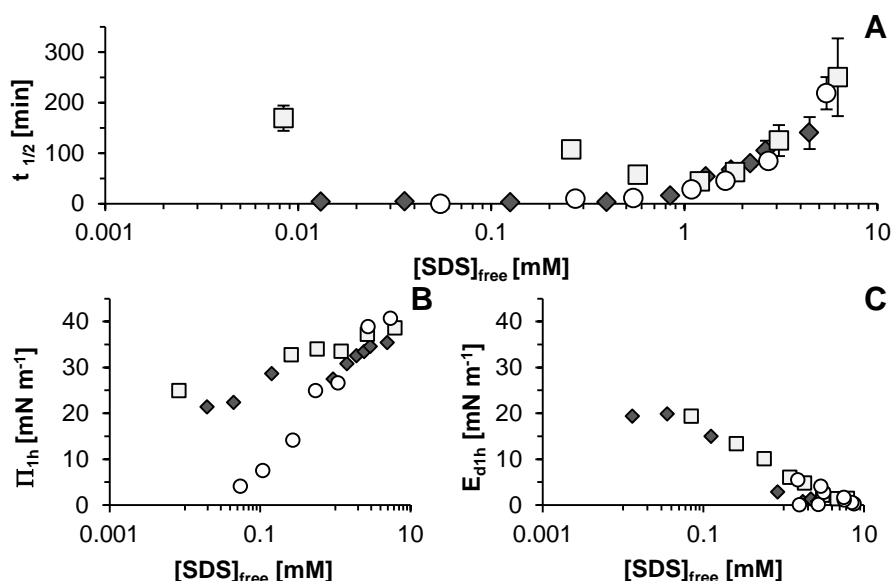


Figure 5.6: A) Foam stability ($t_{1/2}$), B) surface pressure and C) complex dilatational modulus over concentration of free SDS for BSA-SDS (\blacklozenge), BLG-SDS (\blacksquare) and pure SDS (\circ). The $[SDS]_{free}$ for BSA was calculated according to equation 9, for BLG equation 9 and 10 were used. The error bars in A indicate the standard deviation of $t_{1/2}$ between replications.

In case of the rescaled E_{d1h} plots, the curves of coincide at 1 and 0.5 mM for BSA and BLG, respectively. It has to be noted, that after the recalculation, the concentration of free LMWS in the BSA-SDS mixture for solutions above MR 125 (that had concentrations higher than the CMC of SDS) are now lower than the CMC due to binding of SDS to the protein. The binding of SDS to the protein leads to an effective decrease of the concentration of free LMWS, which appears to be typical in case of protein-LMWS interaction².

This good agreement in foam stability and interfacial properties, between the two protein LMWS mixtures and pure SDS, suggests that at high LMWS concentrations ($MR \gg N$), these similarly charged protein-LMWS mixtures behave like pure LMWS systems and with this become comparable. For lower LMWS concentrations ($MR < N$) further experiments supplemented by modelling are needed to show how exactly the foam stability and interfacial properties need to be expressed as function of total and free concentration of both proteins and SDS.

Conclusion

Based on the results obtained, it seems that the concentration of free LMWS is an important variable, which describes the foam stability of similarly charged protein-LMWS mixtures. This variable can be used to describe foam stability of protein LMWS mixtures. The binding ratio X seems to be related to concentration of SDS. Above a certain concentration, the techno-functional properties (e.g. foam properties) of the protein-LMWS mixtures coincide with properties of pure LMWS.

References

1. Lech, F. J.; Steltenpool, P.; Meinders, M. B. J.; Sforza, S.; Gruppen, H.; Wierenga, P. A., Identifying changes in chemical, interfacial and foam properties of β -lactoglobulin-sodium dodecyl sulphate mixtures. *Colloids and Surfaces A: Physicochemical and Engineering Aspects* **2014**, 462, 34-44.
2. Kelley, D.; McClements, D. J., Interactions of bovine serum albumin with ionic surfactants in aqueous solutions. *Food Hydrocolloids* **2003**, 17, 73-85.
3. Valstar, A.; Almgren, M.; Brown, W.; Vasilescu, M., The interaction of bovine serum albumin with surfactants studied by light scattering. *Langmuir* **2000**, 16, 922-927.
4. Jones, M. N.; Wilkinson, A., The interaction between β -lactoglobulin and sodium n-dodecyl sulphate. *Biochemistry Journal* **1976**, 153, 713-718.
5. Loch, J. I.; Bonarek, P.; Polit, A.; Świątek, S.; Dziedzicka-Wasylewska, M.; Lewiński, K., The differences in binding 12-carbon aliphatic ligands by bovine β -lactoglobulin isoform A and B studied by isothermal titration calorimetry and X-ray crystallography. *Journal of Molecular Recognition* **2013**, 26, 357-367.
6. Pitt-Rivers, R.; Impiombato, F. A., The binding of sodium dodecyl sulphate to various proteins. *Biochemical Journal* **1968**, 109, 825.
7. Otzen, D., Protein-surfactant interactions: A tale of many states. *Biochimica et Biophysica Acta (BBA) - Proteins and Proteomics* **2011**, 1814, 562-591.
8. Chakraborty, T.; Chakraborty, I.; Moulik, S. P.; Ghosh, S., Physicochemical and conformational studies on BSA-surfactant interaction in aqueous medium. *Langmuir* **2009**, 25, 3062-3074.
9. Santos, S. F.; Zanette, D.; Fischer, H.; Itri, R., A systematic study of bovine serum albumin (BSA) and sodium dodecyl sulfate (SDS) interactions by surface tension and small angle X-ray scattering. *Journal of Colloid and Interface Science* **2003**, 262, 400-408.
10. Engelhardt, K.; Weichsel, U.; Kraft, E.; Segets, D.; Peukert, W.; Braunschweig, B., Mixed layers of β -lactoglobulin and SDS at air-water interfaces with tunable intermolecular interactions. *The Journal of Physical Chemistry B* **2014**, 118, 4098-4105.
11. Pradines, V.; Krägel, J.; Fainerman, V.; Miller, R., Interfacial properties of mixed β -lactoglobulin-SDS layers at the water/air and water/oil interface. *The Journal of Physical Chemistry B* **2009**, 113, 745-751.
12. Wei, X.; Chang, Z.; Liu, H., Influence of sodium dodecyl sulfate on the characteristics of bovine serum albumin solutions and foams. *Journal of Surfactants and Detergents* **2003**, 6, 107-112.
13. Mikhailovskaya, A. A.; Noskov, B. A.; Lin, S. Y.; Loglio, G.; Miller, R., Formation of protein/surfactant adsorption layer at the air/water interface as studied by dilatational surface rheology. *The Journal of Physical Chemistry B* **2011**, 115, 9971-9979.
14. Uniprot P02754 (LACB_BOVIN) Reviewed, UniProtKB/Swiss-Prot. <http://www.uniprot.org/uniprot/P02754> (03.06.2014),
15. Chernysheva, M. G.; Ivanov, R. A.; Soboleva, O. A.; Badun, G. A., Do low surfactants concentrations change lysozyme colloid properties? *Colloids and Surfaces A: Physicochemical and Engineering Aspects* **2013**, 436, 1121-1129.
16. Freyer, M. W.; Lewis, E. A.; Correia, J.; Detrich, III, H., Isothermal titration calorimetry: Experimental design, data Analysis, and probing macromolecule/ligand binding and kinetic interactions. In *Methods in Cell Biology*, J., C.; Detrich, III, H., Eds. Academic Press: Waltham, MA, USA, **2008**; Vol. Volume 84, pp 79-113.

Chapter 5

17. Wierenga, P. A.; Meinders, M. B. J.; Egmond, M. R.; Voragen, A. G. J.; de Jongh, H. H. J., Quantitative description of the relation between protein net charge and protein adsorption to air–water interfaces. *The Journal of Physical Chemistry B* **2005**, 109, 16946-16952.
18. Engelhardt, K.; Lexis, M.; Gochev, G.; Konnerth, C.; Miller, R.; Willenbacher, N.; Peukert, W.; Braunschweig, B., pH effects on the molecular structure of β -lactoglobulin modified air-water interfaces and its impact on foam rheology. *Langmuir* **2013**, 29, 11646-11655.
19. Benjamins, J.; Cagna, A.; Lucassen-Reynders, E. H., Viscoelastic properties of triacylglycerol/water interfaces covered by proteins. *Colloids and Surfaces A: Physicochemical and Engineering Aspects* **1996**, 114, 245-254.
20. Mackie, A.; Wilde, P., The role of interactions in defining the structure of mixed protein-surfactant interfaces. *Advances in Colloid and Interface Science* **2005**, 117, 3-13.
21. Lund, H.; Christensen, B. P.; Nielsen, A. D.; Westh, P., Proton exchange coupled to the specific binding of alkylsulfonates to serum albumins. *Biochimica et Biophysica Acta (BBA) - Proteins and Proteomics* **2006**, 1764, 1243-1251.
22. Nielsen, A. D.; Borch, K.; Westh, P., Thermochemistry of the specific binding of C12 surfactants to bovine serum albumin. *Biochimica et Biophysica Acta (BBA) - Protein Structure and Molecular Enzymology* **2000**, 1479, 321-331.
23. Chamani, J.; Moosavi-Movahedi, A. A.; Rajabi, O.; Gharanfoli, M.; Momen-Heravi, M.; Hakimelahi, G. H.; Neamati-Baghsiah, A.; Varasteh, A. R., Cooperative α -helix formation of β -lactoglobulin induced by sodium n-alkyl sulfates. *Journal of Colloid and Interface Science* **2006**, 293, 52-60.
24. Paula, S.; Sues, W.; Tuchtenhagen, J.; Blume, A., Thermodynamics of micelle formation as a function of temperature: A high sensitivity titration calorimetry study. *The Journal of Physical Chemistry* **1995**, 99, 11742-11751.
25. Turro, N. J.; Lei, X.-G.; Ananthapadmanabhan, K. P.; Aronson, M., Spectroscopic probe analysis of protein-surfactant interactions: The BSA/SDS system. *Langmuir* **1995**, 11, 2525-2533.
26. Chen, A.; Wu, D.; Johnson, C. S. J., Determination of the binding isotherm and size of the bovine serum albumin-sodium dodecyl sulfate complex by diffusion-ordered 2D NMR. *The Journal of Physical Chemistry* **1995**, 99, 828-834.
27. Tipping, E.; Jones, M. N.; Skinner, H. A., Enthalpy of interaction between some globular proteins and sodium n-dodecyl sulphate in aqueous solution. *Journal of the Chemical Society, Faraday Transactions 1: Physical Chemistry in Condensed Phases* **1974**, 70, 1306-1315.

6. Aggregation in mixtures of lysozyme and sodium dodecyl sulphate determines foam stability by stabilization of the thin films

Abstract

Proteins and low molecular weight surfactants are common ingredients in food applications. The combination of both ingredients can have large effects on the techno-functional properties of the mixtures, like lower foam stability, compared to the pure ingredients. To increase understanding, foam properties of mixtures of lysozyme (LYS) and sodium dodecyl sulphate (SDS) were studied in varying molar ratios (MR) at pH 7.0, where the substances have a charge that is opposite from the other. In addition to experiments, the measured data were compared with modelled thin film stability and foam drainage. This model was based on properties of the adsorbed layer and viscosity of the bulk liquid. The addition of SDS to LYS leads to the formation of LYS-SDS complexes. Between MR 8 - 15, the LYS-SDS complexes aggregate. This is reflected in a maximum in turbidity. In this range, the minimal absolute ζ -potential of the complexes and highest dynamic viscosity were observed. Also the highest foam stability (half-life time 181 minutes at MR 8), and longest drainage times (100 minutes at MR 10) were found in this MR range. From this it was concluded that the presence of aggregated LYS-SDS complexes, which are dispersed in the foam structure, increase the foam stability significantly by stabilizing thin films and slowing down drainage.

Based on: Lech F.J, Gruppen H., Wierenga P.A, Meinders M.B.J. Submitted

Introduction

Proteins and low molecular weight surfactants (LMWS) stabilize air-water interfaces by two different mechanisms, proteins namely by a visco-elastic network and LMWS by the Marangoni mechanism. It has been mentioned in literature that the foam stability of mixtures of proteins and LMWS would be reduced compared to the original solutions^{1, 2}. Usually, complexation of the components is not considered when studying the interfacial and foam properties of protein-surfactant mixtures. Therefore, the effect of the interaction on the functional properties of the mixtures is hardly understood. Recently, the foam properties of mixtures of similarly charged proteins and components were studied (chapters 4 and 5)^{3, 4}. That investigation showed that the binding of surfactant to the protein determines the foam properties of the mixture. It was shown that depending on the molar ratio of surfactant to protein (MR), the mixtures contained protein, soluble protein surfactant complexes, and free LMWS^{3, 4}. Between MR 0 and 20, the foam stability decreased due to complexation, while from MR onwards, it increased with increasing amounts of free LMWS. The charge of protein-surfactant complexes depends on the MR⁵. For oppositely charged mixtures, the net-charge of the lysozyme and sodium dodecyl sulphate (LYS-SDS) complexes decreases with the amount of bound SDS. When the net-charge is too low, the complexes aggregate. The aggregation of the complexes leads to increased turbidity. In the case of mixtures of LYS-SDS, the maximum in turbidity was reported at MR 8^{5, 6}. From MR 15, the aggregated complexes dissociate, resulting in a clear solution (no turbidity) that contains soluble complexes at MR 30⁵⁻⁷. Although the complexation in the bulk is well understood, it is hardly taken into consideration in studies focussed on the interfacial and foam properties of LYS-SDS mixtures⁸⁻¹⁰. Studies on the interfacial properties have shown that the surface pressure (after 20 hours) of LYS-SDS mixtures increases with increased concentration of SDS from 11 mN m⁻¹ (MR 0) to 38 mN m⁻¹ (at MR 400)⁸. In general, it is believed that these interfacial properties also determine thin film and foam properties^{8, 11}. However, recent studies also show the importance of bulk properties for foam stability^{3, 4, 12}. In order to increase insight in the key parameters that control the foam stability of mixed protein-LMWS, we studied the effect of complexation of positively charged protein LYS and the negatively charged LMWS SDS on foam properties (half-life time, drainage, and bubble size). Foam stability is related to interfacial properties as well as the stability of the thin liquid films. Modelling of thin film stability and foam drainage is used to quantify the different phenomena involved.

Materials and Methods

Materials

Lysozyme (LYS; L6876, Lot no. 051K7028; purity N 90 % based on size exclusion chromatography) and sodium dodecyl sulphate were bought from Sigma Aldrich (Zwijndrecht, The Netherlands). All other chemicals were of analytical grade and purchased by Sigma Aldrich or Merck (Darmstadt, Germany). The water for the preparation of the buffer and rinsing of equipment was filtered through a MilliQ filtration

Aggregation in LYS-SDS mixtures of determines foam stability

unit (Millipore, Billerica, MA, USA) with resistivity of 18.2 M Ω cm, 3 ppb total organic carbon and a surface tension of 72.5 \pm 0.5 mN m⁻¹ at 20 °C.

Sample preparation

Stock solutions of LYS (70 $\cdot 10^{-5}$ mol L⁻¹) were prepared by dissolving the powder in sodium phosphate, pH 7, 10 mM). An SDS stock solution (21 $\cdot 10^{-3}$ mol L⁻¹) was prepared by dissolving SDS powder under gentle stirring in the buffer. The pH of the solutions was adjusted to pH 7 by addition of 1 M NaOH or 1 M H₃PO₄. Stock solutions were not kept longer than 3 days at room temperature for SDS and at 6 °C for LYS solution. The molar ratio (MR) is the ratio of SDS molecules per LYS molecule. E.g. the mixture of MR 1 contains 35 $\cdot 10^{-5}$ mol L⁻¹ SDS and 35 $\cdot 10^{-5}$ mol L⁻¹ LYS. Solutions for the experiments were prepared by adding buffer to the LYS stock and afterwards adding the SDS solution to this mix to get the desired MR. The final concentration of lysozyme was kept constant at 35 $\cdot 10^{-5}$ mol L⁻¹. Solutions of pure SDS were used as a reference and they are denoted as an equivalent concentration (EC), which is the real molar concentration of SDS in that solution divided by 35 $\cdot 10^{-5}$.

Foam analysis

Foam was made by sparging N₂ through a metal frit in a closed foam cell of an automated foaming device (Foamsan, Teclis IT-Concept, Longessaigne, France) at 24 °C as described elsewhere⁴. The foam cylinder had a diameter of 34 mm, gas flow rate was 200 mL min⁻¹, the volume of the solution was 40 mL and the maximum foam volume was 200 cm³ in each experiment. The decay of the foam was monitored by a camera and analysed by image analysis by the Foamsan. The foam stability was expressed as the time at which 50 % of the initial foam volume (V_F) had collapsed (half-life time, or t_{1/2}). The drainage of liquid out of the foam was characterized by the time at which 80 % of the liquid (V_L) that was in the foam at the end of sparging had drained to the reservoir under the foam (DT_{80%} (minutes)). The number average mean bubble radius (r_m (mm)) of the foam bubbles was determined by image analysis from pictures taken after 60 seconds to get information about the initial bubble size distribution. The pictures were analysed using a custom Matlab (Version 13b for Windows 7 OS, MathWorks, Natick, MA, USA) script that used the open DIPLib and DIPimage image analysis package for Matlab. A threshold for the analysis of images with the bubbles were automatically applied using the OTSU algorithm (part of the DIPLIP image analysis package) and afterwards segmented to identify individual bubbles. Reported values of t_{1/2}, DT_{80%} and the mean radius are averages of at least three individual foam experiments.

Drop tensiometry

Interfacial tension measurements were performed using an automated drop tensiometer (ADT) (Tracker, Teclis, Longessaigne, France) at 20 °C¹³. A drop of LYS-SDS solution (5 μ L containing 5 mg mL⁻¹ LYS and corresponding amounts of SDS) was formed by a computer controlled syringe hanging from the tip of a needle in air. The interfacial tension was calculated by analysis of the shape of the droplet performed by software provided with the ADT. Changes of the surface tension are expressed as surface pressure, which is the

Chapter 6

surface tension of sodium phosphate buffer (pH 7.0, 10 mM, $71.8 \pm 0.5 \text{ mN}\cdot\text{m}^{-1}$ at 20°C) minus the surface tension of each sample solution ($\Pi = \gamma_{\text{buffer}} - \gamma_{\text{sample}}$). The complex dilatational elastic modulus (E_d) was measured by subjecting the drop to a change in interfacial area ($dA/A = 10\%$) with a frequency of 0.1 Hz for a cycle of 50 seconds followed by a rest period of 50 seconds during 1 hour. The change of the values for Π and E_d after 1 hour was less than $0.005 \text{ mN}\cdot\text{m}^{-1} \cdot \text{s}^{-1}$. The selected time points for Π and E_d (1 hour) are in line with those generally used in similar studies on Π and E_d of LYS-SDS mixtures^{8, 14}. Π and E_d values after 1 hour are denoted Π_{1h} and E_{d1h} . The experiments were performed in duplicate and values of E_{d1h} are expressed as mean of the duplicates. A measurement with buffer over 600 seconds was performed between experiments to verify that the system was clean. Standard deviations between replicates were less than $0.5 \text{ mN}\cdot\text{m}^{-1}$.

ζ-Potential

The ζ -potential of LYS-SDS solutions were determined on a Zetasizer Nano ZSP (Malvern, Malvern, UK) as described elsewhere¹⁵. The measurements were performed at 20°C and 40 V. The ζ -potential was calculated using Henry's equation (equation 1) and values taken from¹⁶.

$$(1) \quad \zeta = \frac{3\eta \cdot \mu_e}{2\varepsilon F(\kappa\alpha)}$$

Where ζ is the ζ -potential (V), η is the viscosity at 20°C ($1.002 \cdot 10^{-3} \text{ Pa}\cdot\text{s}$ ¹⁷), μ_e is the electrophoretic mobility ($\text{m}^2 \cdot \text{V}^{-1} \cdot \text{s}^{-1}$), ε is the dielectric constant of the medium ($7.1 \cdot 10^{-10} \text{ C}^2 \cdot \text{J}^{-1} \cdot \text{m}^{-1}$ ¹⁷) and $F(\kappa\alpha)$ is the dimensionless product of the Debye length in an electrolyte (κ^{-1}) and the dimensions of the protein (α), which equals 1.5 in the Smoluchowski approximation. The ζ -potential was determined in triplicate with a minimum of 25 individual measurements per determination. The presented data is the average and standard deviation of the triplicate measurements for each MR.

Viscosity

The kinematic viscosity was determined using Ubbelohde capillary viscometers (Type 50101, 0.53 mm diameter of the capillary, SI Analytics, Mainz, Germany) at 20°C . 15 mL of LYS-SDS mixtures was equilibrated for 30 minutes in the viscometer, which was immersed in a water bath. The LYS-SDS mixture was drawn from a reservoir up through the capillary by a syringe. After the syringe was removed, the liquid drained back into the reservoir, the draining time was recorded. The kinematic viscosity was calculated according to equation 2

$$(2) \quad \nu = t \times c$$

where ν is the kinematic viscosity ($\text{m}^2 \cdot \text{s}^{-1}$), t is the draining time (s) and c is a constant belonging to the specific viscometer. To calculate the dynamic viscosity, the density of the mixtures was determined with an oscillating U-tube density meter (DMA 5000, Anton Paar, Oosterhout, The Netherlands). The dynamic viscosity was calculated with equation 3

$$(3) \quad \eta = \nu \times \rho$$

where η is the dynamic viscosity ($\text{Pa}\cdot\text{s}$) and ρ is the density of the mixtures ($\text{kg}\cdot\text{m}^{-3}$).

Turbidity

The turbidity of the LYS-SDS mixtures was determined by measuring the absorbance at 595 nm in a UV spectrophotometer (UV-1800, Shimadzu, Kyoto, Japan). SDS stock solution (13.99 mM) and sodium phosphate buffer were mixed in a disposable cuvette (10 mm path length) to obtain 2 mL of SDS solution with the desired concentration of SDS. Then, 2 mL of lysozyme (0.69 mM in sodium phosphate buffer) was added and the cuvette was moved gently to mix the solution without creating air bubbles. The turbidity was expressed relative to the highest measured value, which was set to 1. The turbidity of the solution was measured in triplicate at 20 °C and the average and standard deviations were calculated.

Thin film experiments

Thin liquid films of LYS, SDS and LYS-SDS mixtures were made as described previously¹⁸. In short, thin films were made in a glass capillary cell. The cell is placed under the objective (20 times magnification) of a microscope (Axio Scope.A1, Carl Zeiss, Jena, Germany). Images of the films were recorded using a 5 mega pixel CCD camera (BCE C050-U, Mightex, Toronto, Canada) in reflected light mode. Mixed LYS-SDS solutions were prepared immediately before placing them in the glass annulus of the capillary cell by mixing appropriate quantities of buffer, SDS and LYS to ensure similar equilibration time (15 minutes). After equilibration, liquid was drawn into the capillary by a syringe and a thin film of 200 µm diameter was formed. Full colour images of thin films with aggregates were recorded with the software that was issued by the camera manufacturer (Buffcam app version 1.0 for Windows 7).

Results & Discussion

Foam properties

Solutions of LYS (MR 0) show no foam stability at a concentration of 5 mg mL⁻¹. The foam collapsed before the set volume could be reached (figure 6.1 A). All foams made with the pure SDS or LYS-SDS mixtures reached the desired foam volume within the same amount of time. This indicates good foam ability for the LYS-SDS mixtures at every MR. The foam stability, expressed as foam half-life $t_{1/2}$, of SDS increases continuously with increasing concentration of SDS from 3 ± 1.5 minutes at EC 1.5 until 61.6 ± 8.5 minutes at EC 30. The foam stability of LYS-SDS mixtures increases with increasing MR from MR 0.1 with 13.5 ± 2 minutes until 181.5 ± 13 minutes at MR 8. A further increase of the MR to 30 results in a decrease of $t_{1/2}$ to 26 ± 16 minutes. The poor foam properties of lysozyme in its native state are in agreement with literature and have been reported previously (10 mg mL⁻¹, pH 7; 20 mM sodium phosphate buffer)¹⁹. The increase of the foam stability of SDS foams with increasing EC is in line with reported observations⁴. The foam stability of the mixtures is always greater than that of the SDS solutions. This difference between SDS and the LYS-SDS mixtures is also reflected in the drainage time (DT_{80%}). The DT_{80%} of SDS foam increased from 0.5 ± 0.5 minutes at EC 0.9 until 2.5 ± 0.5 minutes at EC 6 where it levels off (figure 6.1 B). For LYS-SDS mixtures, DT_{80%} increased with increasing MR from 3 ± 0.5 minutes at MR 1 to 9.5 ± 1 minutes at MR 10. From MR 10 the DT_{80%} decreased until 1.5

± 0.5 minutes at MR 30, which is the same $DT_{80\%}$ for SDS (EC 30). The drainage of liquid is related to the mean bubble radius (r_m) and to the viscosity of the solution. $DT_{80\%}$ increase with increasing MR, while the r_m after 0.5 minutes (figure 6.1 C) decreases with increased MR. SDS foams were only stable enough to obtain data on the r_m from EC 1.4 onwards ($r_m = 0.08 \pm 0.007$ mm) from where the r_m decreased with increased concentration to 0.04 ± 0.002 mm at EC 10. A further increase of the EC did not lead to a further decrease of the bubble size. The r_m of LYS-SDS mixtures decreases with increasing MR from 0.12 ± 0.01 mm at MR 0.1 until a minimum is reached at MR 15 with 0.03 ± 0.002 mm. From MR 15 onwards, the r_m increases until a value of 0.04 ± 0.004 mm is reached at MR 30. The similarity of the r_m curve as a function of the concentration indicates that in both SDS solutions as well as LYS-SDS mixtures, the bubble formation is similar.

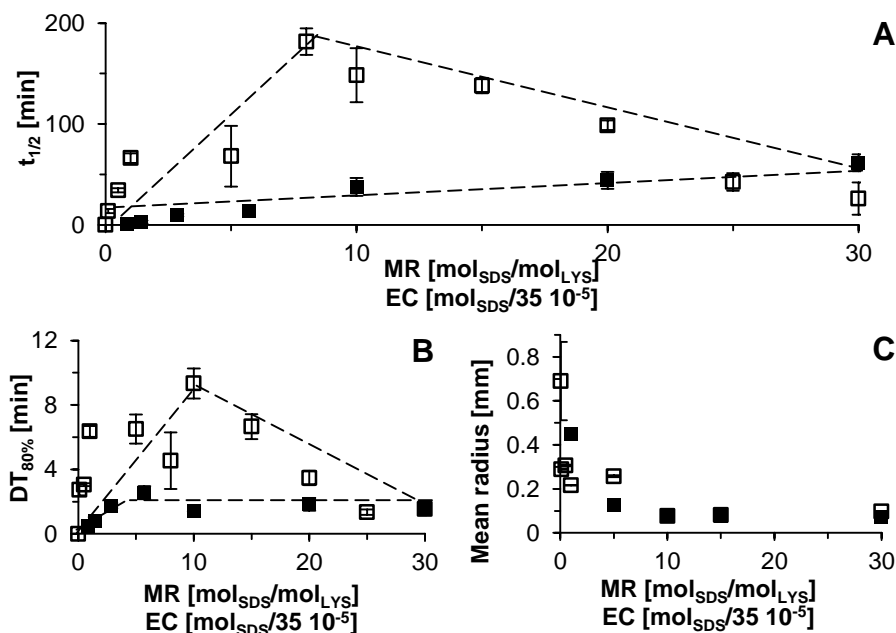


Figure 6.1: A) Foam stability ($t_{1/2}$), B) $DT_{80\%}$ and C) mean radius as a function of the MR for LYS-SDS mixtures (\square) and as a function of the EC for SDS solutions (\blacksquare). The dashed lines are a guide to the eye and the error bars indicate standard deviation between replicates.

Interfacial properties

The Π of LYS after 1 hour of adsorption is 14 mN m^{-1} (figure 6.2 A). Π_{1h} values of the SDS solutions increase with increasing SDS concentration (EC) to 40 mN m^{-1} at a concentration of 3.5 mM. The Π_{1h} of LYS-SDS mixtures is 25 mN m^{-1} at MR 0.05 and it increases with an increasing MR until the Π_{1h} values level off at 31 mN m^{-1} at MR 0.5. Further increase of the MR leads only to a small increase ($\Pi = 33 \text{ mN m}^{-1}$ at MR 30). The E_d of the interface of LYS solution reaches a value of 27 mN m^{-1} after 1 hour of adsorption (figure 6.2 B). The E_{d1h} of the interfacial layer of pure SDS solutions is independent of the SDS concentration measured and was below $10 \pm 1 \text{ mN m}^{-1}$.

The E_{d1h} of the LYS-SDS mixture starts at a value of 15 mN m^{-1} at MR 0.05 and decreases with an increase of the MR until E_{d1h} of the protein surfactant mixtures is similar to that of pure surfactant with values of $10 \pm 1 \text{ mN m}^{-1}$ at MR 30. The adsorption rate, indicated by the Π after 15 s, at different MRs (Figure 6.2 C) is approximated by comparing the Π over $t^{0.5}$ curve. It becomes apparent that the LYS-SDS complexes adsorb much faster than the LYS itself. The adsorption rate of the LYS-SDS mixture increased with increasing MR, though the magnitude of the increase is not large. Which is reflected in the good foam ability of the mixtures. The observed values for Π of pure SDS are in agreement with literature²⁰.

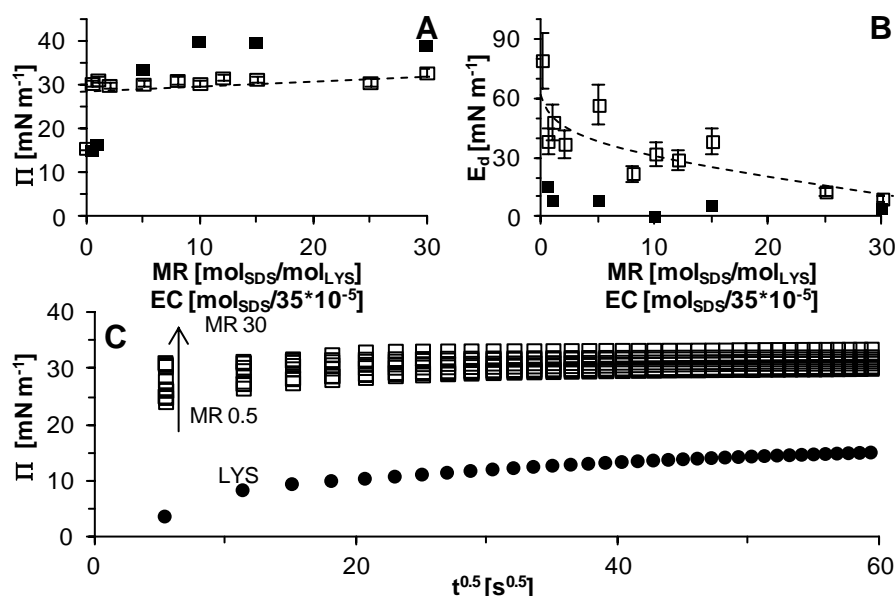


Figure 6.2: Π_{1h} (A) and E_{d1h} (B) as a function of the MR for LYS-SDS mixtures (\square) and as a function of EC for SDS solutions (\blacksquare). The dotted lines are a guide to the eye and not a fit. Deviation between duplicates is indicated by error bars. C) $\Pi(t^{0.5})$ for LYS-SDS mixtures and LYS (\bullet).

It is commonly assumed that foam stability is positively correlated to these interfacial properties of the solutions²¹. To test this correlation in our dataset, the foam stability ($t_{1/2}$) was plotted against the interfacial properties Π_{1h} and E_{d1h} (figure 6.3 A and B). No clear correlation between foam stability and either Π_{1h} or E_{d1h} was found for the oppositely charged protein-surfactant mixtures. In the $t_{1/2}$ over Π_{1h} curve of the LYS-SDS mixtures, very large differences in $t_{1/2}$ occur without large difference in Π_{1h} , the foam stability decreases drastically, with increasing Π . For E_{d1h} , if there is any correlation in the data, it seems to be a negative correlation. The lack of correlations indicates the importance of other factors, which are not reflected by the Π_{1h} and E_{d1h} . It can therefore, be concluded that the foam stability for these systems cannot be predicted from the commonly used measurements of interfacial properties alone. It has to be noted that data

point for MR 30 is located in between the data points of pure SDS, indicating that at this MR the interfacial properties are dominated by the LMWS.

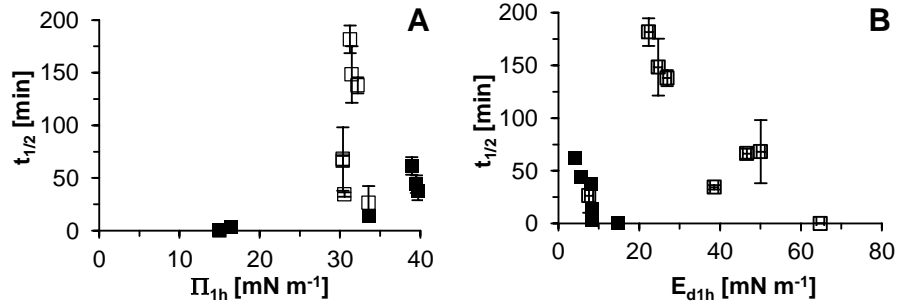


Figure 6.3: Correlation of $t_{1/2}$ and Π_{1h} (A) and E_{d1h} (B) of LYS-SDS mixtures (□) and SDS solutions (■). The error bars indicate the standard deviation between experiments.

Stability of thin films in foam of LYS-SDS mixtures

Drainage of liquid in foam

A multi-scale approach was used to simulate the foam stability. First the liquid drainage of the foam is modeled, giving the liquid volume fraction as function of time and position. Secondly the rupture of thin liquid films is modeled as a function of different liquid volume fractions. Combining both yields an estimation of the foam stability.

The liquid volume fraction ε_l as a function of time t and position in the z -direction was simulated using the drainage model as proposed by Koehler *et al.* (2000) (equation 4)²²

$$(4) \quad \frac{\partial \varepsilon}{\partial t} = - \frac{d}{dz} \left(\frac{K_{1/2} L^2 \sqrt{\varepsilon}}{\eta} \varepsilon \left(\rho g + \sqrt{\delta_p} \frac{d}{dz} \frac{\gamma}{L \sqrt{\varepsilon}} \right) \right)$$

where $K_{1/2} = 8 \cdot 10^{-3}$, $\delta_p = 0.17$, L is the Plateau border length (which is about 0.816 times the bubble radius r_B for dry polyhedral foams), η is the dynamic viscosity, ρ is the density of the liquid (taken to be 10^3 kg m^{-3}), $g = 9.8 \text{ m s}^{-2}$ is the gravitational constant, and $\gamma = \gamma_0 - \Pi$ is the interfacial tension with $\gamma_0 = 72 \text{ mN m}^{-1}$ corresponding to that of the bare interface. The Π values at different MR were taken from figure 6.2. The dynamic viscosity of the liquid phase were taken from figure 6.4, showing the measured values for different MR. These are close to that of water and increase between MR 8 and 15.

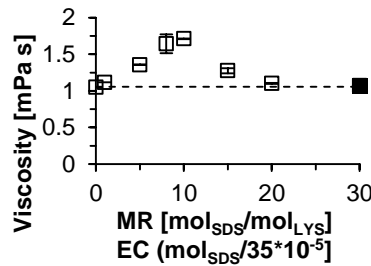


Figure 6.4: Dynamic viscosity of LYS-SDS mixtures at different MR. Error bars are standard deviation between repeated measurements.

Starting with a foam consisting of spherical bubbles with radius $r_b = r_m = 0.1$ mm and an initial volume fraction $\varepsilon_l = 0.36$, (corresponding to a randomly closed packed spheres), ε_l is calculated as a function of time and foam height for different MR. An example is illustrated for LYS-SDS at MR 30 ($\eta = 1$ mPa s, $\Pi = 39$ mN m⁻¹, and foam height $H_0 = 0.3$ m).

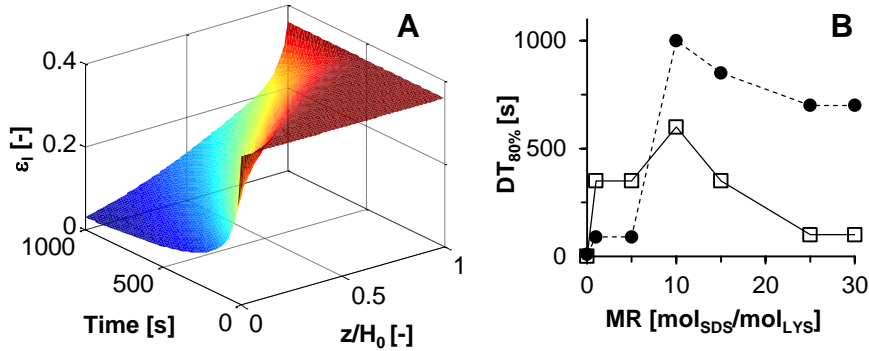


Figure 6.5: A) Simulated ε_l as a function of the position z , relative to the foam height $H_0 = 0.3$ m, and time t for MR 30 ($\eta = 1$ mPa s, $\Pi = 39$ mN m⁻¹). $z = 0$ corresponds to the top of the foam and $z = H_0$ to the bottom. B) Simulated (●) and measured (□) $DT_{80\%}$ for each MR.

At the top of the foam, ε_l decreases quickly with time. The total amount of liquid drained out of the foam with time can be easily calculated by an integration over z . From this, the theoretical $DT_{80\%}$ is estimated for the various MR. These are compared to experimental data in figure 6.5 B. It is seen that the simulated drainage times are of the same order of magnitude as the experimental values and that the change in experimental values of $DT_{80\%}$ with increasing MR is reflected in the simulated data.

To get insights in the coalescence of bubbles the liquid film between bubbles have to be taken into account. As the liquid volume fraction decreases, bubbles will come closer together and liquid drains from the thin film to the Plateau borders. The rupture and drainage of thin films is described using DLVO theory including van der Waals and electrostatic interactions, in combination with Vrij's criterion for thin film stability. This was previously used to describe the stability of thin liquid films of pure water (chapter 2)²³. The change of thickness h of the thin film as function of time t is estimated using equation 5

$$(5) \quad \frac{dh}{dt} = -\frac{2h^3}{3\eta r_f^2} \left(\frac{2\gamma}{r_p} - \Pi_D \right)$$

where r_f is the radius of the thin film, r_p the radius of the Plateau border and Π_D the disjoining pressure. The experimental values for viscosity and interfacial tension are used. The film radius r_f and PB radius r_p are estimated from ε_l and the foam structure. Assuming a foam structure formed by regular pentagonal dodecahedrons, the following relations can be deduced^{24, 25}; $r_f = 0.8 R_b$, $A_p = 0.16r_p^2 + 1.73r_p h$, with A_p the area of the PB, $r_p = 5.4 h + (26.2 h^2 + 6.2 A_p)^{1/2}$, $\varepsilon = v (12 \pi r_f^2 + 10 A_p L)$, $v = (1 - \varepsilon)/V_B$, and $V_B = 4\pi r_B^3/4$.

Chapter 6

From these, r_f and r_p can be estimated given ε_l , h and r_B . As an example: $\varepsilon_l = 0.1$, $h = 100$ nm and $r_B = 0.1$ mm gives $r_f = 80$ μ m and $r_p = 50$ μ m.

As a first approximation, we assume the parameters, except h , to be independent of t . Furthermore, we assume that all SDS binds to LYS, which is in line with literature²⁶. The disjoining pressure is calculated as the sum of the van der Waals and electrostatic contributions (equation 6).

$$(6) \quad \Pi_D = \Pi_{VW} + \Pi_{el}$$

The van der Waals contribution Π_{VW} to the disjoining pressure is estimated by equation 7

$$(7) \quad \Pi_{VW} = -\frac{A_H}{6\pi h^3}$$

where the Hamaker constant A_H is about $7.5 \cdot 10^{-23}$ J for a protein covered interface interacting with another protein interface across water²⁷.

The electrostatic contribution to the disjoining pressure Π_{el} was estimated from equation 8

$$(8) \quad \Pi_{el} = 4k_B T \rho_{\infty} \tanh^2\left(\frac{e\psi_0}{4k_B T}\right) e^{-\kappa h}$$

where $k_B = 1.38 \cdot 10^{-23}$ m² kg s⁻² K⁻¹ is Boltzmann's constant, T is the temperature, $\rho_{\infty} = \sum \rho_{\infty i} / n_i$, with n is the number of ions with same valence and the sum runs over all ions i in solution having a number density in the bulk of $\rho_{i\infty}$, $e = 1.6 \cdot 10^{-19}$ C is the charge of an electron, ψ_0 is the surface potential of the protein interfacial layer, and

$$(9) \quad \kappa = \sqrt{\frac{\sum_i z_i \rho_{i\infty} e}{\varepsilon_0 \varepsilon_r k_B T}}$$

is the Debye screening length, with $\varepsilon_0 = 8.8 \cdot 10^{-12}$ F m⁻¹ is the electric permittivity of vacuum, $\varepsilon_r = 80$ is the relative dielectric constant of water. The surface potential of the protein interfacial layer was derived from the interfacial charge density $\sigma_0 = e Z_c \Gamma_{eq}$, with Γ_{eq} is the adsorbed amount and Z_c is the charge of the adsorbed complexes, and

$$(10) \quad \sigma_0^2 = \frac{\sum \rho_{i\infty} \left(\exp\left(\frac{-e Z_c \psi_0}{k_B T}\right) - 1 \right)}{2 \varepsilon_0 \varepsilon_r k_B T}$$

Γ_{eq} is roughly estimated being 3 mg m⁻², based on various interfacial studies of LYS and LYS-SDS^{9, 11, 28}. It is noted that for the MRs studied here, the adsorbed amount hardly varies with MR¹¹. It also turned out that the results are not very sensitive to the precise value of Γ_{eq} and that the derived conclusions hold even when Γ_{eq} is changed by 1 mg m⁻².

We consider the complex, including the Stern layer, to be a colloidal particle and assume that the ζ -potential is then about equal to the particles surface potential²⁹. Then the charge of the complexes Z_c is estimated using $Z_c = \sigma_c e / A_c$, with σ_c is the (averaged) surface charge density and A_c the surface area of the complex. The surface charge density can be estimated using equation 10, but then with σ_0 and ψ_0 replaced by σ_c and ζ respectively. The radius R_c of the colloidal particle is estimated from its approximated mass $M_c = M_{LYS} + MR \cdot M_{SDS}$, specific volume of proteins $v_p = 0.73 \cdot 10^{-3}$ m³ kg⁻¹³⁰ and thickness of the Stern layer $d_{stern} = 0.4$ nm²⁹. The charge of the complex as function of MR is estimated from the measured ζ -potential, both shown in figure 6.6. The ζ -potential of LYS was 3.2 ± 0.2 mV corresponding with a net charge of $Z_c = 0.4$ for the colloidal particle (figure 6.6 A). This is remarkably lower than the charge of 8, which is expected from the

ionisable groups of LYS at pH = 7. This difference was attributed to the bound counter ions in the Stern layer²⁹.

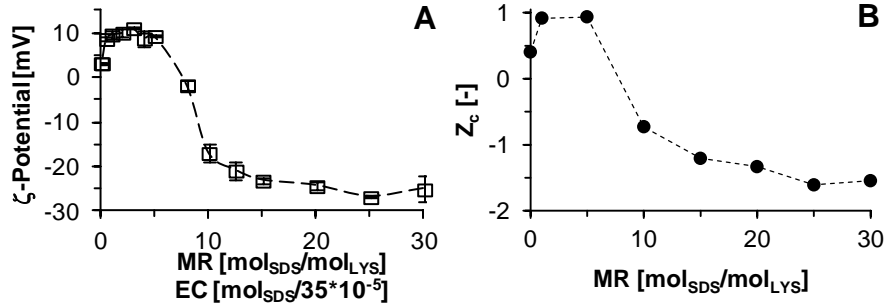


Figure 6.6: A) ζ -potential of LYS-SDS mixtures as function of the MR. The dotted line indicates a ζ -potential of 0 mV. The error bars shows the standard deviation between repetitive measurements. B) The charge Z_c of the LYS-SDS calculated from the ζ -potential as a function of MR. The dashed line is a guide to the eye and does not represent a fit.

Estimations of foam film stability

The rupture times of the thin films, for ε_l ranging from 0.35-0.01, were estimated for the different LYS-SDS MRs, assuming mean bubble radii of 0.1 mm (figure 6.7 A). The bubble radii were based on the values from figure 6.1 C.

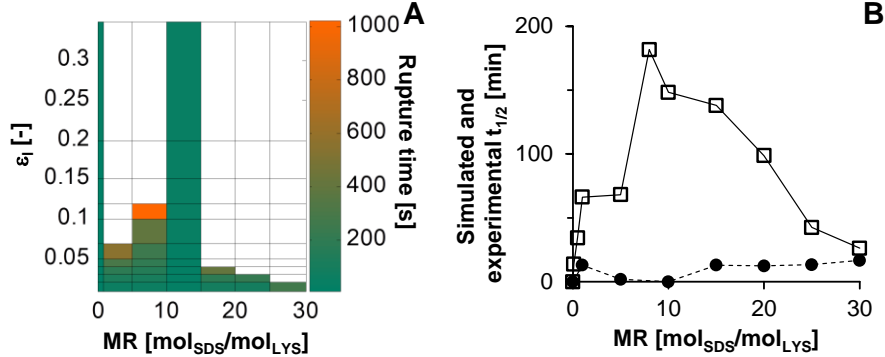


Figure 6.7: A) Simulated rupture times of bubble separating thin films as a function of ε_l and MR for mixtures of LYS-SDS foam and LYS with a mean bubble radius $r_b = 0.1$ mm for different MR (equation 4). B) Foam stability experimental (□) and modelled (onset of coalescence) (●) as function of MR.

The simulation shows that for most values of ε_l the thin films of pure LYS and those of LYS-SDS at MR = 10 rupture at very short time-scales (smaller than about 30 s). This means that bubbles of pure LYS and MR 10 are not stable and will coalesce upon contact with another, i.e. during packing of the bubble layers. At other MRs, stable regimes are observed (white areas figure 6.7 A) where the films will not rupture. For these MRs, rupture will only occur once the ε_l drops below a critical value. For instance, for MR 15,

the films are stable until a critical ε_l is reached at 0.04 where the thin films have rupture time of 1000 s. At $\varepsilon_l = 0.02$ have a rupture time of <200s. Combining the estimation of the rupture times for the thin films with the drainage model, a foam stability α can be estimated. In this approach, the foam stability is the estimated time at which the top layer of the foam reaches the critical ε_l from which onwards, the thin films start to become unstable (figure 6.7 B). It becomes apparent that the simulated foam stability (onset of coalescence) for LYS at MR = 0 and LYS-SDS at MR = 10 is close to zero, which is due to the low repulsive charge of LYS and the LYS-SDS complex at this MR. For LYS this is in line with experimental observation. However, for the mixtures at MR = 10, the simulated foam stability shows the opposite of the experimental observation, which actually shows the largest foam stability at MR = 10. Most probably this discrepancy between the model and the experimental data is due to the bulk interaction of LYS and SDS causing the aggregation of the LYS-SDS complexes, which could stabilize the thin liquid films. The contributions of such aggregates are not included in the theoretical considerations.

Bulk interaction of LYS and SDS

The bulk interaction of LYS and SDS was studied by turbidimetry. Both pure LYS and SDS solutions were clear. The turbidity increased with increasing MR until a maximum between MR 5 and 10 (figure 6.8). At MR > 10, the turbidity of the solution decreased and at MR 30, the mixtures were transparent. The turbidity of the solution is a measure of the number and size of particles dispersed in it.

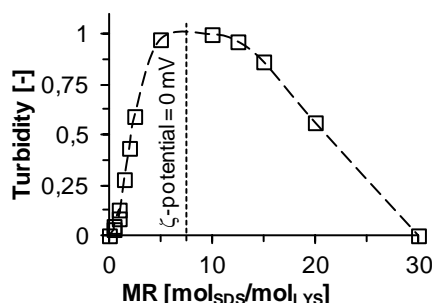


Figure 6.8: Turbidity of LYS-SDS mixtures as function of the MR. The long dashed line is a guide to the eye and does not represent a fit. The dotted line indicates a ζ -potential of 0 mV.

This increase in turbidity with increased MR indicates that the soluble LYS-SDS complexes have formed aggregated complexes. The highest turbidity is observed between MR of 5 and 10, which is in line with observations of LYS-SDS mixtures that have been reported for pH values close to those used in this study (MR-10, pH 5.6⁵; and MR 8-10, pH 6.5⁷). The decrease in turbidity at MR > 10 corresponds to dissociation of the aggregates, which seems typical for LYS-SDS mixtures and is good in agreement with values reported literature⁵⁻⁷. The reason for the increase/decrease in aggregation has been attributed to the decrease/increase of the ζ -potential or net-charge of the complexes, as shown in

figure 6.6. Recently, a foam stabilization mechanism has been proposed for self-associating whey protein microgels, which seem to be comparable to the aggregation of LYS-SDS solutions¹².

Thin films of LYS-SDS mixtures

To get a better understanding of the foam stability in mixed LYS-SDS systems, thin films were studied in the Sheludko cell. As shown in figure 6.9, thin liquid films of LYS (MR 0) drained to common black films. These films were unstable and ruptured within 2 minutes after formation. The thin films made from pure SDS (EC 20) drained to the thickness of a common black films, similar to the pure LYS films, but without the brighter spots. The films of SDS were stable for more than 1 h. Micrographs of thin films of LYS-SDS mixtures at MR 0.5 showed large (10-200 μm) objects in the parallel part of the film as well as in the surrounding meniscus. These objects are most likely the aggregated complexes and seem to be trapped between the two interfaces. The thin films at MR 1 and 5 seem thicker than those at MR 0.5 and did not drain to form the plane parallel parts. It is noted that because of the presence of aggregates, the actual thickness could not be determined by interferometry. Based on the colours in the micrographs, the thickness is estimated to be several 100 nm. In thin films of MR 10 and 15, the plane parallel part is visible again, but still the menisci around the plane parallel part of the films are filled with aggregates. From MR 20 onwards, no objects are visible in the thin films and the thin film looks similar to pure SDS at EC 20.

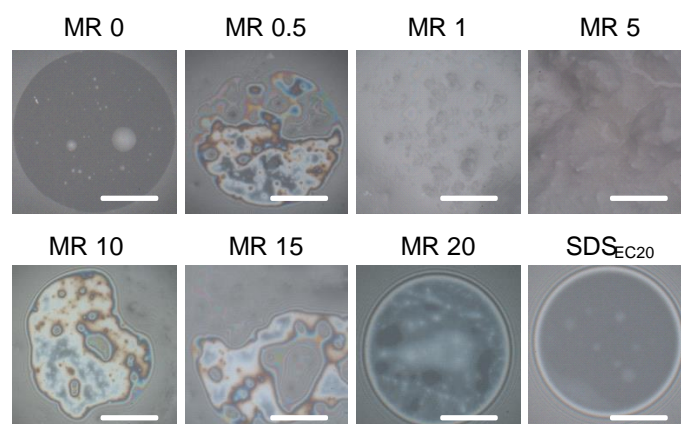


Figure 6.9: Micrographs of typical thin liquid films of LYS-SDS, LYS and SDS solutions, recorded in reflected light 1 minute after film formation. The solutions were equilibrated for 15 minutes prior to film formation. The white bar has a length of 100 μm .

At those MRs, the oppositely charged mixtures behave similar to other (similarly charged) protein-surfactant mixtures at high MR^{3, 4}. For these high MR, the foam stability is similar to the foam properties of pure surfactant. The occurrence of objects (aggregated complexes) in the thin films corresponds with the increase of turbidity as a function of the MR. Similar observations of aggregated complexes, which increased the foam stability have been shown for oppositely charged polymer surfactant mixtures before³¹. In other

Chapter 6

studies, it was shown that protein aggregates are located in the PB^{32, 33}, or in the thin liquid films, depending on the size of the aggregate³⁴. These studies suggest that the particles reduce the drainage rates from PB, which would increase the time until the critical ε_l in the foam is reached. As can be seen from figure 6.7 B, the effect of increasing viscosity at MR 10, which would result in slower PB drainage, is not reflected in the strong decrease in modelled foam stability. Instead of slowing the PB drainage, it is more likely that the aggregated complexes slow the drainage from the thin films, which also increases the time until ε_l is reached and the foam becomes unstable.

Conclusions

The addition of SDS to LYS leads to the formation of aggregates that largely increase the foam stability of the mixture. From the comparison of experimental and modelled drainage and stability data, it was concluded that the presence of aggregated LYS-SDS complexes strongly enhance the stability of thin films, while their role in decreasing PB drainage rates is of less importance. The exact mechanism by which the aggregated complexes increase thin film stability is yet unclear. Especially, the structure of the aggregated complexes might give more insight into their role in stabilizing oppositely charged protein surfactant mixtures.

References

1. Maldonado-Valderrama, J.; Patino, J. M. R., Interfacial rheology of protein-surfactant mixtures. *Current Opinion in Colloid and Interface Science* **2010**, *15*, 271-282.
2. Dickinson, E., Adsorbed protein layers at fluid interfaces: interactions, structure and surface rheology. *Colloids and Surfaces B: Biointerfaces* **1999**, *15*, 161-176.
3. Lech, F. J.; Meinders, M. B. J.; Wierenga, P. A.; Gruppen, H., Comparing foam and interfacial properties of similarly charged protein-surfactant mixtures. *Colloids and Surfaces A: Physicochemical and Engineering Aspects* **2015**, *476*, 18-23.
4. Lech, F. J.; Steltenpool, P.; Meinders, M. B. J.; Sforza, S.; Gruppen, H.; Wierenga, P. A., Identifying changes in chemical, interfacial and foam properties of β -lactoglobulin-sodium dodecyl sulphate mixtures. *Colloids and Surfaces A: Physicochemical and Engineering Aspects* **2014**, *462*, 34-44.
5. Fukushima, K.; Murata, Y.; Nishikido, N.; Sugihara, G.; Tanaka, M., The binding of sodium dodecyl sulfate to lysozyme in aqueous solutions. *Bulletin of the Chemical Society of Japan* **1981**, *54*, 3122-3127.
6. Morén, A. K.; Khan, A., Surfactant hydrophobic effect on the phase behavior of oppositely charged protein and surfactant mixtures: Lysozyme and sodium alkyl sulfates. *Langmuir* **1998**, *14*, 6818-6826.
7. Morén, A. K.; Khan, A., Phase equilibria of an anionic surfactant (sodium dodecyl sulfate) and an oppositely charged protein (lysozyme) in water. *Langmuir* **1995**, *11*, 3636-3643.
8. Alahverdjieva, V. S.; Khristov, K.; Exerova, D.; Miller, R., Correlation between adsorption isotherm, thin liquid films and foam properties of protein/surfactant mixtures: Lysozyme/C₁₀DMPO and lysozyme/SDS. *Colloids and Surfaces A: Physicochemical and Engineering Aspects* **2008**, *323*, 132-138.
9. Green, R. J.; Su, T. J.; Joy, H.; Lu, J. R., Interaction of lysozyme and sodium dodecyl sulfate at the air-liquid interface. *Langmuir* **2000**, *16*, 5797-5805.
10. Sun, M. L.; Tilton, R. D., Adsorption of protein/surfactant complexes at the air/aqueous interface. *Colloids and Surfaces B: Biointerfaces* **2001**, *20*, 281-293.
11. Alahverdjieva, V. S.; Grigoriev, D. O.; Fainerman, V. B.; Aksenenko, E. V.; Miller, R.; Möhwal, H., Competitive adsorption from mixed hen egg-white lysozyme/surfactant solutions at the

air–water interface studied by tensiometry, ellipsometry, and surface dilational rheology. *The Journal of Physical Chemistry B* **2008**, 112, 2136-2143.

12. Schmitt, C.; Bovay, C.; Rouvet, M., Bulk self-aggregation drives foam stabilization properties of whey protein microgels. *Food Hydrocolloids* **2014**, 42, 139-148.

13. Wierenga, P. A.; Meinders, M. B. J.; Egmond, M. R.; Voragen, A. G. J.; de Jongh, H. H. J., Quantitative description of the relation between protein net charge and protein adsorption to air–water interfaces. *The Journal of Physical Chemistry B* **2005**, 109, 16946-16952.

14. Chernysheva, M. G.; Ivanov, R. A.; Soboleva, O. A.; Badun, G. A., Do low surfactants concentrations change lysozyme colloid properties? *Colloids and Surfaces A: Physicochemical and Engineering Aspects* **2013**, 436, 1121-1129.

15. Delahaije, R. J. B. M.; Wierenga, P. A.; Giuseppin, M. L. F.; Gruppen, H., Improved emulsion stability by succinylation of patatin is caused by partial unfolding rather than charge effects. *Journal of Colloid and Interface Science* **2014**, 430, 69-77.

16. Jachimska, B.; Wasilewska, M.; Adamczyk, Z., Characterization of globular protein solutions by dynamic light scattering, electrophoretic mobility, and viscosity measurements. *Langmuir* **2008**, 24, 6866-6872.

17. Walstra, P., Appendix H: Physical properties of water at 0°C to 100°C. In *Physical Chemistry of Foods*, Marcel Dekker: New York, NY, USA, **2009**; p 807.

18. Wierenga, P. A.; van Norél, L.; Basheva, E. S., Reconsidering the importance of interfacial properties in foam stability. *Colloids and Surfaces A: Physicochemical and Engineering Aspects* **2009**, 344, 72-78.

19. Le Floch-Fouéré, C.; Pezenec, S.; Lechevalier, V.; Beaufils, S.; Desbat, B.; Pézolet, M.; Renault, A., Synergy between ovalbumin and lysozyme leads to non-additive interfacial and foaming properties of mixtures. *Food Hydrocolloids* **2009**, 23, 352-365.

20. Bahri, M. A.; Hoebeke, M.; Grammenos, A.; Delanaye, L.; Vandewalle, N.; Seret, A., Investigation of SDS, DTAB and CTAB micelle microviscosities by electron spin resonance. *Colloids and Surfaces A: Physicochemical and Engineering Aspects* **2006**, 290, 206-212.

21. Walstra, P., Formation of emulsions and foams. In *Physical Chemistry of Foods*, 1 ed.; Marcel Dekker: New York, NY, USA, **2003**; p 807.

22. Koehler, S. A.; Hilgenfeldt, S.; Stone, H. A., A generalized view of foam drainage: Experiment and theory. *Langmuir* **2000**, 16, 6327-6341.

23. Lech, F. J.; Wierenga, P. A.; Gruppen, H.; Meinders, M. B. J., Stability properties of surfactant-free thin films at different ionic strengths: Measurements and modeling. *Langmuir* **2015**, 31, 2777-2782.

24. Desai, D.; Kumar, R., Liquid holdup in semi-batch cellular foams. *Chemical Engineering Science* **1983**, 38, 1525-1534.

25. Leonard, R. A.; Lemlich, R., A study of interstitial liquid flow in foam. Part I. Theoretical model and application to foam fractionation. *American Institute of Chemical Engineers Journal* **1965**, 11, 18-25.

26. Lad, M. D.; Ledger, V. M.; Briggs, B.; Green, R. J.; Frazier, R. A., Analysis of the SDS–lysozyme binding isotherm. *Langmuir* **2003**, 19, 5098-5103.

27. Israelachvili, J. N., *Intermolecular and surface forces*. 3 ed.; Academic Press (Elsevier): Santa Barbara, CA, USA, **2011**; p 674.

28. Hunter, J. R.; Kilpatrick, P. K.; Carbonell, R. G., Lysozyme adsorption at the air/water interface. *Journal of Colloid and Interface Science* **1990**, 137, 462-482.

29. Norde, W.; Lyklema, J., Why proteins prefer interfaces. *Journal of Biomaterials Science, Polymer Edition* **1991**, 2, 183-202.

30. Millero, F. J.; Ward, G. K.; Chetirkin, P., Partial specific volume, expansibility, compressibility, and heat capacity of aqueous lysozyme solutions. *Journal of Biological Chemistry* **1976**, 251, 4001-4004.

31. Monteux, C.; Fuller, G. G.; Bergeron, V., Shear and dilational surface rheology of oppositely charged polyelectrolyte/surfactant microgels adsorbed at the air–water interface. Influence on foam stability. *The Journal of Physical Chemistry B* **2004**, 108, 16473-16482.

32. Carn, F.; Colin, A.; Pitois, O.; Vignes-Adler, M.; Backov, R., Foam drainage in the presence of nanoparticle–surfactant mixtures. *Langmuir* **2009**, 25, 7847-7856.

33. Carn, F.; Colin, A.; Pitois, O.; Backov, R., Foam drainage study during plateau border mineralisation. *Soft Matter* **2012**, 8, 61-65.

34. Carl, A.; Bannuscher, A.; von Klitzing, R., Particle stabilized aqueous foams at different length scales: Synergy between silica particles and alkylamines. *Langmuir* **2014**.

7. General Discussion

The aim of the research described in this thesis was to understand of the effects that the addition of low molecular weight surfactants (LMWS) to proteins have on the foam properties of the mixtures. In **chapter 1** it was hypothesized that the formation of the complexes as well as the composition of the mixtures i.e. the presence of protein-LMWS complexes and free LMWS determine the foam properties of the mixtures. Both proteins and LMWS can be similarly or oppositely charged to each other. Hence, the charge of compounds will lead to different protein-LMWS complexes. It is, therefore, hypothesized that the foam properties of the mixtures / complexes depend on the relative charge both substances possess and on the effect this has on interfacial and thin film properties.

The data provided in this thesis make it unequivocally clear that there is a large effect of the addition of LMWS to protein solutions on the foam properties of the mixtures (**chapters 4-6**). The foam properties of the mixtures show a non-linear relation with MR. In two cases of similarly charged mixtures (**chapters 4 and 5**) a minimum foam stability was observed at intermediate MR, while in a third case of an oppositely charged mixture (**chapter 6**) a maximum of the foam stability was found.

The use of different proteins and LMWS in combination with different measurement methods allowed us to reach the following conclusions: (1) The key parameter describing the foam properties of mixtures of similarly charged LMWS and proteins is the amount of bound and free LMWS. In general, taking the foam stability of the protein as a reference, a decrease of the foam stability was found at low MR, i.e. before all high affinity binding sites are saturated. At higher MR, the foam stability followed the curve of foam stability of LMWS. This confirms the first hypothesis stated in the general introduction; (2) When proteins are mixed with oppositely charged LMWS, the presence of aggregated complexes can result in an increase in foam stability. This confirms the second hypothesis stated in the general introduction. (3) For pure protein solutions, the foam ability depends on the adsorption rate of the protein, which depends on the concentration as well as on the molecular properties of the protein. Three regimes; a surfactant poor, an intermediate and a surfactant rich regime, separated by two critical concentrations can be discriminated. The critical concentrations and with it the foam ability varied with pH, which was explained by a difference in adsorption rates.

Foam properties of similarly charged protein-LMWS mixtures: Importance of the binding sites in similarly charged mixtures

As mentioned above, there is a large effect of the addition of LMWS to proteins on the foam stability. In the case of BSA-SDS mixtures, the foam half-life time ($t_{1/2}$) showed a minimum at MR 50, which is a reduction of 90 % compared to the solely protein based foam (under conditions as described in **chapter 5**). Similarly, the foam stability of a BLG-

Chapter 7

SDS mixture at MR 20 was reduced by 86 % compared to MR 0 (under conditions as described in **chapter 4**). The MR at which this minimum occurs is the MR at which the free LMWS start to dominate the interfacial and foam properties. This MR can be estimated by quantifying the number of binding sites and therewith the concentration of free LMWS (**chapter 5**). The question is how the number of low and high affinity binding sites can be determined. There are databases, such as the *binding database*¹ or *binding MOAD* (mother of all databases)², that provide data on for instance the binding affinity or half maximum effective concentration (EC_{50}) values. However, they do not provide data on the number of high and or low affinity binding sites. Experimentally, the number of high affinity binding sites (1 for BLG and 5 for BSA) can be successfully determined by isothermal titration calorimetry (ITC). The number of low affinity binding sites is more difficult to quantify. The use of ITC for this purpose is limited, since at high MRs proteins unfold, which hinders the analysis³. Another method is to quantify the amount of free LMWS (SDS) by a colorimetric method⁴. However, the quantification was not accurate enough to determine free SDS at MR < 10, where the transition between high and low affinity binding is located. In **chapter 5** we referred to literature that shows binding isotherms that were obtained by equilibrium dialysis. As described in **chapter 1**, the number of low-affinity binding sites depends on the concentration of LMWS and increases until the protein is saturated, as can exemplarily be seen for BSA-SDS mixtures⁵. The binding data for BSA-SDS mixtures⁵⁻⁷, as discussed in **chapter 5**, was used to calculate a binding ratio of 80 % (± 5 %). The binding ratio assumes that at any given concentration above the number of high affinity binding sites a fraction (e.g. the binding ratio is 80 % for SDS and BSA⁵⁻⁷) of LMWS binds to the protein, while the remainder of the LMWS is dissolved in the bulk solution. This allowed the comparison of foam stability of BSA and BLG in the presence of SDS.

Foam properties of oppositely charged protein-LMWS mixtures

In **chapter 6**, it was concluded that for oppositely charged mixtures, the presence of aggregated LYS-SDS complexes is responsible for the improved foam stability at low MR. The presence of these aggregates leads to an increase in foam stability from 13 min at MR 0.1 to 181 minutes at MR 8. The question arose whether this observation of enhanced foam stability is unique for mixtures of LYS and SDS, or a generic feature of oppositely charged protein-LMWS mixtures. Here we show additional data on two other oppositely charged protein-LMWS systems. In one system, the cationic LMWS cetyltrimethylammonium bromide (CTAB) was added to BLG at pH 7. In the other system SDS was added to BLG at pH 3. The foam stability ($t_{1/2}$) of BLG-SDS at pH 3 increases from 12 minutes at MR 0 to a maximum of 216 minutes at MR 10 and then drops to 10 minutes at MR 30 and increases again to 57 minutes at MR 100 (figure 7.1 A). At the same time, the $t_{1/2}$ of SDS alone increases monotonically up to 220 minutes at EC 100. The $t_{1/2}$ of the BLG-CTAB mixtures initially decreases with increasing MR, from 250 minutes at MR 0 down to 15 minutes at MR 10 (figure 7.1 B). Further increase of the MR leads to an increase of $t_{1/2}$ to 190 minutes at MR 21 from where the $t_{1/2}$ becomes independent of the MR. In comparison, the $t_{1/2}$ of CTAB alone increases monotonically up to 197 minutes at EC 50.

It seems that the foam stability of mixture of BLG-SDS at pH 3 is comparable to the foam stability of the LYS-SDS mixtures, while the foam stability of BLG-CTAB is following the opposite trend than that of the LYS-SDS mixture. While there are differences in foam stability, in all three cases aggregation of the protein-LMWS complexes is observed. This aggregation seems to be a generic feature, which can be predicted based on the net charge of the protein⁸ and the chain length of the LMWS molecule⁹.

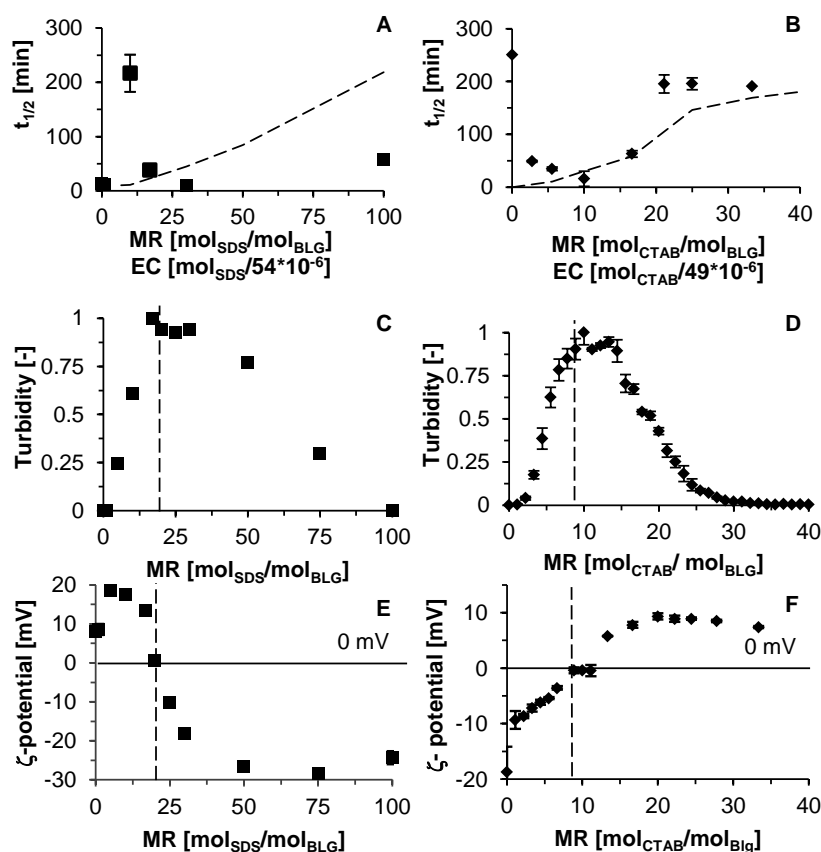


Figure 7.1: $t_{1/2}$, relative turbidity and ζ -potential of BLG-SDS (A, C and E, McIlvaine buffer (cf. chapter 3) pH 3.0) and BLG-CTAB (B, D and F, 10 mM sodium phosphate pH 7.0). The solid lines indicate the ζ -potential of 0 mV; the dashed lines indicate the MR where the maximum turbidity is observed.

The mixtures of BLG-SDS at pH 3 and BLG-CTAB show an increase of turbidity as a function of the MR until a maximum, followed by a decrease (figure 7.1 C+D). The absolute ζ -potential of the complexes decreases until it is at a minimum at the same MR where the turbidity is at the maximum (figure 7.1 E+F). In terms of aggregation of the complexes, both mixtures are similar to LYS-SDS mixtures (chapter 6). The aggregation of complexes of BLG-CTAB (at pH 7) is in good agreement with literature^{10, 11}. It can be seen that in all three oppositely charged mixtures the interaction in bulk, i.e. the aggregation and the ζ -

potential of the complexes follow similar rules. The maximum aggregation of the complexes is reflected by the net-charge of the protein (at the pH of the solution). This indicates that the charge of the protein can be used to predict the bulk interaction at MR below the maximum turbidity.

Characterization of aggregated complexes in mixtures of oppositely charged components

In the case of the oppositely charged protein-LMWS, aggregated protein-LMWS complexes were formed. For LYS-SDS and BLG-SDS at pH3, an improved foam stability was observed at the MRs (LYS-SDS: MR 0-8, BLG-SDS pH 3 MR 0-10) where these aggregates were formed. For BLG-CTAB, the foam stability in these MRs (MR 0 - 10) were lower than the pure protein solution, similar as observed for similarly charged protein-LMWS mixtures. This could be due to the properties of the particles, which may lead to anti-foam properties as has been shown for hydrophobic particles¹². To test this, thin film experiments were performed using solutions of aggregated complexes of LYS-SDS (high foam stability) and BLG-CTAB (low foam stability) mixtures (figure 7.2 A).

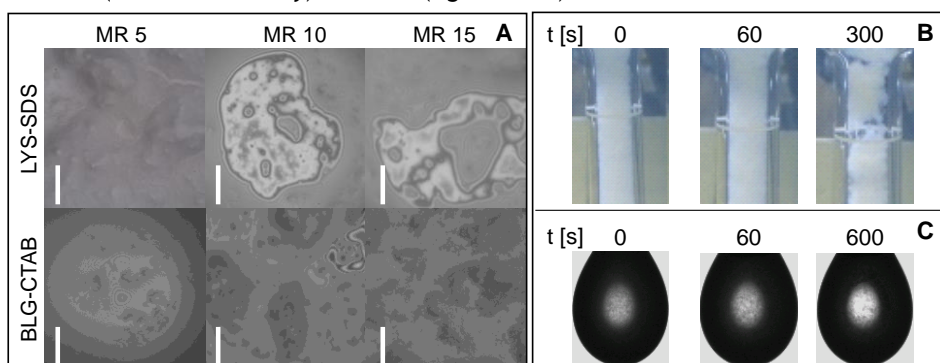


Figure 7.2: A) Micrographs of thin liquid films of LYS-SDS and BLG-CTAB at different MR. The white bar is 100 μm . B) and C) Phase separation and sedimentation of LYS-SDS mixtures as a function of time. MR 10 in the Ubbelohde capillary (panel B) and MR 1 in a pendant drop (panel C)

In both cases the aggregates were clearly observed in the thin films, but in both cases the films were stable. This shows that the aggregated complexes formed from BLG-CTAB do not act as anti-foam agents. Still, the foam stability experiments suggest that there are properties of the BLG-CTAB aggregates that are different from the aggregates formed by BLG-SDS (at pH 3) and LYS-SDS (chapter 6).

During preliminary experiments to characterize these aggregated complexes by light scattering it was found that they were so large that they sedimented. The sedimentation was also observed during other experiments, such as viscosimetry and automated drop tensiometry (figure 7.2 C). The aggregated complexes are instable, slight stirring was enough to break them up. This break-up of the aggregated complexes, was also observed during analysis of viscosity in the Ubbelohde capillary viscometer (figure 7.2 B). Since the aggregated complexes cluster and break apart depending on the shear forces, the interpretation of data from viscosity measurements becomes impossible. An attempt to

separate and measure the size of the aggregated complexes by asymmetric flow field flow fractionation (AF4) (Eclipse, Wyatt Technologies, Santa Barbara, CA, USA) was unsuccessful, since the aggregated complexes bound to the membrane in the flow channel and did not elute. Another preliminary experiment to study the effect of the concentration of the aggregated complexes showed the importance of the equilibrium of complexed and free SDS. For this experiment, aggregated complexes were separated from the solution (LYS-SDS, MR 10) by centrifugation. The aggregated complexes were re-dispersed in an SDS solution that had the same concentration of SDS as supernatant of MR 10 after centrifugation. Dissolving the complexes at different concentrations in the SDS solutions showed the delicate equilibrium between complexed and free SDS. The aggregated complexes either dissolved, when the concentration of aggregated complexes was lower than in the original solution or they aggregated further at concentrations that were higher than the original solution. This indicates that the aggregates are in equilibrium with non-adsorbed SDS in solution.

Foam properties of other mixtures of protein and a non-ionic LMWS

In foods, not only ionic LMWS, but also non-ionic LMWS are used. To extend the observations on ionic LMWS described above, experiments were performed using mixtures of the non-ionic Tween20 and BLG. The interfacial properties (Π and E_d) as function of MR show a similar trend as observed for the ionic surfactants. The Π and E_d after 1h adsorption time increased from the value of the pure protein to that of the pure surfactant (figure 7.3 A and B). The foam stability of the protein-LMWS mixture at pH 7 and 9 (figure 7.3 C) shows a similar behaviour as the mixtures with ionic LMWS. The only difference in this case is perhaps that the pure surfactant does not show very high values of $t_{1/2}$ as were observed for SDS or CTAB.

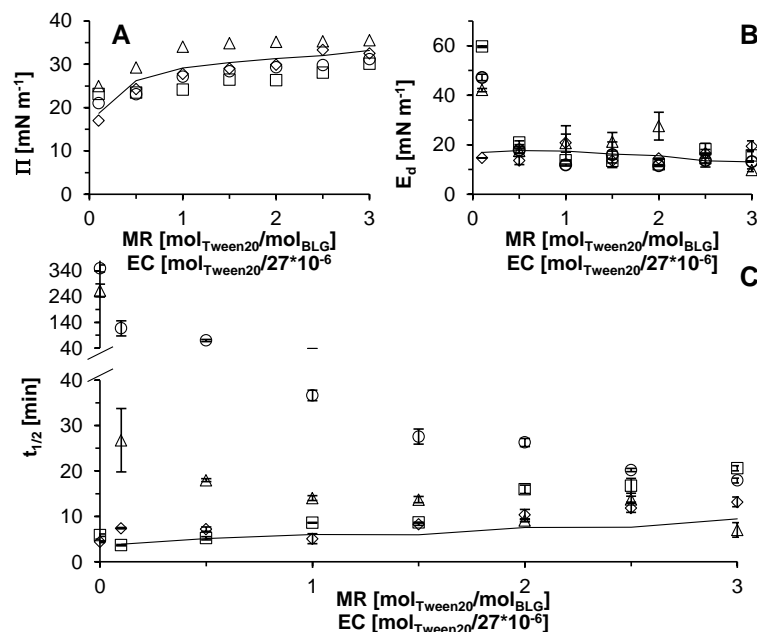


Figure 7.3: A) Π_{3600} , B) E_{d3600} and C) $t_{1/2}$ as a function of the MR of Tween20 for BLG (0.5 mg mL⁻¹). BLG was dissolved in pH 3 (◇), pH 5 (□), pH 7 (△) and pH 9 (○) in Mcllvaine buffer as described in chapter 3. The line represents data for Tween 20. Error bars indicate the standard deviation between replicate experiments.

With decreasing pH, the foam stability of the pure protein decreases. Because of the low foam stability of the protein under these conditions (pH 3 and 5) the foam stability in those mixtures is dominated by the LMWS for all MR > 0. At pH 7 and 9 the foam stability of the mixture becomes similar to the foam stability of the pure LMWS from a MR of 1.5. This signifies that MR 1.5 is the MR above which the free LMWS dominate the foam stability of the mixture. From this, in combination with the results with the ionic surfactants, it becomes clear that it is important to understand the parameters that determine the critical molar ratio.

The effect of the MR on the composition of protein-LMWS mixtures: Introducing the critical MR

In all systems studied, i.e. oppositely, similarly charged protein-LMWS mixtures and mixtures with proteins and non-ionic LMWS, a critical MR (MR_{cr}) was identified above which the foam stability was dominated by the LMWS. This was attributed (chapter 5) to the fact above the MR_{cr} the LMWS concentrations becomes high enough to dominate the interfacial and foam properties. The concentration of free LMWS can be calculated from the number of high binding sites (N) and the binding ratio of the low affinity binding sites (X) and the concentration of protein. In other words, at MR_{crit} , $t_{1/2mix} = t_{1/2LMWSCrit}$ when

$[LMWS]_{free} = [LMWS]_{crit}$. For SDS, $[LMWS]_{crit}$ was 1 mM. From equation 10 in chapter 5 it follows that MR_{crit} can be calculated with equation 1

$$(1) \quad MR_{crit} = N + \frac{[LMWS]_{free}}{[prot] - X * [prot]}$$

where MR_{crit} is the critical MR, N is the number of high affinity binding sites (-), $[LMWS]_{free}$ is the specific free surfactant concentration (mol L⁻¹), $[prot]$ is the concentration of protein (mol L⁻¹) and X is the specific low affinity binding ratio for the protein (-).

The critical MR, as well as N and X for SDS-BLG and SDS-BSA mixtures are listed in table 7.1. This approach is still a first approximation to formulate guidelines to understand the foam properties of mixed protein-LMWS mixtures. Of course, more detailed studies should be performed to identify the exact binding mechanism and to obtain direct experimental data on the low-affinity binding sites. Still, the approach shows that the behaviour of mixed protein-LMWS systems can be described and maybe predicted if the foam properties of the pure systems and the number of binding sites are known.

Table 7.1: Critical MR for similarly charged mixtures used in this research.

Protein/ LMWS	BLG/ SDS	BSA/ SDS
$[prot] \cdot 10^{-5}$ [mol L ⁻¹]	4.5	4.5
N [-]	0.8	5.5
X [-]	0.11	0.8
MR_{crit}	26	117

For oppositely charged mixtures (cf. chapter 6 and the mixtures, discussed above), the bulk interactions are similar for the different mixtures, i.e. similar trends in turbidity and ζ -potential as a function of the MR. Yet, in the MR range where aggregated complexes are present, different trends in foam stability curves were observed. Still, in all cases, a MR_{cr} is observed above which the foam properties start to be similar to that of the pure surfactant. In addition, above a certain MR, the interfacial properties will be dominated by the free LMWS. However, the MR above which the LMWS dominate the interfacial properties (MR_{cr}) is not necessarily the same as the MR above which they dominate the foam properties. This is due to the presence of aggregated complexes in the mixtures, found in oppositely charged protein-LMWS mixtures. Therefore, a second critical MR (MR_D) was defined as the MR above which the aggregated complexes are dissociated and the foam stability is similar to that of the pure LMWS. The MR_D would be expected to relate to the charge of the protein-LMWS complex. However, as becomes clear from figure 7.1, the ζ -potential measured on the suspensions does not give a clear indication of this point. This may be due to the fact that the method measures the ζ -potential of the aggregates and not of the individual protein-LMWS complex in the aggregate. Still, MR_D depends on the number of high affinity binding sites and a specific binding ratio of the low affinity binding sites. In the case of LYS-SDS, the number of high affinity binding sites were derived from the concentration of free SDS determined by a colorimetric assay⁴. At MR 5 no free SDS

Chapter 7

was determined, but at MR 10 7 % of the added SDS was found back as free SDS. This indicates that the number of high affinity binding sites is between 5 and 10. This corresponds with the MR at which the complexes have a ζ -potential of 0 mV (MR 8). Based on this, and the amount of free SDS at MR 10, the binding ratio of the low affinity binding sites (X) is calculated to be 0.34. With these values, it was calculated that the $[LMWS]_{free}$ at the MR_D where the complexes dissociate (MR 30) is 2.6 mM. This is close to the $[LMWS]_{free}$ at MR_{crit} for similarly charged surfactants (cf. **chapter 5**). Equation 1 was rewritten to equation 2, to calculate N and X for the BLG-CTAB and BLG-SDS (at pH 3) mixtures. We have assumed that the number of high affinity binding sites equals the net charge at that pH. This is based on the fact that for lysozyme the concentration of free LMWS was 0 until the MR where the complexes have a ζ -potential of 0 mV. Using these assumptions, the binding ratio of low affinity binding sites in oppositely charged mixtures can be calculated with equation 2.

$$(2) \quad X = \frac{[LMWS]_{free}}{(MR_D - N) * [prot]}$$

The values for the MR_D as well as N and X for the oppositely charged mixtures are summarized in table 7.2.

Table 7.2: MR_D , N and X in oppositely charged mixtures used in this research.

<i>Protein</i> <i>LMWS</i>	<i>LYS</i> <i>SDS</i>	<i>BLG</i> <i>CTAB</i>	<i>BLG_{pH3}</i> <i>SDS</i>
[prot] 10^{-5} M	35	4.5	4.5
N	8*	8	17
X	0.34*	0.93	0.26
MR_D	30*	32	100

*N and MR_D are discussed in the text, X was calculated with equation 2.

From the results presented in tables 7.1 and 7.2 it becomes clear that this set of quantifiable parameters allows the calculation of the two critical MR (MR_{crit} and MR_D) above which the foam stability of the mixture becomes similar to the foam stability of the pure LMWS. This allowed us to reconsider the 2 models for interfacial adsorption of mixed protein-LMWS systems that were presented in the **chapter 1**; i.e. the separate adsorption model and the complex adsorption model (figure 1.7). A schematic overview of the effect of addition of LMWS to protein solutions, based on the results of this thesis, is presented in figure 7.4.

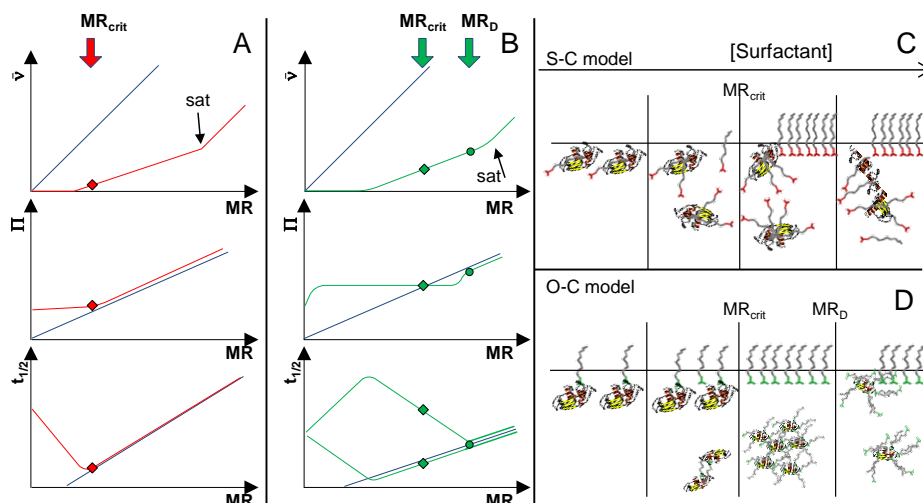


Figure 7.4: Schematic overview of binding, Π and $t_{1/2}$ for similarly charged (A) and oppositely charged (B) protein-LMWS mixtures. The critical MRs (MR_{crit} (♦, ◆) and MR_D (●)) are indicated by the arrows. The saturation of all protein binding sites is marked by a black arrow. The blue indicates the pure LMWS. C and D) Interfacial model for adsorption of similarly charged mixtures (S-C model) and oppositely charged mixtures (O-C model), respectively. The free LMWS that are in solution are not depicted.

For similarly charged mixtures, at $0 < MR \leq MR_{cr}$, the interface is filled with protein-LMWS complexes, with perhaps a small amount of free surfactant. At $MR > MR_{cr}$, the free LMWS at the interface dominate the interfacial properties. There may still be a certain amount of protein-LMWS complexes at the interface, but they do not contribute significantly to the foam properties. For oppositely charged mixtures, the picture is similar, except for the fact that until $MR = MR_D$ aggregated complexes are present. It may therefore be possible that there are cases where at $MR < MR_D$ the interfacial properties are dominated by free LMWS, while the foam properties are still dominated by the presence of the aggregated complexes.

Understanding foam ability

From the above, it is clear that based on the MR, N and X, the change in foam properties of mixed protein-LMWS systems can be described, at least qualitatively. To come to a quantitative prediction of the absolute value of the foam stability, a quantitative understanding of the foam properties of the pure protein and surfactant systems are needed. In chapter 3 it was shown that the foam ability (FA) as function of concentration can be divided into three regimes. In the surfactant poor regime, the foam volume increases with increasing concentration until at a critical concentration for the foam ability (C_{crFA}), the set foam volume is reached. In the intermediate regime, the initial bubble radius (r_{32}) decreases with increasing protein concentration until it becomes independent of the protein concentration. This point is referred to as the critical

Chapter 7

concentration for the radius (C_{cr32}) and is the start of the last, protein rich regime. It seems that to make a fair comparison of the foam stabilising properties of different proteins under different conditions, the samples should be compared in the protein rich regime ($C > C_{cr32}$). At least, the comparison of samples in that regime will reduce effects induced by differences in the initial foam structure (i.e. volume and bubble radius). The question is then how these critical concentrations (C_{crFA} and C_{cr32}) depend on the system conditions.

Effect of ionic strength

In **chapter 3** the foam ability (FA) was defined as the amount of foam formed after a certain sparging time (60 s), relative to the maximum amount possible. Below the critical concentration C_{crFA} the set maximum foam volume of 400 cm³ was not reached. Note, that FA is a parameter that depends on the chosen experimental conditions (e.g. desired foam volume, gas flow rate and temperature). It was concluded that C_{crFA} was related to the adsorption rate of the protein (**chapter 3**). Since the adsorption rate of proteins is, amongst others, related to the ionic strength of the solution¹³, it was hypothesized that by increasing the ionic strength the C_{crFA} of a protein solution is decreased. Consequently, at a constant protein concentration the FA would increase. Furthermore, a decrease of C_{cr32} is expected. If C_{cr32} becomes lower than the protein concentration tested, this should result in an increase in foam stability.

To further test this hypothesis, additional experiments with increasing NaCl concentration were performed. Data on the foam ability FA and stability $t_{1/2}$ of BLG (0.5 mg/mL⁻¹) in water and NaCl solutions at pH 3 and pH 6.5 are shown in figure 7.5. At pH 3, the protein concentration is below the C_{crFA} (0.75 mg mL⁻¹). The C_{crFA} for BLG at pH 6.5 is unknown, it can be assumed that it is close the C_{crFA} of pH 7 (0.25 mg mL⁻¹).

The FA of BLG at pH 3 increases with increasing concentration of NaCl (C_{NaCl}) from 0.25 in H₂O to 0.99 in 200 mM NaCl (figure 7.5 A). For BLG at pH 3, the FA increases with increased C_{NaCl} . This increase was expected since the adsorption rate increases with increasing C_{NaCl} ^{14, 15}. Only at a C_{NaCl} of 200 mM BLG at pH 3 reaches the C_{crFA} . For BLG at pH 6.5, differences between the samples dissolved in H₂O and NaCl were observed. The FA for 10 and 200 mM NaCl were similar and maximal. Since the FA for BLG at pH 6.5 in H₂O is not maximal, it is concluded that in H₂O the concentration of 0.5 mg mL⁻¹ is below the C_{crFA} . The fact that in both NaCl solutions FA is maximal indicates that at those C_{NaCl} , the BLG solutions are above C_{crFA} .

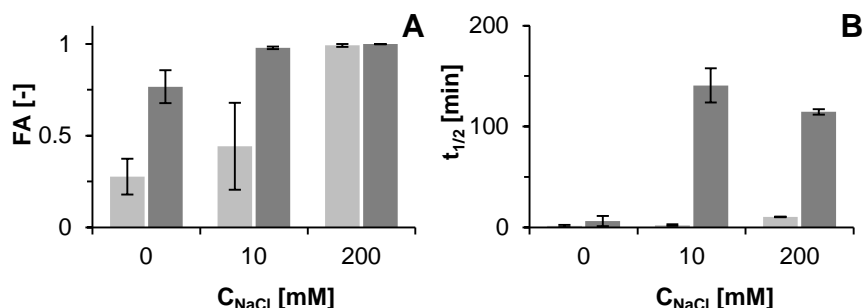


Figure 7.5: A) FA of BLG (0.5 mg mL^{-1}) in H_2O and NaCl solutions at pH 3 (■) and 6.5 (■). B) $t_{1/2}$ of the same solutions. Error bars indicate standard deviation.

Based on results shown in **chapter 3**, it was expected that for solutions in which the protein concentration $C < C_{\text{crr}32}$, the foam stability should be lower than for solutions where $C > C_{\text{crr}32}$. The foam stability in the BLG solutions at pH 3 increased with increased C_{NaCl} (1, 2 and 10 minutes, respectively) (figure 7.5 B). Those values are close to the foam stability values obtained in **chapter 3** for different concentrations. In **chapter 3** it was concluded that the protein rich regime for BLG at pH 3 begins around 10 mg mL^{-1} with a $t_{1/2}$ of 11 minutes. It seems that by changing C_{NaCl} , the foam stability of a sample from the protein rich regime can be matched by using a 20 times lower concentration. In other words, by increasing C_{NaCl} the boundary of the protein rich regime can be lowered. For BLG at pH 6.5, $t_{1/2}$ in H_2O was low (6 minutes) compared to the samples in 10 and 200 mM NaCl (140 and 114 minutes, respectively). The value obtained for 10 mM at NaCl solution (140 minutes) at pH 6.5 is between the values for BLG at pH 6 (50 minutes) and pH 7 (300 minutes) reported in **chapter 3**. At least for pH 7 with 0.5 mg mL^{-1} , the concentration was close to the $C_{\text{crr}32}$. We assume that those two concentration, which are above CRFA, are close to the $C_{\text{crr}32}$. Since the $t_{1/2}$ of 10 and 200 mM NaCl are much higher than those of BLG in H_2O , it becomes clear that the foam stability of the samples with and without added NaCl should not be compared. Only when the solutions are in the protein rich regime, a fair comparison seems possible, which strengthens the point we made **chapter 3**. Although the $t_{1/2}$ of BLG at pH 6.5 in NaCl solution is in the same order of magnitude as the $t_{1/2}$ of BLG at pH 7 (170 minutes at $0.25, 5$ and 10 mg mL^{-1} , respectively, cf. **chapter 3**), it does by no means indicate that this has to be the case for BLG at all pH's in the protein rich regime. The reason for absolute differences of $t_{1/2}$ of BLG at different pH values is still unknown. Modelling, as was shown in **chapter 6**, of the foam drainage and stability the thin liquid films might be used to determine the underlying mechanisms of the instability.

Outlook

The myth of predicting foam properties with interfacial properties

The field of protein and surfactant stabilised interfaces and foams has a long history. Still, a quantitative prediction of foam properties based on molecular properties of the surfactants does not exist. A lot of research in this field has been focussed on the

Chapter 7

assumption that interfacial properties, such as Π or E_d can be used to predict foam stability¹⁶⁻¹⁸. However, this view has been challenged in several occasions¹⁹⁻²¹.

In this thesis (**chapter 3**) we proved that the foam ability and bubble radius are indeed reflected by the adsorption rate of protein, which can be derived from the development of surface pressure in time. However, the foam stability did not correlate with the adsorption rate or by any of the 'long term' interfacial properties, such as the Π or E_d after 1 hour and the foam stability. Still, a link between foam ability and foam stability (and therefore with adsorption kinetics) was established. In the protein poor regime ($C < C_{cr32}$) the foam stability is low, while in the protein rich regime the foam stability is consistently higher.

During our research, we collected data on the foam stability and interfacial properties of an array of different protein solutions and mixtures of protein and LMWS. Here, we present these data and discuss them in relation to the hypothesis, postulated by many researchers, e.g.^{17, 18, 22}, i.e. that the foam stability can be predicted by determining the interfacial properties alone. In figure 7.6, we show the data for LYS-SDS, BLG-SDS and BSA-SDS. As was mentioned above, comparison of the foam stability is only possible in the protein rich regime. In the case of BLG-SDS (pH 7), the protein concentration was 0.82 mg mL^{-1} , which is above the C_{cr32} (**chapter 3**). For BSA (2.95 mg mL^{-1}) as well as for LYS (5 mg mL^{-1}), the critical concentrations are unknown. Since in all cases, LMWS molecules are added to the protein solution, the total concentration of surfactants is higher than the protein concentration. Therefore, we assume that in the other two cases of protein-LMWS mixtures, the concentrations of surfactant are close to or in the protein rich regime or to be more correct, in the surfactant rich regime, which allows a comparison of the foam stability.

The plots of $t_{1/2}$ over interfacial properties (Π and E_d) of mixtures show no positive correlation between both parameters and the foam stability (figure 7.6). This indicates that in mixtures of protein and LMWS, the hypothesis¹⁶⁻¹⁸ that Π or E_d can be used to predict the foam stability is disproven.

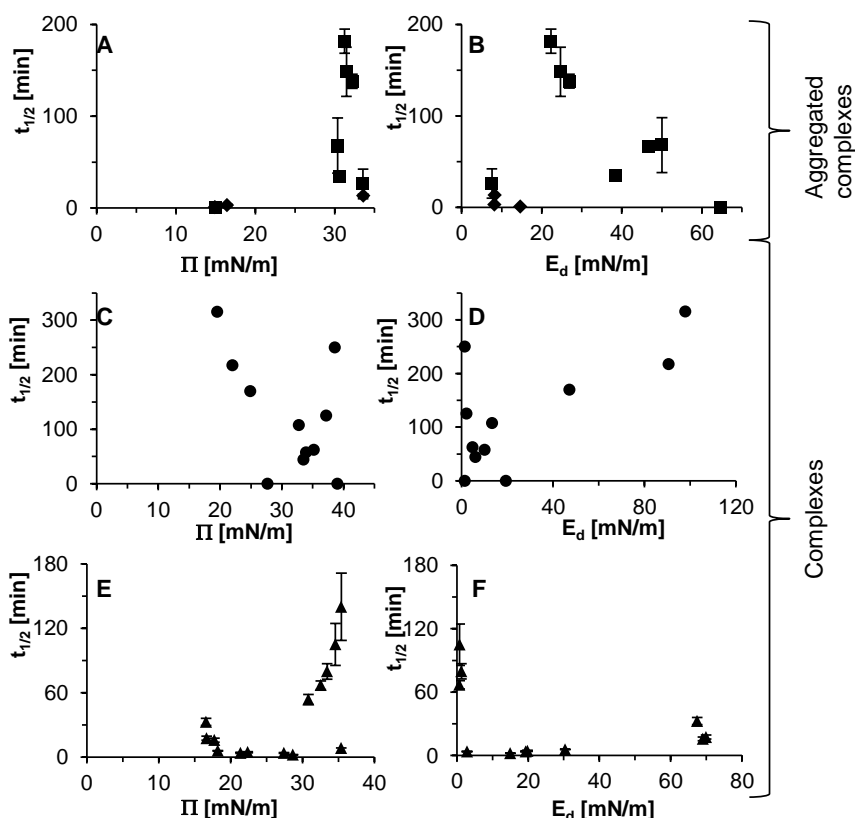


Figure 7.6: $t_{1/2}$ plotted over Π and E_d after 1 hour LYS-SDS (A and B, chapter 6), BLG-SDS (C and D, chapter 4) and BSA-SDS (E and F, chapter 5) mixtures. Error bars indicate standard deviation between replicates.

Further, we tested a system containing a single protein (BLG at 0.5 mg mL^{-1} , chapter 3) at different pH values (figure 7.7 A and B). Also in this case, no correlation between $t_{1/2}$ and Π or E_d was found. In chapter 3 it was shown that the foam ability depended on the concentration and the pH of the solution. In the case of BLG at pH 3, the concentration of 0.5 mg mL^{-1} is below the critical concentrations (C_{crFA} and C_{cr32}). This leads to differences in the foam structure and can lead to an incorrect comparison of the foam stabilities. To exclude possible effects of structural differences in foam, we compared Π of BLG at pH 3.0 with $C > C_{cr32}$ (20 mg mL^{-1}) to BLG at pH 7 (0.5 mg mL^{-1}) (figure 7.7 C). At 20 mg mL^{-1} , BLG at pH 3 shows faster adsorption and higher absolute values of Π than BLG at pH 7. Hence, it might be expected that the foam stability of BLG at pH 3 (20 mg mL^{-1}) would be higher than at pH 7. As can be seen in figure 7.7 D, this is not the case. Rather, the foam stability of BLG at pH 3, is still significantly lower than at pH 7, even at 20 mg mL^{-1} . This shows that the difference in foam stability of BLG at pH 3 and 7 is not reflected by differences in Π . Based on this, we conclude that the foam stability cannot be predicted by Π .

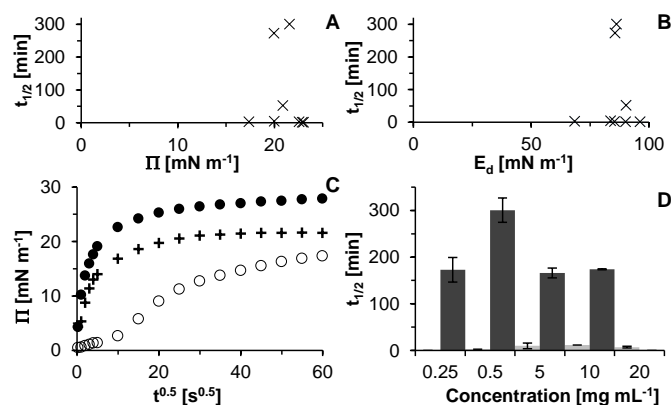


Figure 7.7: A) Plot of $t_{1/2}$ over the Π after 1 hour, B) plot of $t_{1/2}$ over E_d for BLG (0.5 mg mL⁻¹) at different pH values. C) Plot of Π over $t^{0.5}$ of BLG at pH 3 (20 mg mL⁻¹ (●)) and pH 7 (0.5 mg mL⁻¹ (+)). As a reference, also pH 3 with 0.5 mg mL⁻¹ (○) is shown. D) Foam stability of BLG at pH 7 (■) and pH 3 (▨) at different concentrations.

The comparison of $t_{1/2}$ to the interfacial properties (figures 7.6 and 7.7) shows that these interfacial properties do not provide the required detail to understand and predict the foam stability. Of course, interfacial properties can be measured and described in many different ways. This makes it difficult to identify the parameters that link to foam stability. In fact, the authors suggesting the prediction of foam stability by interfacial properties should provide more detail on the parameters to be used in such predictions (e.g. the frequency used to measure E_d). Also, the manner in which these parameters are quantitatively linked to the foam stability should be provided.

In chapters 2 and 6 we proposed a quantitative model to predict the foam stability based on the disjoining pressure (extended DLVO theory) and rupture times of the thin liquid films based on physical parameters, including the surface pressure. This is a step towards the prediction of the foam stability, yet other parameters, such as steric repulsion need to be included into the model to predict the foam stability (chapter 6). It should be noted that the overall generic statement that foam properties can be predicted by interfacial properties is not trivial.

Concluding remarks

The work presented in this thesis has shown that the foam stability of these mixtures can be predicted over a broad range of MRs. Using the foam stabilities of the pure protein and pure LMWS, the magnitude of change in foam stability can be estimated. The MR where the largest changes in foam stability are expected can be estimated from the critical parameters i.e. the critical MR, the number of high affinity binding sites and the binding ratio to the low affinity binding sites. The concentration of free LMWS enables a rescaling of the x-axis in different protein-LMWS system. It shows that the quantification of the bulk interaction between protein and LMWS is a valuable tool to predict the foam stability of the mixtures.

References

1. Gilson, M. The binding database. <https://www.bindingdb.org/bind/index.jsp> (3.9.2015),
2. Hu, L.; Benson, M. L.; Smith, R. D.; Lerner, M. G.; Carlson, H. A., Binding MOAD (Mother of all databases). *Proteins: Structure, Function, and Bioinformatics* **2005**, 60, 333-340.
3. Ding, Y.; Shu, Y.; Ge, L.; Guo, R., The effect of sodium dodecyl sulfate on the conformation of bovine serum albumin. *Colloids and Surfaces A: Physicochemical and Engineering Aspects* **2007**, 298, 163-169.
4. Rusconi, F.; Valton, É.; Nguyen, R.; Dufourc, E., Quantification of sodium dodecyl sulfate in microliter-volume biochemical samples by visible light spectroscopy. *Analytical Biochemistry* **2001**, 295, 31-37.
5. Chen, A.; Wu, D.; Johnson, C. S. J., Determination of the binding isotherm and size of the bovine serum albumin-sodium dodecyl sulfate complex by diffusion-ordered 2D NMR. *The Journal of Physical Chemistry* **1995**, 99, 828-834.
6. Tipping, E.; Jones, M. N.; Skinner, H. A., Enthalpy of interaction between some globular proteins and sodium n-dodecyl sulphate in aqueous solution. *Journal of the Chemical Society, Faraday Transactions 1: Physical Chemistry in Condensed Phases* **1974**, 70, 1306-1315.
7. Turro, N. J.; Lei, X.-G.; Ananthapadmanabhan, K. P.; Aronson, M., Spectroscopic probe analysis of protein-surfactant interactions: The BSA/SDS system. *Langmuir* **1995**, 11, 2525-2533.
8. Morén, A. K.; Khan, A., Phase equilibria of an anionic surfactant (sodium dodecyl sulfate) and an oppositely charged protein (lysozyme) in water. *Langmuir* **1995**, 11, 3636-3643.
9. Morén, A. K.; Khan, A., Surfactant hydrophobic effect on the phase behavior of oppositely charged protein and surfactant mixtures: Lysozyme and sodium alkyl sulfates. *Langmuir* **1998**, 14, 6818-6826.
10. Maulik, S.; Dutta, P.; Chatteraj, D. K.; Moulik, S. P., Biopolymer-surfactant interactions: 5 Equilibrium studies on the binding of cetyltrimethyl ammonium bromide and sodium dodecyl sulfate with bovine serum albumin, β -lactoglobulin, hemoglobin, gelatin, lysozyme and deoxyribonucleic. *Colloids and Surfaces B: Biointerfaces* **1998**, 11, 1-8.
11. Waninge, R.; Paulsson, M.; Nylander, T.; Ninham, B.; Sellers, P., Binding of sodium dodecyl sulphate and dodecyl trimethyl ammonium chloride to β -lactoglobulin: A calorimetric study. *International Dairy Journal* **1998**, 8, 141-148.
12. Pelton, R.; Flaherty, T., Defoamers: linking fundamentals to formulations. *Polymer International* **2003**, 52, 479-485.
13. Schwenzfeier, A.; Lech, F.; Wierenga, P. A.; Eppink, M. H. M.; Gruppen, H., Foam properties of algae soluble protein isolate: Effect of pH and ionic strength. *Food Hydrocolloids* **2013**, 33, 111-117.
14. Delahaije, R. J. B. M.; Wierenga, P. A.; Giuseppin, M. L. F.; Gruppen, H., Improved emulsion stability by succinylation of patatin is caused by partial unfolding rather than charge effects. *Journal of Colloid and Interface Science* **2014**, 430, 69-77.
15. Wierenga, P. A.; Meinders, M. B. J.; Egmond, M. R.; Voragen, A. G. J.; de Jongh, H. H. J., Quantitative description of the relation between protein net charge and protein adsorption to air-water interfaces. *The Journal of Physical Chemistry B* **2005**, 109, 16946-16952.
16. Rodríguez Patino, J. M.; Carrera Sánchez, C.; Rodríguez Niño, M. R., Implications of interfacial characteristics of food foaming agents in foam formulations. *Advances in Colloid and Interface Science* **2008**, 140, 95-113.
17. Schmidt, D. L., Nonaqueous foams. In *Foams*, Prud'homme, R.; Khan, S., Eds. Marcel Dekker: New York, NY, USA, 1996; Vol. 1, pp 287-314.

Chapter 7

18. Wilde, P.; Mackie, A.; Husband, F.; Gunning, P.; Morris, V., Proteins and emulsifiers at liquid interfaces. *Advances in Colloid and Interface Science* **2004**, 108-109, 63-71.
19. Bals, A.; Kulozik, U., Effect of pre-heating on the foaming properties of whey protein isolate using a membrane foaming apparatus. *International Dairy Journal* **2003**, 13, 903-908.
20. Davis, J. P.; Foegeding, E. A., Foaming and interfacial properties of polymerized whey protein isolate. *Journal of Food Science* **2004**, 69, C404-C410.
21. Wierenga, P. A.; van Norél, L.; Basheva, E. S., Reconsidering the importance of interfacial properties in foam stability. *Colloids and Surfaces A: Physicochemical and Engineering Aspects* **2009**, 344, 72-78.
22. Foegeding, E. A.; Luck, P. J.; Davis, J. P., Factors determining the physical properties of protein foams. *Food Hydrocolloids* **2006**, 20, 284-292.

Summary

Foods typically contain mixtures of surface-active components, such as proteins and low molecular weight surfactants (LMWS). Although the mechanisms determining the individual foam properties of protein and LMWS are known, the mechanisms that determine the foam properties of protein-LMWS mixtures are still unknown. Therefore, the aim of this thesis is to gain understand the foam properties of protein-LMWS mixtures. In **chapter 1**, the underlying mechanisms of foam formation and stabilization at different length scales (e.g. solution, interface, thin liquid film and foam) are introduced. Next, an introduction into properties of LMWS and proteins in the bulk solution, at the interface and in the foam is given. A screening of the current literature on protein-LMWS mixtures showed that the research on bulk interaction as well as the research on interfacial properties use similar conditions (e.g. concentration, conditions and compounds). Still, both fields are not tightly connected. The literature overview also showed that little data on foam properties of protein-LMWS mixtures is available, although many studies claim the importance of their findings for foam properties. Based on the information available, it was hypothesized that the foam properties depend on the molar ratio (MR) of LMWS to protein as well as on the formation of protein-LMWS complexes. Further, it was hypothesized that the foam properties of the complexes are determined by the charge of the proteins and LMWS. In other words, the complexes that are formed if both substances are similarly charged will be different from properties of complexes that are formed in oppositely charged protein-LMWS mixtures.

To understand the parameters that describe the stability of thin liquid films, a model based on an extended DLVO theory was developed (**chapter 2**). It was shown experimentally that the surface charges of surfactant free films can be screened by the addition of an electrolyte, which results in unstable thin films and lower rupture times ($> 7 \cdot 10^{-4} \text{ mol L}^{-1}$). The model uses the surface potential of water films, the hydrophobic interaction and the hydrophobic decay length to predict the drainage and equilibrium thickness of thin liquid films. Combining the model with the stability criterion, the rupture times of films of surfactant free water and NaCl solutions could be modelled. This model was later used in **chapter 6** to quantify the rupture times of thin liquid films to provide a theoretical estimation of the stability of lysozyme-SDS foams.

Next, the effects of concentration on the foam ability and stability of a single protein (β -lactoglobulin, BLG) system were studied. The results were compared to a recently developed concept that describes the concentration dependence of the droplet sizes obtained during production of protein-stabilized emulsions. It was shown that a similar concept can be used to describe the concentration dependence in the formation of protein-stabilized foam (**chapter 3**). A minimal protein concentration (C_{crFA}) is needed to form a set volume of foam. The concentration range below C_{crFA} is called the protein poor

Summary

regime. Increasing the concentration above C_{crFA} results in a decrease of the mean bubble radius (Sauter mean, r_{32}) in the foam until a second critical concentration (C_{cr32}). Above this concentration the r_{32} becomes independent of the concentration. The concentration range between C_{crFA} and C_{cr32} is called the intermediate regime and the concentration range above C_{cr32} is called the protein rich regime. In addition to the foam ability, the foam stability showed a transition to higher values- at concentrations above C_{cr32} . From this it was concluded that the foam stability at $C < C_{cr32}$ is also affected by the foam volume and bubble size. Consequently, comparison of foam stability between different samples should be done at concentrations above C_{cr32} .

To understand the behaviour of mixtures of protein and LMWS, we characterized the bulk, interfacial and foam properties of BLG and sodium dodecyl sulphate (SDS) mixtures (**chapter 4**). Both substances are commonly used in studies on the bulk as well as interfacial properties of protein-LMWS mixtures. They are similarly charged under at pH7, the pH of use in this chapter. The protein concentration used in this chapter is above the critical concentrations (C_{cr32}) determined in **chapter 3**. This means that the foam stability of solutions with different of LMWS to protein molar ratios (MRs) are compared in the protein rich regime. Using isothermal titration calorimetry a single high affinity binding site was identified. Mass spectrometry showed binding at additional low affinity binding sites. The foam stability of the BLG-SDS mixtures decreased between MR 0-20. MR 20 is the critical MR (MR_{cr}), since at $MR > MR_{cr}$ the foam stability increased, following the behaviour of the pure SDS. The interfacial properties monotonically change with increasing MR from values typically associated with proteins towards values that are similar to the ones of SDS. These interfacial properties, namely the surface pressure Π and the dilatational elastic modulus E_d can however, not explain the change of the foam stability as a function of the MR. Furthermore, it was shown by bulk exchange experiments that once BLG or a BLG-SDS complexes are adsorbed to the interface, they cannot be 'washed out' and do not desorb from the interface.

To investigate whether the observations of BLG-SDS are typical for similarly charged protein-LMWS mixtures, the results from **chapter 4** are compared with results obtained for a second mixture of similarly charged bovine serum albumin (BSA) and SDS (**chapter 5**). The foam stability of BSA-SDS mixtures followed a similar trend as the BLG-SDS mixtures. In other words, a decrease in foam stability was observed until a certain critical MR, above which the foam stability increased again. However, the MR_{cr} of BSA-SDS was higher (MR 50) than that of BLG-SDS (MR 20). This was attributed to the fact that BSA has ~5 high affinity binding sites. Using the number of high affinity binding sites and the binding ratio for low affinity binding sites (0.8 for BSA-SDS and 0.1 for BLG-SDS), the concentration of free SDS in solution was calculated. When the foam stability for both systems was plotted against the concentration of free SDS, the data for both systems collapse onto a single curve. From this it was concluded that the initial decrease of the foam stability was due to the formation of protein-SDS complexes, while at higher MR, the foam stability was related to an increase of the concentration of free SDS.

In **chapter 6**, an oppositely charged protein-LMWS mixture (lysozyme (LYS) and SDS) was studied. The concentration of LYS was below the C_{crFA} , since the desired foam volume could not be reached. However, the addition of minute amounts of SDS (MR 0.05) was

sufficient for the solution to reach the foam volume set. The foam stability of the mixtures increased with increasing MR until MR 10. Further increase of the MR lead to a decrease of the foam stability of the mixtures until it was similar to that of pure SDS at MR 30. The increase in foam stability was attributed to the formation of aggregated protein-LMWS complexes. Turbidity measurements showed increasing aggregate formation with increasing MR until MR 8. With further increase of MR up to MR 30, the aggregated complexes dissociated. The experimental foam stability was compared to theoretical estimates of the foam stability. This theoretical estimation was based on a prediction of the stability of the thin liquid films using the model developed in **chapter 2**, combined with a model to describe the drainage in the foam. The stability of the thin films was predicted based on DLVO interactions not taking into account the presence of aggregates. From the comparison of experimental and modelled drainage and stability data, it was concluded that the presence of aggregated LYS-SDS complexes strongly enhance the stability of thin films, while their role in decreasing Plateau border drainage rates is of less importance.

The main findings described in the experimental chapters are discussed in connection to each other in **chapter 7**. First, the effect of the binding of LMWS molecules to protein in similarly and oppositely charged protein-LMWS mixtures is discussed (**chapters 4-6**). The data are supplemented with data on other oppositely charged mixtures (BLG-SDS at pH 3 and BLG and cetyltrimethylammonium bromide) as well as with data on a mixture of a non-ionic LMWS (Tween20) with a BLG. We show that the foam stability of the mixtures can be estimated by quantifying the number of high affinity binding sites and the binding ratio of low affinity binding sites. This relates to a critical MR, which denotes the MR at which a critical concentration of free LMWS molecules in the mixtures is reached.

In conclusion, mixtures of proteins and LMWS can to a certain extent be understood in terms of the concentration of LMWS, the charge of the protein and the LMWS, as well as the number of high affinity sites and the binding ratio of the low affinity binding sites.

Acknowledgements

After four years, writing acknowledgements feels like a big reward. It means that I am about to finish my thesis project and will be ready for the next step. Finishing it would not have been possible without the contribution of many people to whom I am indebted. I would like to use this space to express my sincere gratitude to those people.

First, I would like to thank my co-promotor Peter. Thank you for your help in shaping this thesis and for guiding me through the last 4 years. As a supervisor, you did not only demand but left enough room to grow and develop myself, which I appreciate a lot. You were the sparring partner I needed to make the next step or to find the answers to the issues at hand! Secondly, I would like to thank Marcel, who initiated the project, in which I could perform the research described in this thesis. Thank you for your constant encouragement and enthusiasm about new results and ideas as well as your critical attitude and correctness concerning the communication of the results. Your different background and specialization made it possible for me to work on the interface between chemistry and physics. Thirdly, I would like to thank my promotor Harry for sharing his experience on how to do science with me. Without your critical attitude to all our work, we could not produce such high quality research as we do. Thank you for all the hours (early or late) you spend so that your PhD students can finish their theses. You have my utmost respect for your commitment to our work!

Next, I would like to thank the Laboratory of Food Chemistry and especially Jolanda, the heart and soul of the Laboratory. Thank you for all your help with administration and of course, the candy. Further, I would like to thank René for his patient help with the chromatography and electrophoresis equipment as well as Edwin and Stephano for their help with the Synapt MS.

Thanks also go to the 'protein buddies', who are never shy to volunteer their help and who always have good suggestions!

Of course, I have to thank my old lab mates, Surender and Rianne as well as my new lab mates (Alexandra, Roy, Claire, Emma and Surender) for the good times we had in the lab. It was always nice to share a joke or a litre of buffer with you!

Many thanks go to the other people, students, PhD students, technicians, analysts and guests of the Laboratory of Food Chemistry who create an environment that is more than just a place to work!

I also have to thank some people outside of the Laboratory of Food Chemistry for their support: Harry Baptist for his help with rheology equipment, Jos Sewalt and Maurice

Acknowledgements

Strubel for their help with isothermal titration calorimetry and dynamic light scattering and Adri Westphal for his help with circular dichroism.

For the lively and fruitful discussions, I would like to thank the TIFN team of FS003, also known as the ‘foam project’. Min, Christian, Tijs, Franklin, Eric, Ruud, Guido and Hans, it was a pleasure to work with you.

Some say that you learn the most while teaching. This was true for me as I learned a lot from all my B.Sc. and M.Sc. thesis project students, Frank, Paulien, Lianne, Blanca, Letizia, Marlies, Jurre and Jack! I had a good time guiding you through your theses and I learned a lot from all our discussions.

Since only part of the work during a thesis is performed in the lab, many thanks go to my ‘old’ office mates Koos and Abishek and my ‘new’ office mates Red, Matthias and Roeland for all the talks, jokes and of course chocolate.

Thanks to all my friends who were interested in my progress and did not ask how many papers I had published already. Ein großer Dank geht alle meine Freunde, die sich für meine Arbeit interessiert haben und trotzdem nicht immer fragten, wie viele Paper schon veröffentlicht seien.

Many thanks go to my two paranymphs Alexandra and Roy, who were supporting me an infinite amount of times during my thesis and in the preparation of my defence!

Nur durch die Unterstützung meiner Familie bin ich da, wo ich heute bin. Vielen Dank an meine Eltern, Sabine und Alfred, an Malte, Sonja, Angelika, Gerhard und den Rest der Familie, für all Eure Unterstützung!

Bei einer Person kann ich mich nicht genug bedanken. Sie war immer für mich da, hat mir in schlechten Zeiten gut zugesprochen, mich ermuntert und motiviert. Danke Luisa! Für Alles! Für Dich! Für uns!

Curriculum Vitae

Frederik Jürgen Lech was born on October 30th 1983 in Bremen, Germany. He finished his secondary education at the KGS Leeste in 2003 and completed his community service in 2004. Afterwards, he started working as an apprentice skilled worker in food technology (Fachkraft für Lebensmitteltechnik) at Kellogg's Manufacturing GmbH & Co. KG in Bremen. In 2006, he started his study of bakery and confectionary technology at the HS OWL in Lemgo, Germany.



He finalized his B.Sc. with a thesis on the application of a protein isolate from lupines as fat replacement in a chocolate mousse at the Fraunhofer IVV, Freising. He graduated in 2009 and enrolled afterwards at Wageningen University for the M.Sc. program Food Technology, specializing in ingredient functionality. He completed his M.Sc. with a thesis at the Laboratory of Food Chemistry, Wageningen. The thesis was entitled 'Investigation of the influence of heating time on physical and chemical properties of lysozyme'. Afterwards he did an internship with PepsiCo Nederland, where he developed methods to determine the crispiness and colour of baked cereal products. In September 2011, he started to work as a researcher for the Top Institute Food and Nutrition at the Laboratory of Food Chemistry. This work is described in this thesis. Frederik continues to work at the Laboratory of Food Chemistry as researcher.

Contact: Frederik.Lech@gmail.com

About the author

List of publications

Schwenzfeier, A.; Lech, F. J.; Wierenga, P. A.; Eppink, M. H. M.; Gruppen, H., Foam properties of algae soluble protein isolate: Effect of pH and ionic strength. *Food Hydrocolloids* **2013**, 33, 111-117.

Lech, F. J.; Steltenpool, P.; Meinders, M. B. J.; Sforza, S.; Gruppen, H.; Wierenga, P. A., Identifying changes in chemical, interfacial and foam properties of β -lactoglobulin-sodium dodecyl sulphate mixtures. *Colloids and Surfaces A: Physicochemical and Engineering Aspects* **2014**, 462, 34-44.

Lech, F. J.; Meinders, M. B. J.; Wierenga, P. A.; Gruppen, H., Comparing foam and interfacial properties of similarly charged protein-surfactant mixtures. *Colloids and Surfaces A: Physicochemical and Engineering Aspects* **2015**, 476, 18-23.

Lech, F. J.; Wierenga, P. A.; Gruppen, H., Meinders, M. B. J., Stability properties of surfactant-free thin films at different ionic strengths: Measurements and modeling. *Langmuir* **2015**, 31, 2777-2782.

Lech, F. J.; Delahaije, R. J. B. M.; Meinders, M. B. J.; Gruppen, H.; Wierenga, P. A., Identification of critical concentrations determining foam ability and stability of β -lactoglobulin. Submitted.

Lech, F. J.; Gruppen, H.; Wierenga, P. A.; Meinders, M. B. J., Aggregation in mixtures of lysozyme and sodium dodecyl sulphate determines foam stability by stabilization of the thin films. Submitted.

Overview of completed training activities

Discipline specific courses

Han-sur-Lesse Winterschool, Han-sur-Lesse, Belgium,	2012
Food Structure and Rheology (VLAG), Wageningen, the Netherlands,	2012
Advanced Food Analysis (VLAG), Wageningen, the Netherlands,	2013 ¹
Industrial Food Proteins (VLAG),	2013 ¹

Conferences

EUFoam, Lisbon, Portugal,	2012
Food Colloids, Copenhagen, Denmark,	2012
EUFoam, Thessaloniki, Greece,	2014 ²
Food Colloids, Karlsruhe, Germany,	2014 ¹

General courses / activities

PhD introduction week (VLAG),	2011
Scientific writing (WGS),	2012
Interpersonal communication (WGS),	2012
Voice Matters (WGS),	2014
Career perspectives (WGS)	2014
Statistics for Food Technologists (WGS),	2012
Basic $i\pi$ for TIFN researchers (TIFN),	2012
Feedback course (YoungAFGS),	2012
Networking course (YoungAFSG),	2013
Pitch yourself (YoungAFSG),	2014

Additional activities

Preparing PhD research proposal,	2012
Food Chemistry PhD-trip Singapore and Malaysia ^{1,2} ,	2012 ^{1,2}
Food Chemistry PhD-trip Germany, Denmark, Sweden and Finland,	2014 ^{1,2}
B.Sc./M.Sc. thesis student presentation and colloquia,	2011-2015
PhD presentations Food Chemistry,	2011-2015

¹ Poster presentation

² Oral presentation

The work described in this thesis was performed at the Laboratory of Food Chemistry, Wageningen University, The Netherlands.

The research described in this thesis was financially supported by the Top Institute Food & Nutrition, Wageningen, The Netherlands

Financial support from Wageningen University and the Top Institute Food & Nutrition for printing this thesis is gratefully acknowledged.

Cover design: Frederik Lech

This thesis was printed by Gildeprint drukkerijen, Enschede, The Netherlands.

Frederik J. Lech, 2015